

Particles and Plasmas in the Universe

Johann Rafelski

Quark-Hadron part in collaboration with **Cheng Tao Yang**

Neutrino Freeze-out in collaboration with **Jeremiah Birrell & Cheng Tao Yang**

e^+e^- Plasma and BBN in collaboration with **Chris Grayson & Cheng Tao Yang**

Presentation artistry and more by **Andrew Steinmetz & Johann Rafelski**

Department of Physics, The University of Arizona, Tucson 85721



Latest update:
Dec. 2nd, 2022

**Background credit: Planck
Microwave Background Radiation**

Quark-Hadron part: Cheng Tao Yang, Inga Kuznetova, Mike Fromerth

- Yang, Cheng Tao, and Johann Rafelski. "Cosmological strangeness abundance." *Physics Letters B* 827 (2022): 136944. <https://doi.org/10.1016/j.physletb.2022.136944>
- Yang, Cheng Tao, and Johann Rafelski. "Reactions Governing Strangeness Abundance in Primordial Universe." EPJ Web of Conferences. Vol. 259. EDP Sciences, 2022. <https://doi.org/10.1051/epjconf/202225913001>
- Rafelski, J., and C. T. Yang. "The Muon Abundance in the Primordial Universe." *Acta Physica Polonica B* 52.3 (2021): 277. <https://doi.org/10.5506/APhysPolB.52.277>
- Yang, Cheng Tao, and Johann Rafelski. "Possibility of bottom-catalyzed matter genesis near to primordial QGP hadronization." *arXiv preprint arXiv:2004.06771* (2020) (update pending)
- Fromerth, Michael J., Inga Kuznetova, et al. "From quark-gluon universe to neutrino decoupling: $200 < T < 2 \text{ MeV}$." *Acta Phys. Pol. B* 43, 2261 (2012) <https://doi.org/10.5506/APhysPolB.43.2261>



Neutrino Freeze-out in collaboration with Jeremiah Birrell & Cheng Tao Yang

- Birrell, Jeremiah, Cheng Tao Yang, and Johann Rafelski. "Relic neutrino freeze-out: Dependence on natural constants." *Nuclear Physics B* 890 (2015): 481-517. <https://doi.org/10.1016/j.nuclphysb.2014.11.020>
- Birrell, Jeremiah, Jon Wilkening, and Johann Rafelski. "Boltzmann equation solver adapted to emergent chemical non-equilibrium." *Journal of Computational Physics* 281 (2015): 896-916. <https://doi.org/10.1016/j.jcp.2014.10.056>
- Birrell, Jeremiah, et al. "Relic neutrinos: Physically consistent treatment of effective number of neutrinos and neutrino mass." *Physical Review D* 89.2 (2014): 023008. <https://doi.org/10.1103/PhysRevD.89.023008>



$e^+ e^-$ Plasma and BBN in collaboration with Chris Grayson & Cheng Tao Yang

- Grayson, Christopher, et al. "Dynamic Magnetic Response of Quark-Gluon Plasma to Electromagnetic Fields." *Phys. Rev. D* 106 (2022): 014011 <https://doi.org/10.1103/PhysRevD.106.014011>
- Formanek, Martin, et al. "Current-conserving relativistic linear response for collisional plasmas." *Annals of Physics* 434 (2021): 168605. <https://doi.org/10.1016/j.aop.2021.168605>



The Universe: Making matter and nuclei

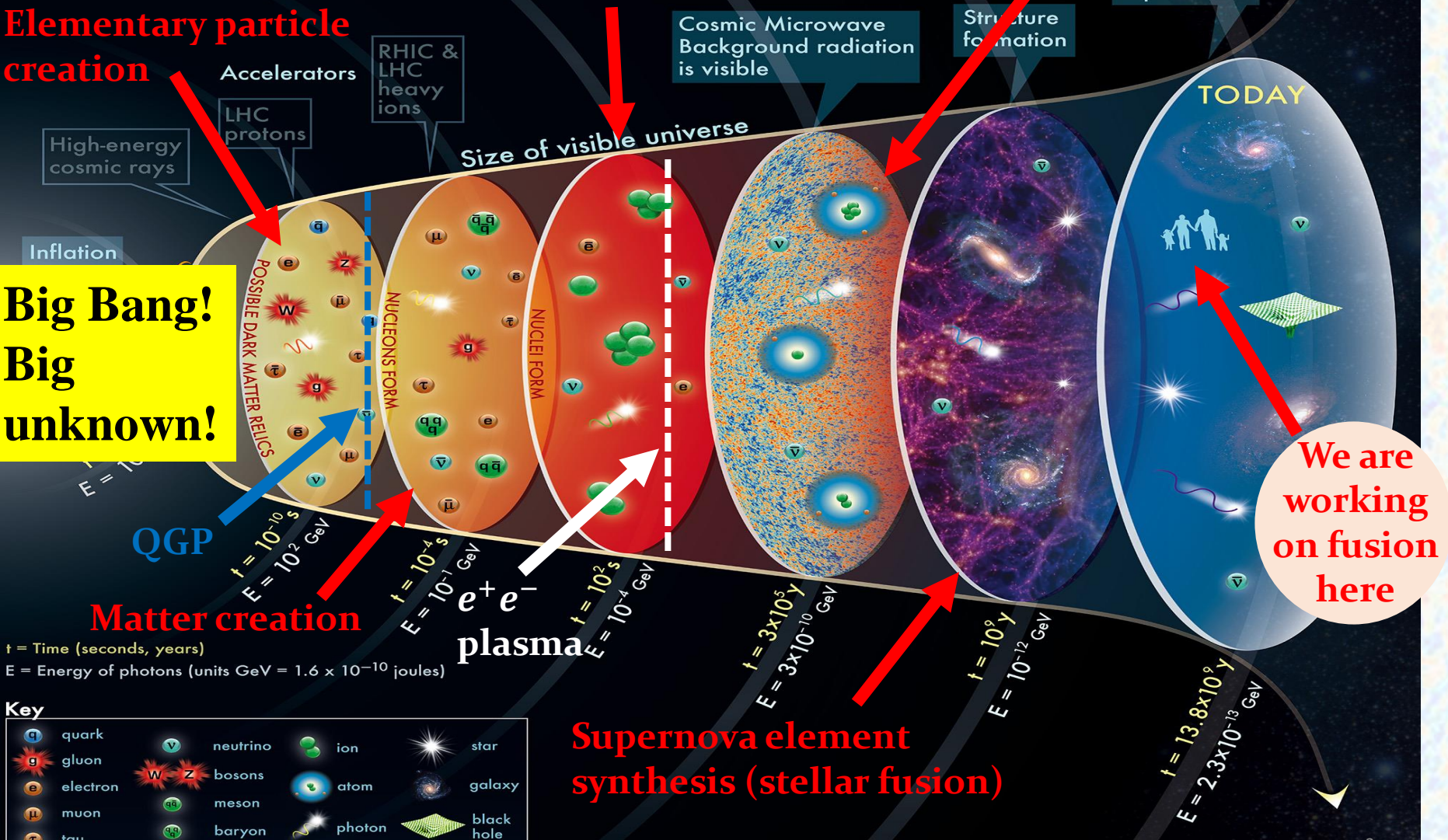
Direct observational cosmology begins here

HISTORY OF THE UNIVERSE

Big Bang nucleosynthesis (first fusion)

Elementary particle creation

Big Bang! Big unknown!



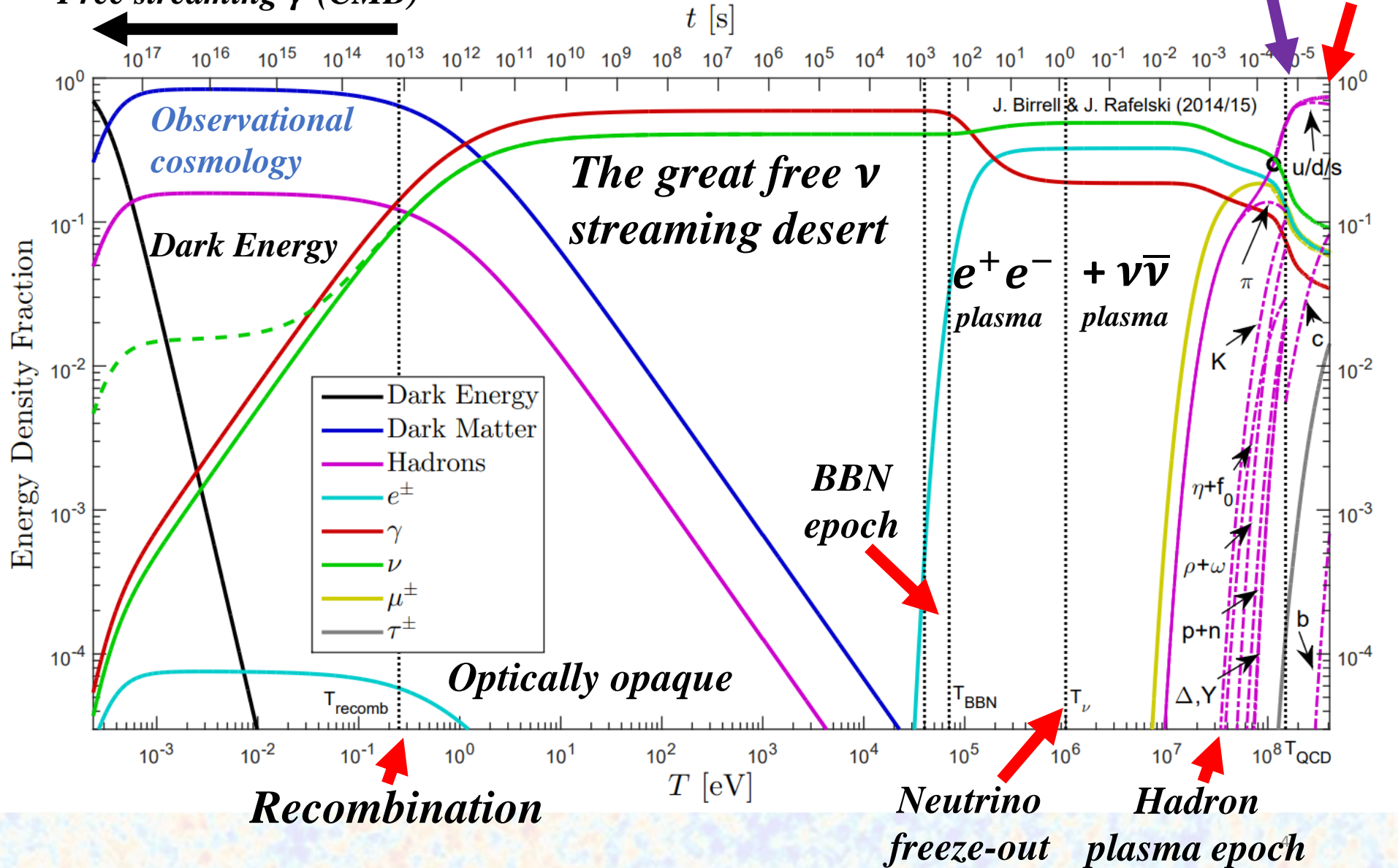
Key

	quark		neutrino		ion		star
	gluon		bosons		atom		galaxy
	electron		meson		photon		black hole
	muon		baryon				
	tau						

The concept for the above figure originated in a 1986 paper by Michael Turner.


A quick look at the Universe's composition

Free streaming γ (CMB)



Choice of Zimanyi School 2022 lecture material

1. **Universe evolution**
2. **Connecting new phases of matter in the laboratory & Universe**
3. Baryons in the Universe
4. Strangeness epochs in the Universe
5. Muon abundance is the doorway to Kaons
6. Kinetic theory of hadronic strangeness
 - Special topic: Heavy quarks
7. Neutrino freeze-out in the Early Universe
8. **Big Bang Nucleosynthesis (BBN) epoch**
9. **Fusion energy for mankind**
 - Natural fusion
 - Brute force & clever paths to manmade fusion
 - Tabletop approaches to fusion
 - Muon-catalyzed fusion
 - Two beam pB-laser fusion
 - Antennas for light – plasmonic fusion
10. **Moving nuclei in non-relativistic electron-positron plasma**



Quantum
jump to
slide 40

Module 1: Universe evolution

Basis of Λ CDM

Hubble parameter

$$H \equiv \frac{\dot{a}}{a}$$

Deceleration parameter

$$q \equiv -\frac{a\ddot{a}}{\dot{a}^2} = -\frac{1}{H^2} \frac{\ddot{a}}{a}$$

Einstein's Λ plus cold dark matter plus FLRW metric.

The Friedman-Lemaître-Robertson-Walker (FLRW) metric is given by:

$$\text{diag}(g_{\mu\nu}) = (1, -a^2(t), -a^2(t), -a^2(t))$$

The universe's evolution is described by the Einstein Field Equations (EFE)

$$\mathcal{R}_{\mu\nu} - \frac{1}{2}g_{\mu\nu}\mathcal{R} + \Lambda g_{\mu\nu} = 8\pi T_{\mu\nu} \leftarrow \text{diag}(T_{\mu\nu}) = (\rho, P, P, P)$$

Relation of Dark Energy to Lambda

$$\rho_{DE} = \frac{\Lambda}{8\pi G}$$

In a perfectly homogenous isotropic universe, the FLRW metric is a solution of the Einstein Field Equations. Under the FLRW assumptions, the EFE reduce to two dynamical equations:

$$P_{DE} = \frac{-\Lambda}{8\pi G}$$

$$\frac{\Lambda}{3} + \frac{8\pi G}{3}\rho = \frac{\dot{a}^2 + k}{a^2} = H^2 \left(1 + \frac{k}{\dot{a}^2}\right)$$

$$\frac{\Lambda}{3} - \frac{4\pi G}{3}(\rho + 3P) = \frac{\ddot{a}}{a} = -qH^2$$

$$H^2 = \frac{8\pi G}{3}\rho$$

For most of the Universe's history, the primary driver of expansion was energy density.

From particle data group, the Hubble constant **today** :

$$1/H_0 \approx 4.58 \times 10^{17} \text{ s}$$

An important nuance A: Deceleration parameter

$$\frac{\Lambda}{3} + \frac{8\pi G}{3} \rho = \frac{\dot{a}^2 + k}{a^2} = H^2 \left(1 + \frac{k}{\dot{a}^2} \right)$$

Solve for constant and set two equations as equal.

$$\frac{\Lambda}{3} - \frac{4\pi G}{3} (\rho + 3P) = \frac{\ddot{a}}{a} = -qH^2$$

This provides an expression for q in terms of H , ρ , and P .

Hubble parameter

$$H \equiv \frac{\dot{a}}{a}$$

Deceleration parameter

$$q \equiv -\frac{a\ddot{a}}{\dot{a}^2} = -\frac{1}{H^2} \frac{\ddot{a}}{a}$$

The deceleration (or acceleration) of the universe's expansion is written in terms of the second derivative of the expansion coefficient. Using the Friedman equations, this can also be written

as:

$$q = \frac{1}{2} \left(1 + \frac{3P}{\rho} \right) \left(1 + \frac{k}{\dot{a}^2} \right) - \left(1 + \frac{P}{\rho} \right) \frac{\Lambda}{H^2}$$

Relation of Dark Energy to Lambda

$$\rho_{DE} = \frac{\Lambda}{8\pi G}$$

$$P_{DE} = \frac{-\Lambda}{8\pi G}$$

Universes with different energy content types results in different q values:

- **Radiation dominated universe:** $P = \rho/3 \Rightarrow q = 1$
- **Matter dominated universe:** $P \ll \rho \Rightarrow q = 1/2$
- **Dark energy (Λ) dominated universe:** $P = -\rho \Rightarrow q = -1$

Today evolving into a Dark Energy dominated accelerating universe!

An important nuance B:

Freeze-out & non-equilibrium in a dynamic Universe

In cosmology, freeze-out refers to the epoch where a given type of particle ceases to interact with other particles as the Universe expands:

$$\frac{1}{\Delta T_f} \equiv \left[\frac{1}{(\Gamma/H)} \frac{d(\Gamma/H)}{dT} \right]_{T_f}, \quad \Gamma \equiv \frac{1}{\tau}$$

- **This is traditional freeze-out:**

Rate of production become slower than the rate of Universe expansion.

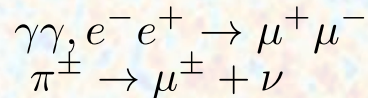
- **The case of muons is different:**

$$\tau_{ab \rightarrow c} = \tau_{c \rightarrow ab} < 1/H$$

Muons decoupling from the primordial plasma is driven by the production process slowing down at low temperature and not being able to keep up with decay of muons.

J. Rafelski and C.T. Yang, Acta Phys. Polon. B 52, 277 (2021)

The total relaxation time



$$\tau_{\text{source}} \geq \tau_{\text{decay}}$$

Lifespan of muon $\mu^\pm \rightarrow e^\pm \nu_e \nu_\mu$

Muon abundance thus disappears as soon as a decay rate crosses the dominant production rate. **Where this happen depend on temperature. Duration of reaction depends on the momentary value of H.**

- **Neutrinos, however, freeze-out very slowly because of the weakness of the interaction:**
 - a. Neutrinos do not decay unlike muons, pions, etc...
 - b. The chemical (abundance) and kinetic (equi-distribution of energy) freezes out nearly at same temperature. $T = 3 \pm 1$ MeV

J. Birrell, C.T. Yang and J. Rafelski, Nucl. Phys. B 890, 481-517 (2014)

- **Exceptional case of pions:**

The production $\gamma\gamma \rightarrow \pi^0$ is faster than the expansion of Universe, and all pions remain in full thermal equilibrium.

I. Kuznetsova, D. Habs and J. Rafelski Phys. Rev. D 78, 014027 (2008)

Module 2: Connecting new phases of matter in the laboratory and in the Universe

- **RECREATE THE EARLY UNIVERSE IN LABORATORY**

Recreate and understand the high energy density conditions prevailing in the Universe when matter formed from elementary degrees of freedom (quarks, gluons) at about $20\mu\text{s}$ after the Big-Bang.

- **PROBE ORIGIN OF FLAVOR**

Normal matter made of first flavor family (d, u, e, $[\nu_e]$). Strangeness-rich quark-gluon plasma the sole laboratory environment filled 'to the rim' with 2nd family matter (s, c, $[\mu, \nu_\mu]$). and considerable abundance of b and even t.

- **PROBING OVER A 'LARGE' DISTANCE THE (DE)CONFINING QUANTUM VACUUM STRUCTURE**

The quantum vacuum, the present day relativistic æther, determines prevailing form of matter and laws of nature.

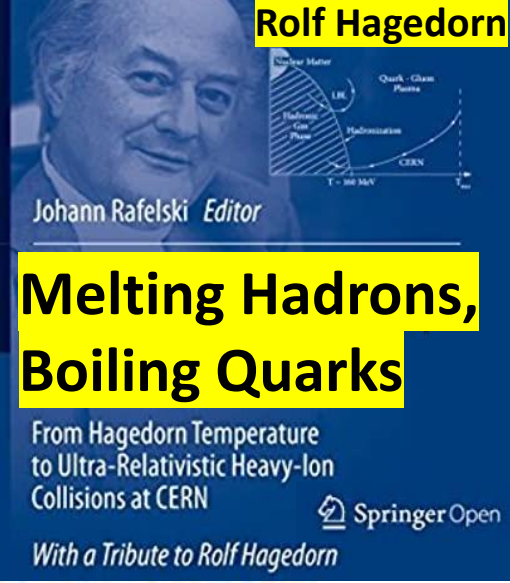
- **STUDY OF THE ORIGIN OF MATTER & OF MASS**

Matter and antimatter created when QGP 'hadronizes'. Mass of matter originates in the confining vacuum structure.

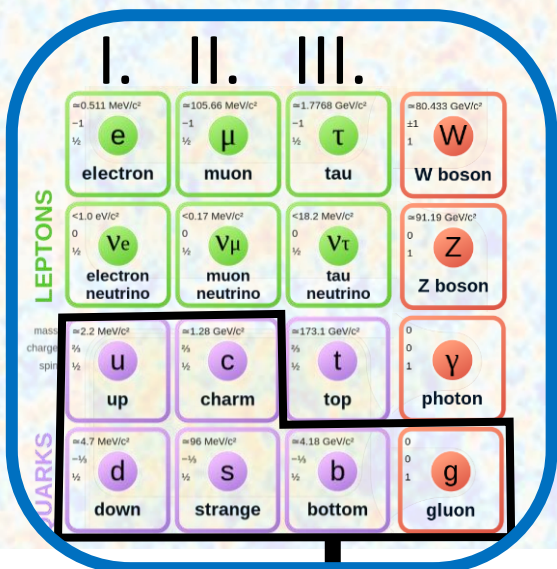
- **PROBE STRONGEST FORCES IN THE UNIVERSE**

For a short-times the relativistic approach and separation of large charges $Ze \leftrightarrow Ze$ generates EM fields 1000s time stronger than those in Magnetars; strong fields=strong force=strong acceleration

Rolf Hagedorn



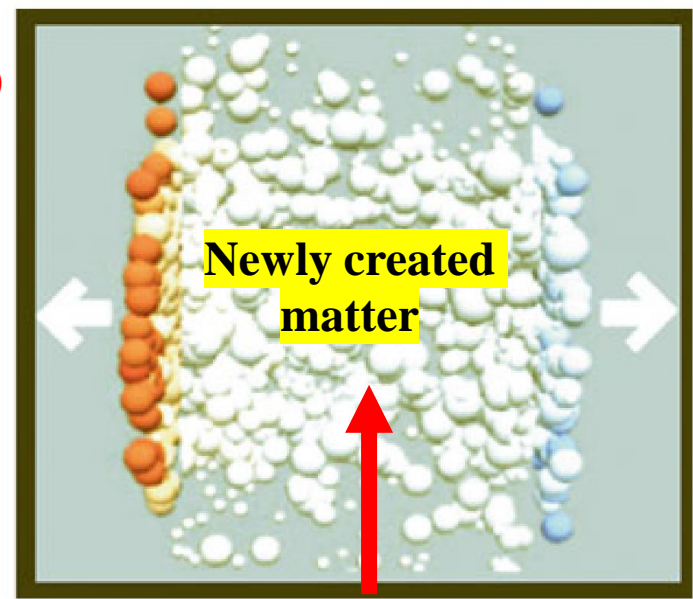
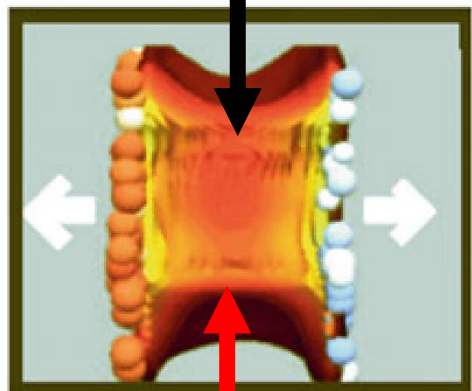
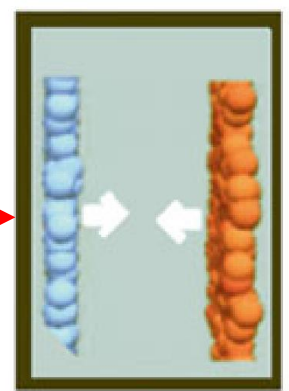
Melting Hadrons, Boiling Quarks



- Matter we see in the Universe today is Family I.
- Early Universe had everything in the particle soup.
- Heavy-ion collisions allow all three families to appear.

Just after initial collision, hot primordial plasma forms (recreating early Universe)

Lorentz contracted nuclei collide.



Ongoing experiments utilize Lorentz gamma of 5-5,000 today.

Quark Universe in the laboratory

Hadron Universe in the laboratory

Particle input in adiabatic expansion

Comoving entropy density in universe:

$$\text{Const.} = sa^3 = \left[\frac{\rho + P}{T} - \sum_i \frac{\mu_i}{T} n_i \right] a^3 \equiv \frac{2\pi^2}{45} g_*^s T^3 a^3$$

130 GeV >
T > 150 MeV

Gluons : g
Quarks : u, d, s, c, b, t
Weak bosons : W^\pm, Z

g_*^s = 'entropy' degrees of freedom

150 MeV >
T > 5 MeV

Photon : γ Heavy leptons : τ^\pm
Neutrino : $\nu_e, \nu_\mu, \nu_\tau, \bar{\nu}_e, \bar{\nu}_\tau, \bar{\nu}_\mu$

Hubble parameter:

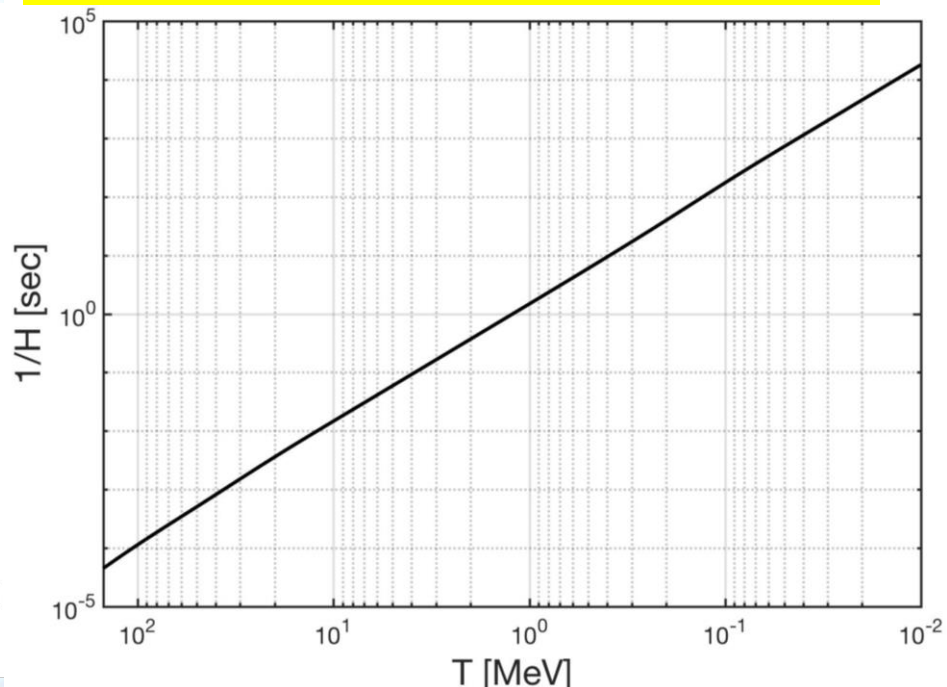
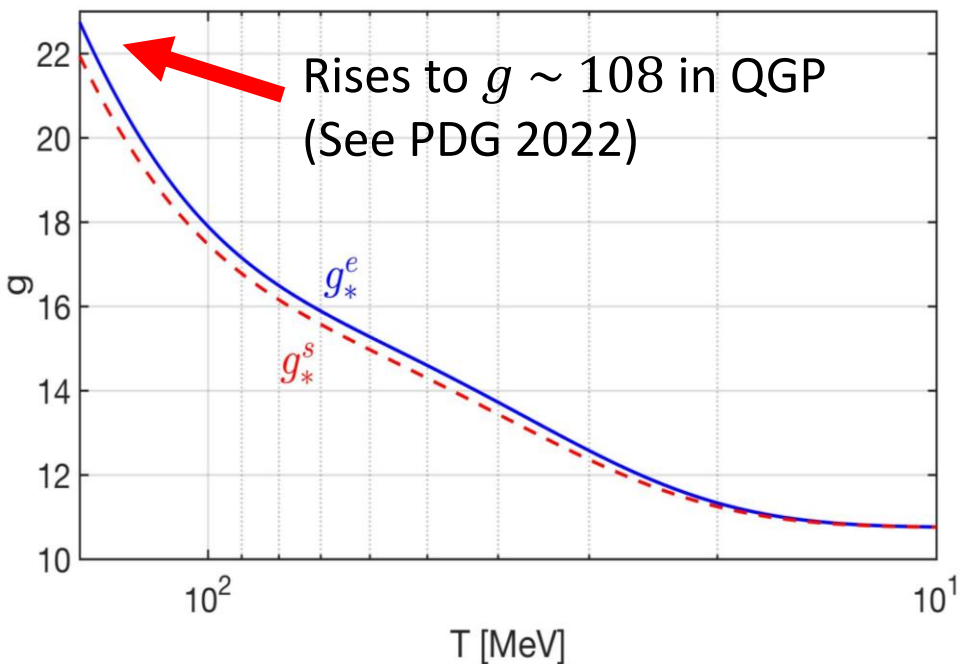
$$H^2 = H_{rad}^2 \left(1 + \frac{\rho_{\pi, \mu, \rho}}{\rho_{rad}} + \frac{\rho_{strange}}{\rho_{rad}} \right) = \frac{8\pi^3 G_N}{90} g_*^e T^4$$

Charged lepton : e^-, e^+, μ^-, μ^+

Hadron : π^0, π^+, π^- .

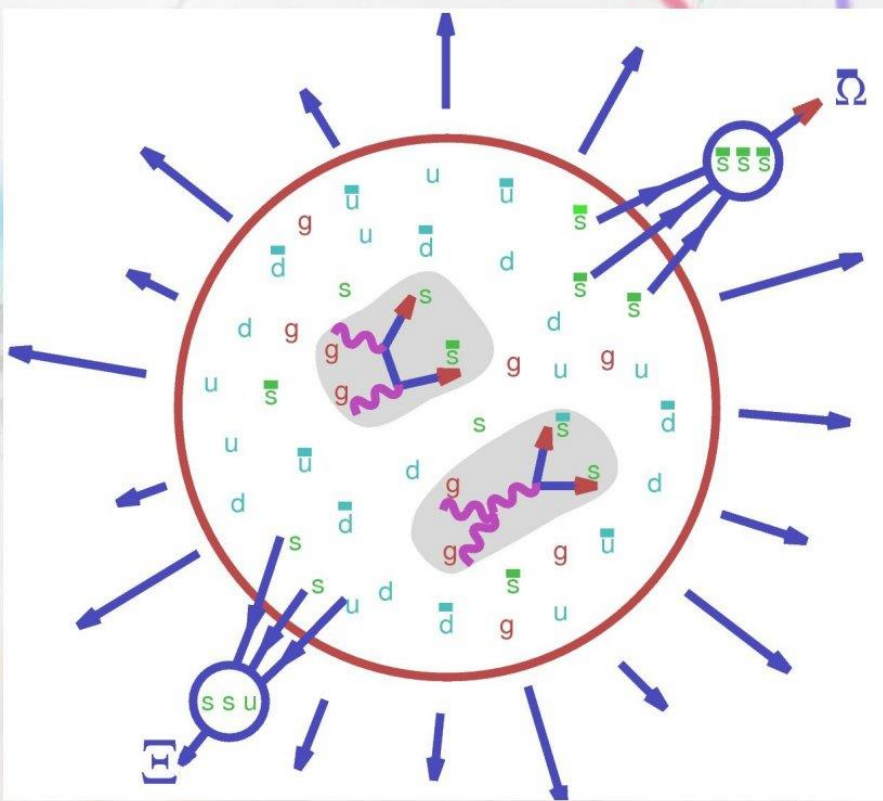
Strangeness : $K^0, K^\pm, K^*, \eta, \eta'$

g_*^e = relativistic 'energy' degrees of freedom



Pions remain always remain in chemical equilibrium, muons disappear at 4-5 MeV.

Cooking flavors, forming hadrons



- 1 $GG \rightarrow s\bar{s}$ (thermal gluons collide)
 $GG \rightarrow c\bar{c}$ (initial parton collision)
gluon dominated reactions
- 2 hadronization of pre-formed $s, \bar{s}, c, \bar{c}, b, \bar{b}$ quarks



Berndt Muller, Peter Koch, and JR

30 years after: [Phys.Rept. 88 \(1982\) p331](#).

Evaporation-recombination formation of complex rarely produced (multi)exotic flavor (anti)particles from QGP is a key QGP property leading to abundant production of flavored (strange, charm, bottom) (anti)baryons progressing with 'exotic' flavor content.

Module 3: Baryons in the Universe

Asymmetry in the Universe $n_B \neq 0$; $n_B + n_l = 0$:

Quark chemical potentials near hadronization

Chemical potentials control particle/antiparticle abundances:

$$f_{p/a} = \frac{1}{e^{\beta(\varepsilon \mp \mu)} \pm 1}, \quad \varepsilon = \sqrt{p^2 + m^2}$$

- **Quark side:** $d \leftrightarrow s \leftrightarrow b_{\text{ottom}}$ oscillation means $\mu_d = \mu_s = \mu_{\text{bottom}}$ and similarly $\mu_{\nu_e} = \mu_{\nu_\mu} = \mu_{\nu_\tau}$. WI reaction e.g. $d \rightarrow u + e^- + \bar{\nu}_e$ imply $\mu_d - \mu_u = \Delta\mu_l$ with

$$\Delta\mu_l = \mu_e - \mu_{\nu_e} = \mu_\mu - \mu_{\nu_\mu} = \mu_\tau - \mu_{\nu_\tau}$$

- **Hadron side:** Quark chemical potentials control valence quarks and can be used in the hadron phase, e.g. $\Sigma^0 (uds)$ has chemical potential $\mu_{\Sigma^0} = \mu_u + \mu_d + \mu_s$. The baryochemical potential μ_B is:

$$\mu_B = \frac{1}{2}(\mu_p + \mu_n) = \frac{3}{2}(\mu_d + \mu_u) = 3\mu_d - \frac{3}{2}\Delta\mu_l$$

Three constraints

The chemistry of particle reaction and equilibration in the Universe has three chemical potentials 'free' i.e. not only baryochemical potential μ_B . We need three physics constraints

Michael J. Fromerth , JR e-Print: [astro-ph/0211346](https://arxiv.org/abs/astro-ph/0211346):

- i. Charge neutrality eliminates Coulomb energy

$$n_Q \equiv \sum Q_i n_i(\mu_i, T) = 0,$$

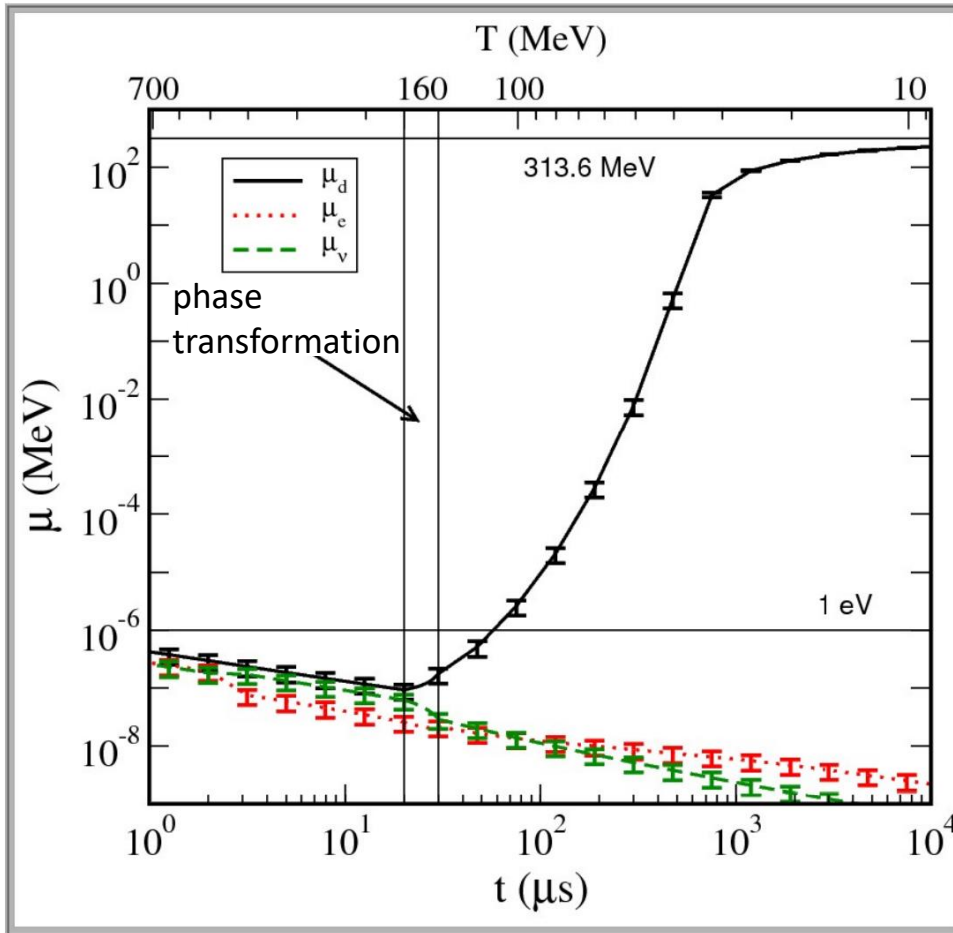
Q_i and n_i charge and number density of species i .

- ii. Net lepton number equals net baryon number However, possible neutrino-antineutrino asymmetry can hide an imbalance
- iii. Prescribed value of entropy-per-baryon

$$\frac{\sigma}{n_B} \equiv \frac{\sum_i \sigma_i(\mu_i, T)}{\sum_i B_i n_i(\mu_i, T)} = 3.2 \dots 4.5 \times 10^{10}$$

Today best est. $S/B = 3.5 \times 10^{10}$, results shown for 4.5×10^{10}

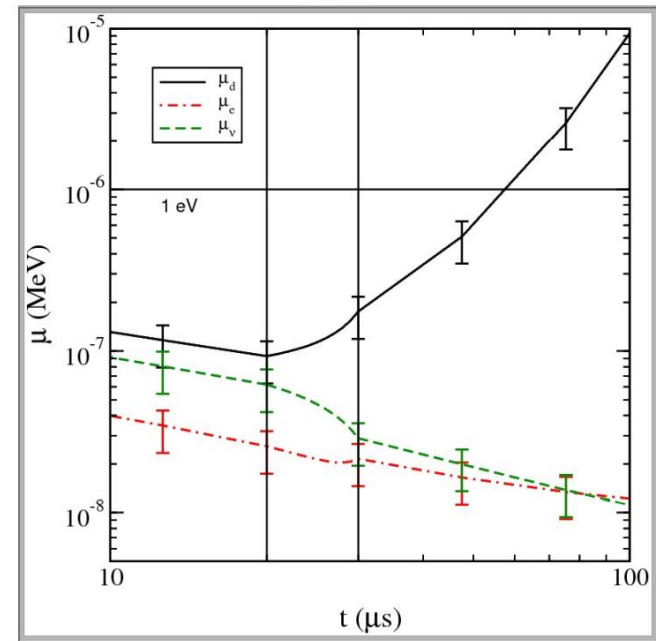
Chemical potential created by baryon asymmetry



2002 input data:
Changes nearly within the
error bars and hardly visible

Minimum:

$$\mu_B = 0.33^{+0.11}_{-0.08} \text{ eV}$$



$\Rightarrow \mu_B$ defines remainder of matter after annihilation

Review chemical equilibrium and potential

From the QGP study, in high temperature range the the strangeness formation processes studied in the laboratory are fast enough to assure chemical equilibrium.

- Considering the Universe evolves adiabatically, we have constant baryon-per-entropy ratio, i.e.

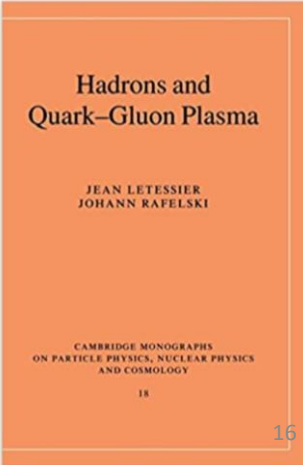
$$\frac{n_B - n_{\bar{B}}}{s} = \left(\frac{n_B - n_{\bar{B}}}{s} \right)_{t_0} = (0.865 \pm 0.008) \times 10^{-10} \quad \text{2020 input data}$$

Input: $(n_B - n_{\bar{B}}) / n_\gamma = (0.609 \pm 0.06) \times 10^{-9}$ (CMB)

- As long as strong interactions dominate production of strangeness the evolution of baryon and strangeness chemical potentials is constrained by $\langle s - \bar{s} \rangle = 0$, we have

$$\lambda_s = \lambda_q \sqrt{\frac{F_K + \lambda_q^{-3} F_Y}{F_K + \lambda_q^3 F_Y}} \quad \mu_s = T \ln \lambda_s \quad \mu_B = 3T \ln \lambda_q$$

$$F_i = \sum_i g_i \left(\frac{m_i}{T} \right)^2 K_2(m_i/T)$$



Jean Letessier, Johann Rafelski, "Hadrons and Quark-Gluon Plasma", p 220

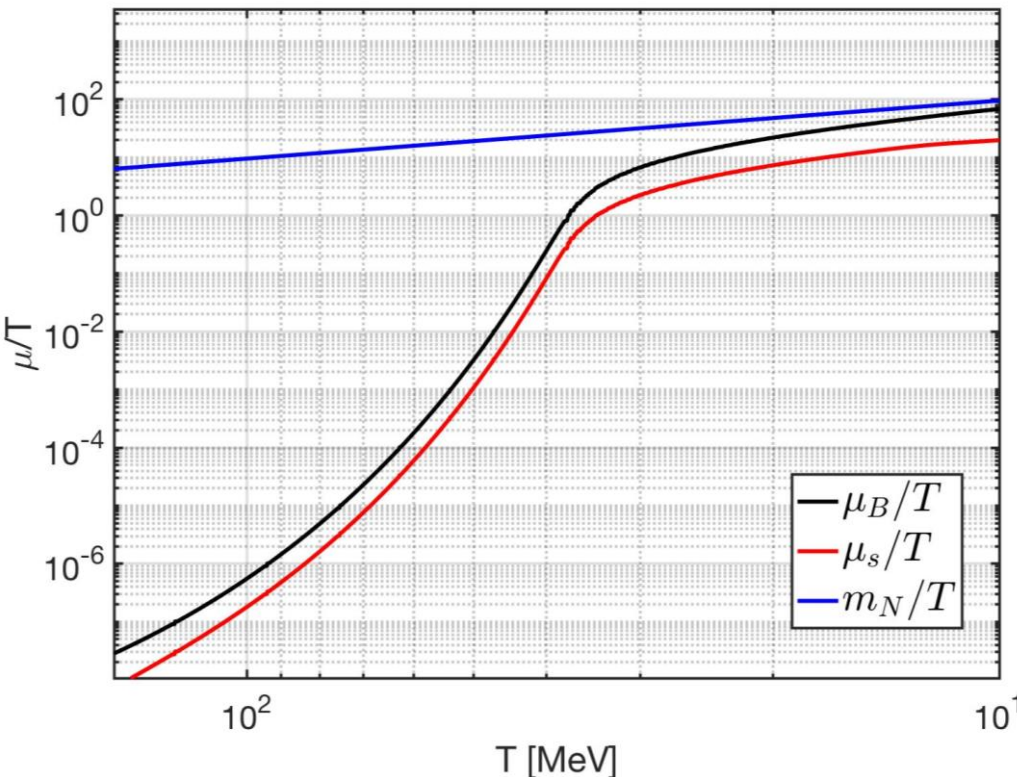
M.J.Fromerth, I. Kuznetsova, L. Labun, J. Letessier and J. Rafelski, "From Quark-Gluon Universe to Neutrino Decoupling: 200 <T <2MeV," Acta Phys. Polon. B 43, no.12, 2261-2284 (2012)

Chemical potentials of μ_B and μ_s in hadronic era

We use the **conservation of strangeness** and the **conserved entropy-per-baryon-ratio** to determine the chemical potentials of baryons and strangeness in the early Universe

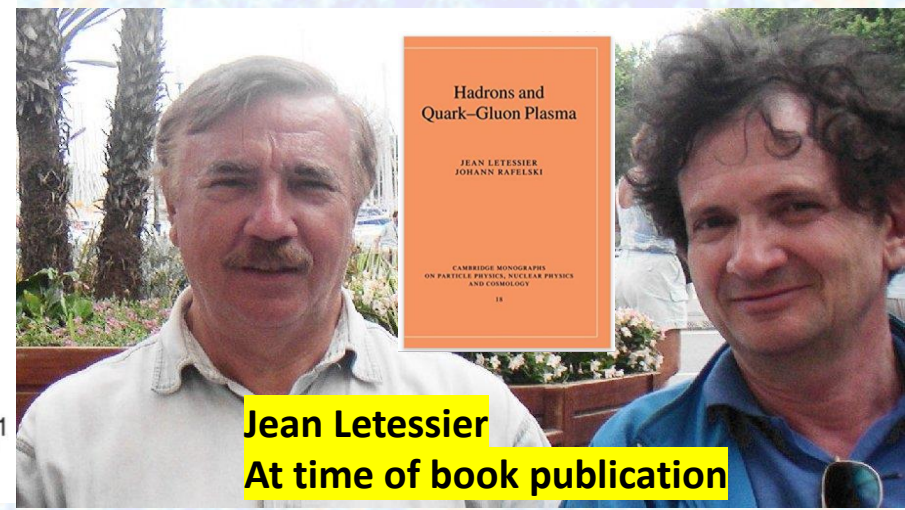
$$\left(\frac{n_B - n_{\bar{B}}}{s} \right)_{t_0} = \frac{45}{2\pi^4 g_*^s} \sinh \left[\frac{\mu_B}{T} \right] F_N \left[1 - \frac{F_Y}{F_N} \sqrt{\frac{1 + e^{-\mu_B/T} F_Y/F_K}{1 + e^{\mu_B/T} F_Y/F_K}} \right].$$

Input: $(n_B - n_{\bar{B}})/n_\gamma = (0.609 \pm 0.06) \times 10^{-9}$ (CMB)



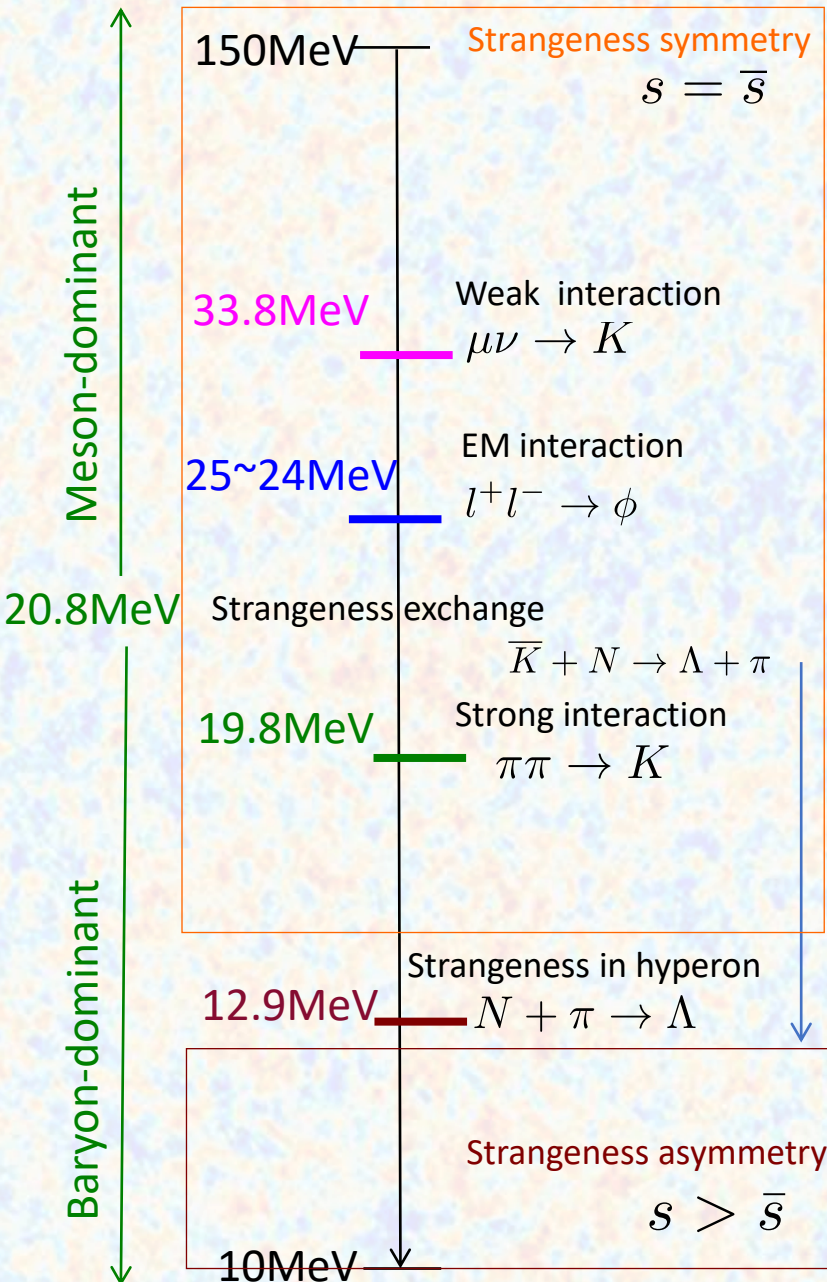
The chemical potentials change dramatically in the temperature window $T = 50 \sim 30$ MeV which is an important period for antibaryon annihilation.

Jean Letessier, Johann Rafelski, "Hadrons and Quark-Gluon Plasma"



Jean Letessier
At time of book publication

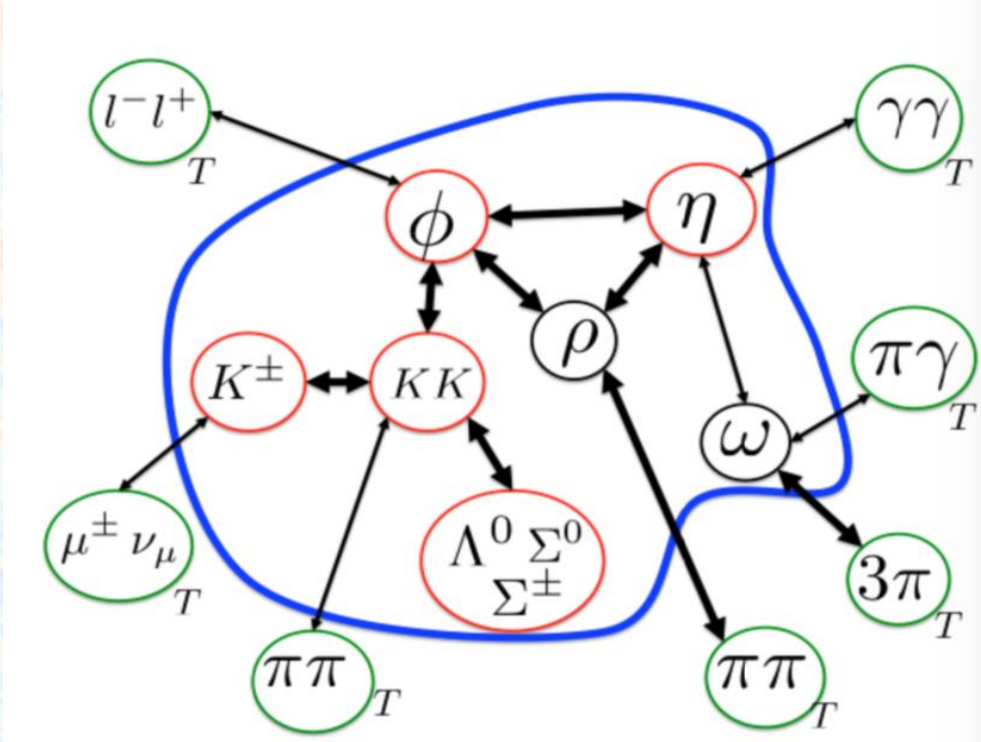
Module 4: Strangeness epochs in the Universe



- For temperature $T > 20.8$ MeV, the strangeness is predominantly present in the mesons with $s = \bar{s}$
- The first freezeout reaction is the weak interaction $\mu\nu \rightarrow K$ at $T=33.8$ MeV.
- The second freezeout reaction is the electromagnetic process: $l^+l^- \rightarrow \phi$ at $T=25\sim 24$ MeV .
- The last freezeout reaction is the hadronic reaction $\pi\pi \rightarrow K$ at $T=19.8$ MeV.
- For temperature $20.8 > T > 12.8$ MeV, the strangeness is predominantly present in the hyperons and anti-strangeness in kaon, then keep $s = \bar{s}$
- For $T < 12.9$ MeV the reaction $K + N \rightarrow \Lambda + \pi$ becomes slower than the strangeness decay $N + \pi \leftrightarrow \Lambda$, and we have $s > \bar{s}$

Hadro-chemical equilibrium in the Universe

The relevant reactions in the Universe following on QGP hadronization in the temperature interval $150 > T > 10$ MeV range.



- The blue boundary is drawn around hadronic particles expected to fall out of abundance equilibrium.
- The red circles within this domain represent strangeness-carrying mesons
- The green circles represent the equilibrium (index T) heat bath of particles.

We need to know what is the dominant strangeness and their reaction in early universe from $150 > T > 10$ MeV.

Strangeness in the hadronic Universe

Strangeness flavor is abundant and found in chemical equilibrium in the primordial Quark-Gluon Plasma(QGP) filling the early Universe. Upon hadronization near to $T = 150 \text{ MeV}$ **one may think that relatively short lived massive strange hadrons decay rapidly and strangeness disappears.**



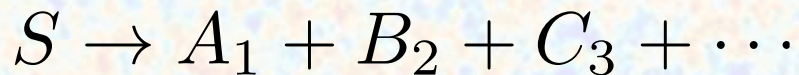
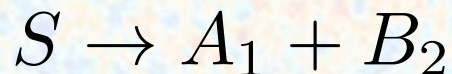
$$\text{Mass } m = 497.611 \pm 0.013 \text{ MeV}$$

$$\text{Mean life } \tau = (0.8954 \pm 0.0004) \times 10^{-10} \text{ s}$$

- The time it takes for the Universe to evolve from 150 MeV to 10 MeV, about $\Delta t \approx 10^{-3} \text{ s}$, is much longer compared to K^0 life span.

However, strangeness can be produced by the inverse decay reactions in the early universe:

Strangeness Decay



Strangeness production



- The freezeout processes can break the detailed balance and make the reactions departure from the equilibrium.
- Nonequilibrium processes have important impact in the early universe evolution

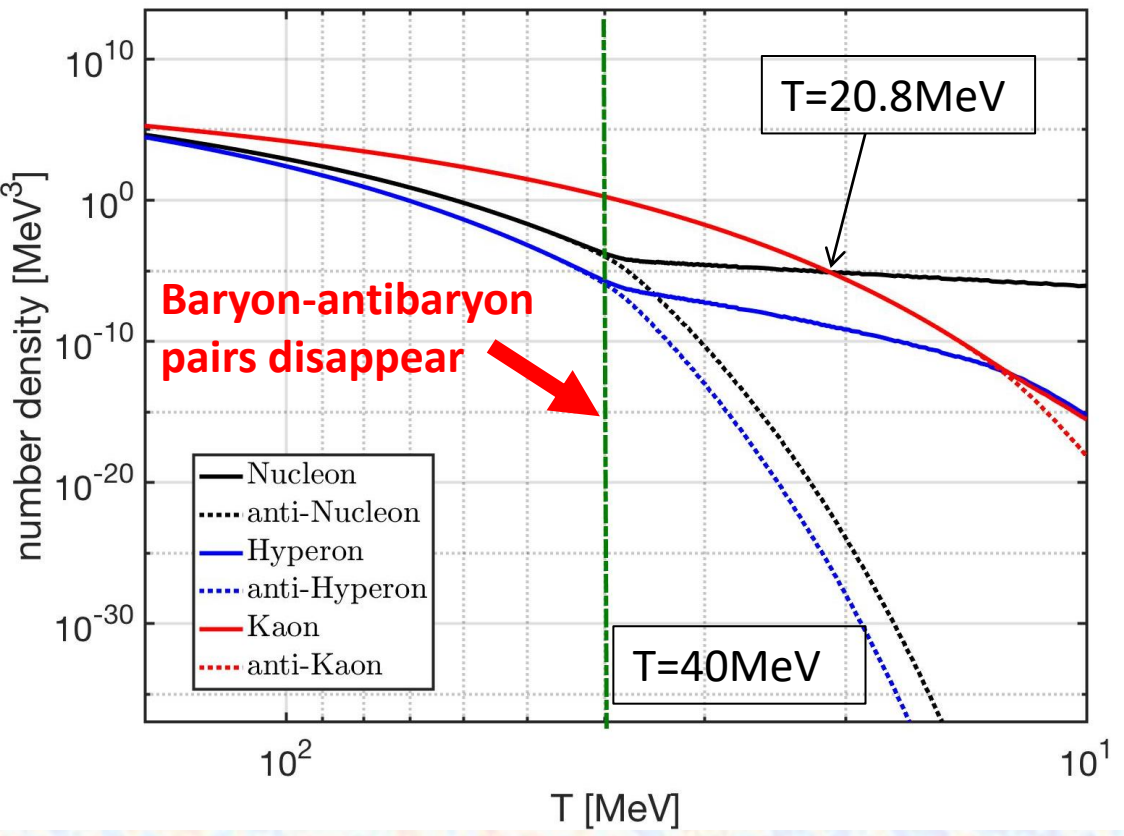
Our interest is to study in detail how long can strangeness stay in the Universe

We need to explore the influence of strangeness decay and production reactions on strangeness flavor freezeout process.

Strangeness abundance from μ_B and μ_s

The number density of baryon and strangeness as a function of temperature $150 \text{ MeV} > T > 10 \text{ MeV}$ in early universe.

Onset of anti-baryon start disappearance:

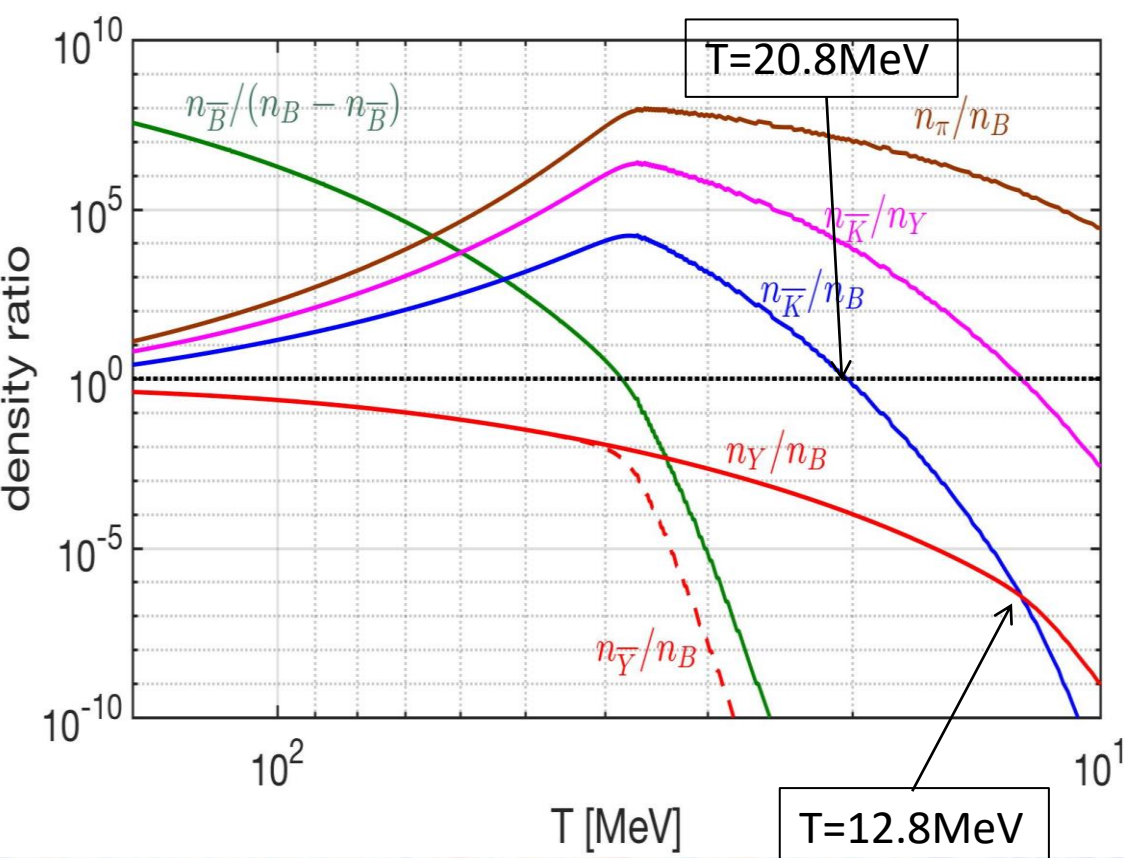


- We show that the Universe in the range $T > 20 \text{ MeV}$ is rich in physics phenomena involving strange mesons, (anti)baryons including (anti)hyperon abundances.
- In relative chemical equilibrium, the chemical potential of hadrons is equal to the sum of the chemical potentials of their constituent quarks.

Composition of the Universe (chemical equilibrium)

For $T > 20$ MeV the ratio $n_{\bar{K}}/n_B \gg 1$ which implies the universe is meson-dominant, and for $T < 20$ MeV the ratio $n_{\bar{K}}/n_B \ll 1$ we have baryon-dominant universe.

$n_{\bar{K}} \gg n_B$ ← → $n_B \gg n_{\bar{K}}$



For $T > 20$ MeV, the strangeness is dominantly present in the meson with: $s = \bar{s}$

Strangeness exchange reaction:
 $\bar{K} + N \rightarrow \Lambda + \pi$

For $20 > T > 12$ MeV, the strangeness can present in the hyperons and anti-strangeness in kaon keeping symmetric: $s = \bar{s}$

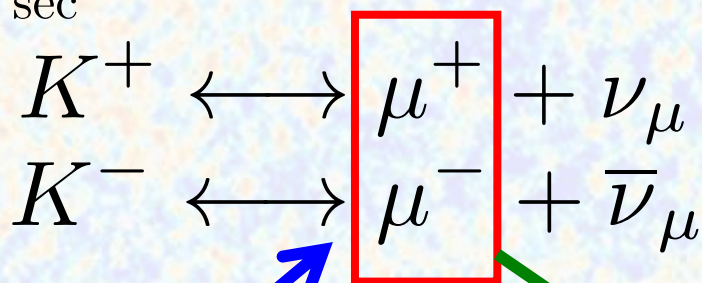
$n_Y/n_B = 3.6 \times 10^{-7}$

Module 5: Muon abundance is the low energy doorway to Kaon production

Our interest in strangeness flavor freeze-out in the early Universe requires the understanding of the abundance of muons in the early Universe.

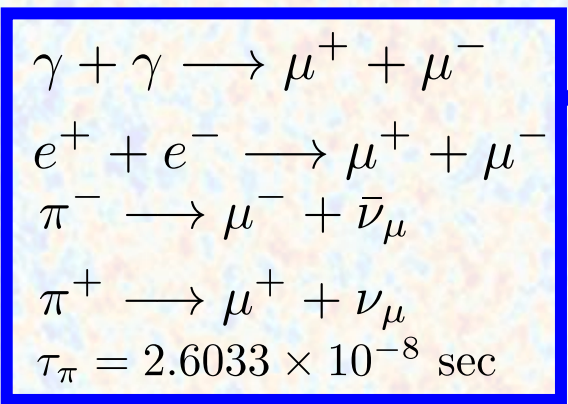
Motivation:

$$\tau_{K^\pm} = 1.238 \times 10^{-8} \text{sec}$$



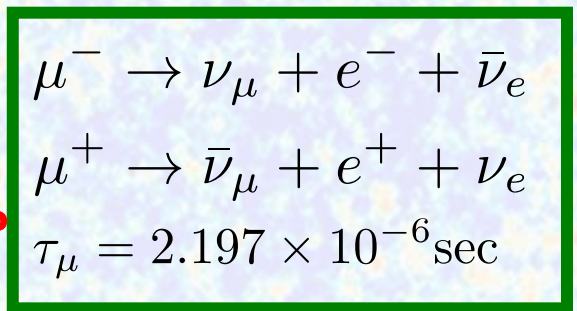
The muon abundances allow detailed-balance back-reactions to influence strangeness abundance.

Muon Production



Do muon abundances still retain their chemical equilibrium? If so, how long?

Muon Decay

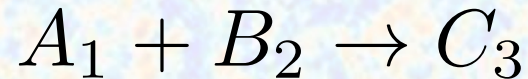


J. Rafelski and C.T. Yang, Acta Phys. Polon. B 52, 277 (2021)

We thus must establish the range of temperature in which production processes exceed in speed the decay process that keep muons remain in abundance (chemical) equilibrium

Particle production rate

In a dense and high temperature thermal ambient phase particles A_1 and B_2 are present, and the **inverse decay reaction** can occur to produce the particle:



- In general, the **thermal reaction rate per time and volume for two body to n final-state particles reaction $1+2 \rightarrow n$** can be written as

$$R_{12 \rightarrow n} = \frac{g_1 g_2}{(2\pi)^5} \frac{T}{1 + I} \frac{|\mathcal{M}_{12 \rightarrow n}|^2}{(2\pi)^{3n-3}} \int_{s_{th}}^{\infty} ds \sqrt{s} \text{IMS}(s; 2) \text{IMS}(s; n) K_1(\sqrt{s}/T).$$

$$\text{IMS}(s; 2) = \frac{\pi}{2} \frac{\sqrt{[s - (m_1 + m_2)^2][s - (m_1 - m_2)^2]}}{s} \quad \text{IMS}(s; n) = \int \prod_{i=1}^n d^4 p_i \delta_0(p_i^2 - m_i^2) \delta^4 \left(p_1 + p_2 - \sum_i^n p_i \right)$$

P.Koch, B.Muller and J.Rafelski, 'Strangeness in Relativistic Heavy Ion Collisions', Phys. Rept. 142 167-262 (1986)

- In order to compare the reaction time with Hubble time $1/H$, it is also convenient to define the relaxation time as follow

Relaxation time

$$\tau_{12 \rightarrow 3} \equiv \frac{n_1^{eq}}{R_{12 \rightarrow 3}}$$

Muon persistence temperature

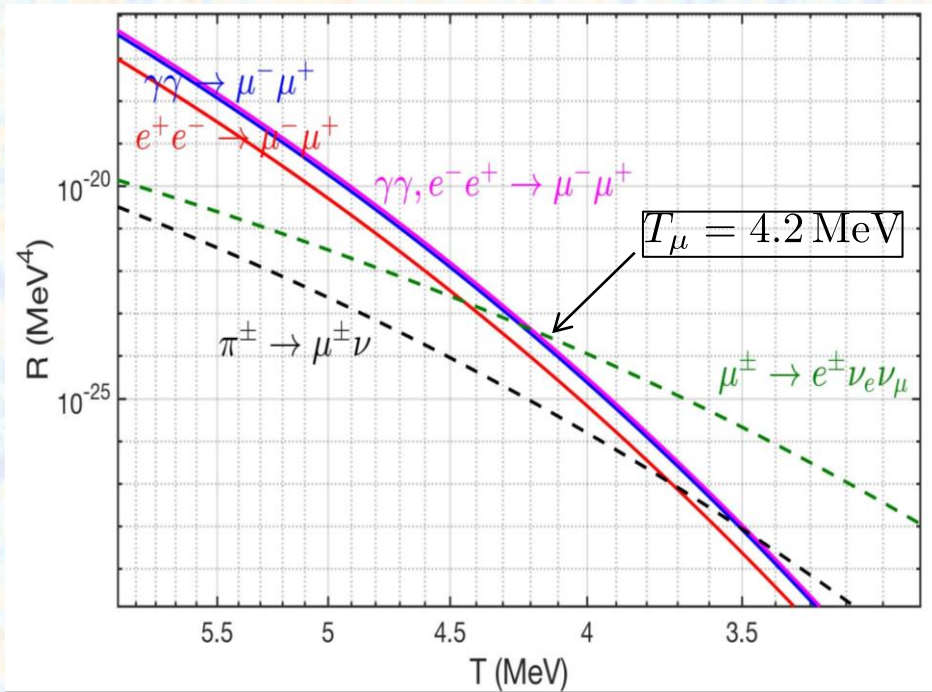
The thermal reaction rate per time and volume for two particles scattering and decay in Boltzmann approximation:

$$R_{a\bar{a} \rightarrow b\bar{b}} = \frac{g_a g_{\bar{a}}}{1 + I} \frac{T}{32\pi^4} \int_{s_{th}}^{\infty} ds \frac{s(s - 4m_a^2)}{\sqrt{s}} \sigma_{a\bar{a} \rightarrow b\bar{b}} K_1(\sqrt{s}/T)$$

$\sigma_{a\bar{a} \rightarrow b\bar{b}}$ = cross section for the reaction $a\bar{a} \rightarrow b\bar{b}$

$$R_c = \frac{g_c}{2\pi^2} \left(\frac{T^3}{\tau_c}\right) \left(\frac{m_c}{T}\right)^2 K_1(m_c/T)$$

τ_c = lifespan of particle c



- As the temperature decreases in the expanding Universe, the muon abundance disappears as soon as any decay rate is faster than the fastest production rate.
- Specifically, after the Universe cools below the temperature $T_\mu = 4.2 \text{ MeV}$, the dominant reaction is the muon decay.

Muons persist in abundance (chemical) equilibrium established predominantly by electromagnetic and weak interaction processes until $T = 4.2 \text{ MeV}$

Surprising coincidence: Muons disappeared when their density matched the density of baryons.

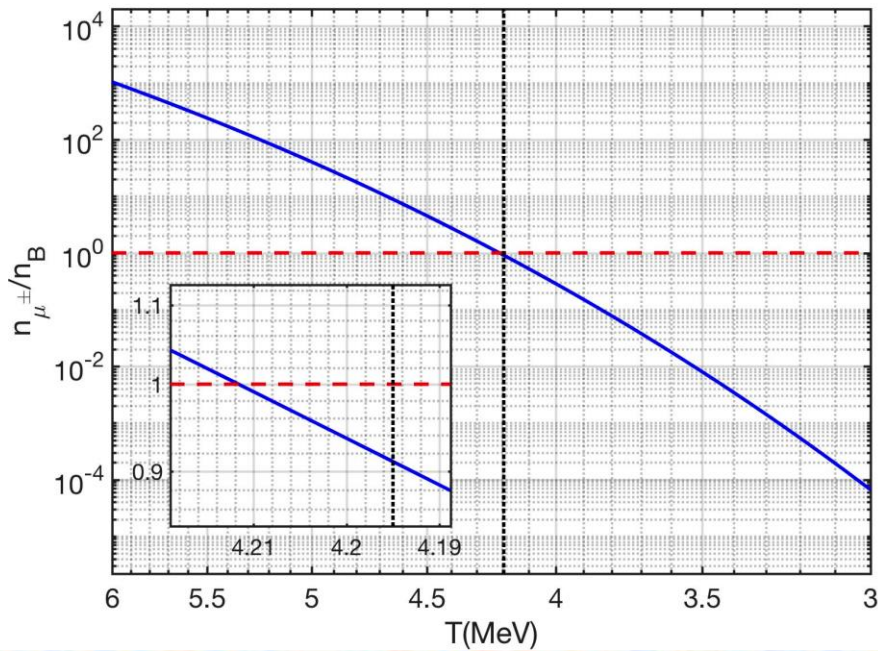
Using constant baryon-per-entropy ratio, the density between muon and baryon can be written as

$$\frac{n_{\mu^\pm}}{n_B} = \frac{n_{\mu^\pm}}{s} \frac{s}{n_B} = \frac{n_{\mu^\pm}}{s} \left(\frac{s_{\gamma e} (1 + s_\nu / s_{\gamma e})}{n_B} \right)_{t_0}$$

$$(n_B - n_{\bar{B}}) / n_\gamma = (0.609 \pm 0.06) \times 10^{-9} (\text{CMB})$$

$$s = \frac{2\pi^2}{45} g_*^s T^3$$

$$n_{\mu^\pm} = \frac{g_{\mu^\pm}}{2\pi^2} T^3 \left(\frac{m_\mu}{T} \right)^2 K_2(m_\mu/T)$$



- This muon-baryon density ratio at persistence temperature:

$$T_\mu = 4.2 \text{ MeV}$$

$$n_{\mu^\pm} / n_B(T_\mu) \approx 0.911$$

- We also find that at the temperature for density ratio is unit

$$T_{\text{equal}} \approx 4.212 \text{ MeV}$$

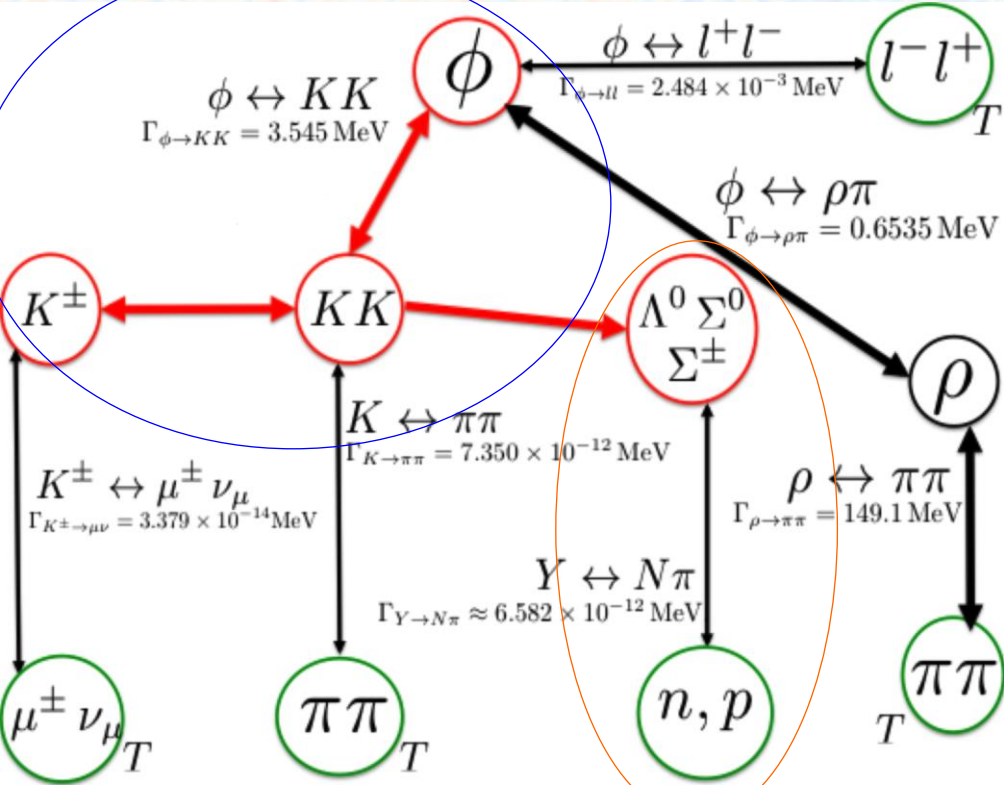
$$n_{\mu^\pm} / n_B(T_{\text{equal}}) = 1$$

This could be numerical coincidence, or a consequence of unknown physics.

Module 6: Kinetic theory of hadronic strangeness

We characterize the number of strange quark $s = \bar{s}$ abundance in the early Universe. The strange quark abundance is equal to the sum of strange baryons and strange mesons. Based on low T reaction rates, we can focus attention onto a smaller most relevant reaction system:

Strangeness in mesons



Strangeness in hyperons

- Below $T = 55 \text{ MeV}$ all ρ created can convert faster to ϕ than they are resupplied, and ϕ will break out into kaons which populate hyperons.
- ρ abundance is controlled by the production and decay rates \rightarrow **dynamic abundance**
- Pions retain their chemical equilibrium until $T = 5 \text{ MeV}$.

I. Kuznetsova, D.Habs and J.Rafelski Phys. Rev. D 78, 014027 (2008)

Strangeness creation/annihilation in mesons

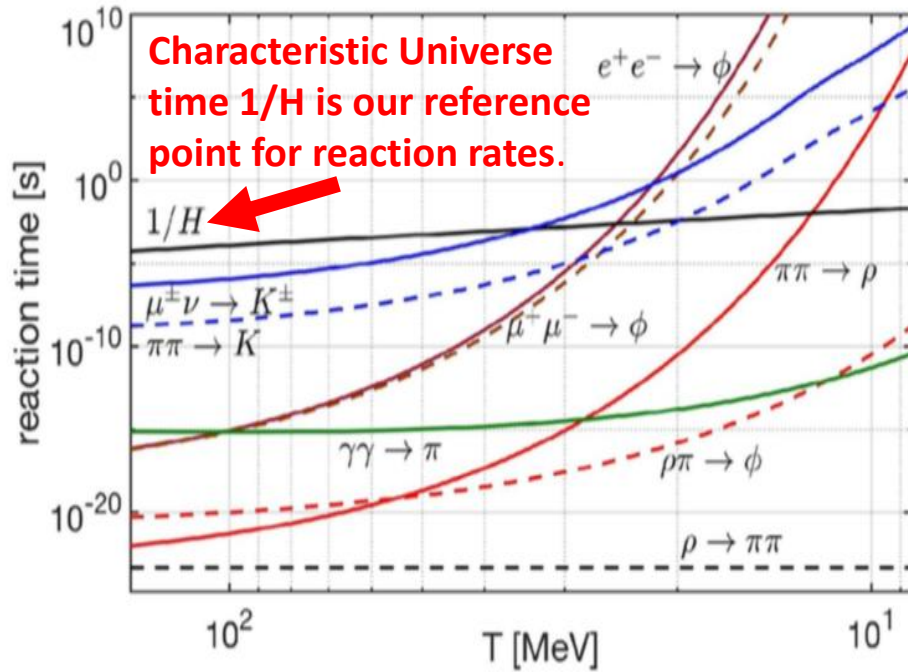


Table 1: For a sample of values of temperature T we show the characteristic Universe time constant $H^{-1} = \dot{a}/a$, the age of hadron phase t_h , and the number N of e-folds.

T [MeV]	H^{-1} [s]	t_h [s]	N [e-folds]
150	4.51×10^{-5}	0	0
100	1.14×10^{-4}	3.45×10^{-5}	0.46
50	5.07×10^{-4}	2.31×10^{-4}	1.21
10	1.49×10^{-2}	7.44×10^{-3}	2.90
5	5.90×10^{-2}	2.95×10^{-2}	3.59

Definition of N-folding:

$$\frac{a(t_f)}{a(t_i)} = e^N \longrightarrow N \equiv \ln \left(\frac{a(t_f)}{a(t_i)} \right) = \int_{t_i}^{t_f} H dt$$

Freeze-out Condition:

$$\tau_{12 \rightarrow 3}(T_f) = 1/H(T_f)$$

Below $T=55\text{MeV}$ all ρ created can convert faster to ϕ than they are resupplied, and ϕ will break out into kaons which populate hyperons.

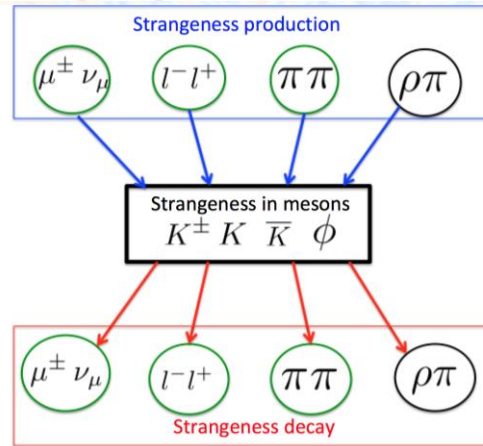


Table 2: The characteristic strangeness reaction and their freezeout temperature and temperature width in early Universe.

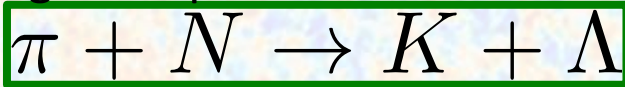
Reactions	Freezeout Temperature (MeV)	ΔT_f (MeV)
$\mu^\pm \nu \rightarrow K^\pm$	$T_f = 33.8 \text{ MeV}$	3.5 MeV
$e^+ e^- \rightarrow \phi$	$T_f = 24.9 \text{ MeV}$	0.6 MeV
$\mu^+ \mu^- \rightarrow \phi$	$T_f = 23.5 \text{ MeV}$	0.6 MeV
$\pi\pi \rightarrow K$	$T_f = 19.8 \text{ MeV}$	1.2 MeV
$\pi\pi \rightarrow \rho$	$T_f = 12.3 \text{ MeV}$	0.2 MeV

Once the reactions decouple from the cosmic plasma, the corresponding detailed balance can be broken and the inverse decay reactions are acting like a "hole" in the strangeness abundance "pot".

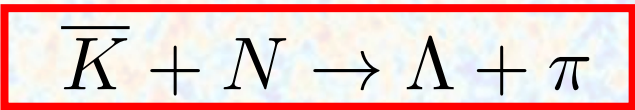
Strangeness production/exchange in hyperons

We now consider the strangeness production reaction, the strangeness exchange reaction; and the strangeness decay in the universe

Strangeness production reaction



Strangeness exchange reaction

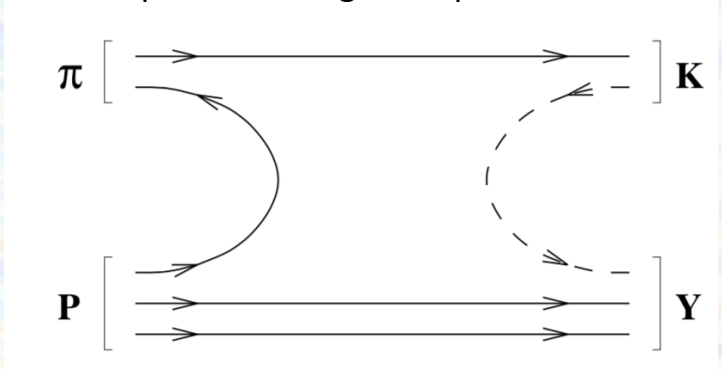


Strangeness decay

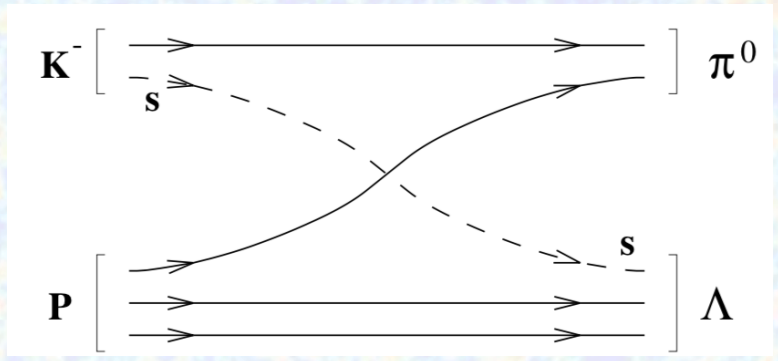


These reactions allow strange hyperons and anti hyperons to influence the dynamic nonequilibrium condition including development of $\langle s - \bar{s} \rangle = 0$

An example of a strangeness-production:



An example of a strangeness-exchange reaction



Strangeness reaction rate with hyperons

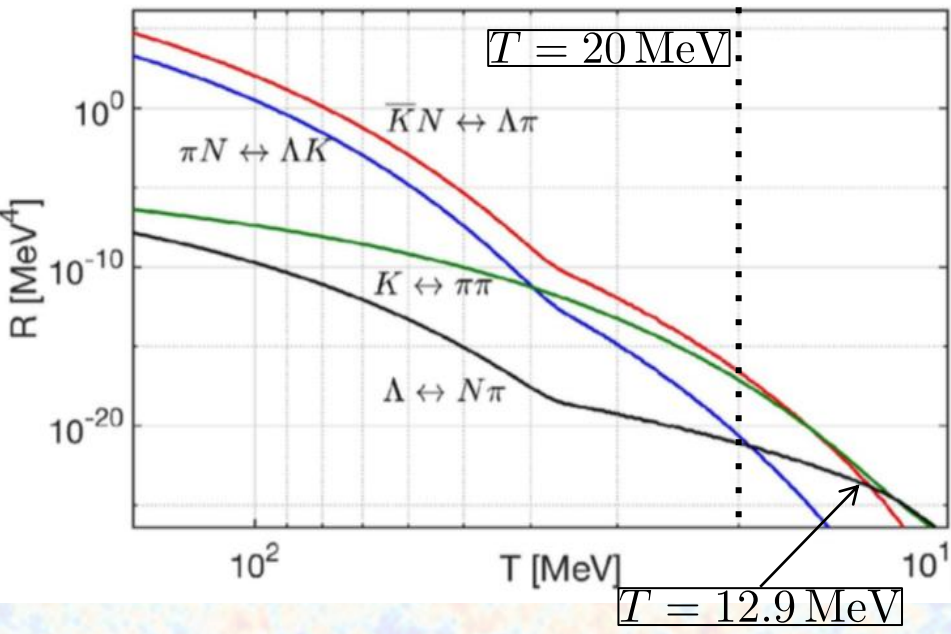
In general, to evaluate the reaction rate per volume in two-body reaction $1 + 2 \rightarrow 3 + 4$ in the Boltzmann approximation we can use reaction cross section and the relation:

$$R_{12 \rightarrow 34} = \frac{g_1 g_2}{32\pi^4} \frac{T}{1 + I_{12}} \int_{s_{th}}^{\infty} ds \sigma(s) \frac{[2 - (m_1 + m_2)^2] [2 - (m_1 - m_2)^2]}{\sqrt{s}} K_1(\sqrt{s}/T),$$

The cross section can be estimated base on experiments

$$\sigma_{\pi N \rightarrow K \Lambda} = \frac{1}{4} \times \sigma_{\pi p \rightarrow K^0 \Lambda} \approx 0.1 \text{mb} \quad \sigma_{\bar{K} N \rightarrow \Lambda \pi} = \frac{1}{2} (\sigma_{K^- p \rightarrow \Lambda \pi^0} + \sigma_{K^- n \rightarrow \Lambda \pi^-}) \approx 1 \sim 3 \text{mb}$$

P.Koch, B.Muller and J.Rafelski, 'Strangeness in Relativistic Heavy Ion Collisions', Phys. Rept. 142} 167-262 (1986)

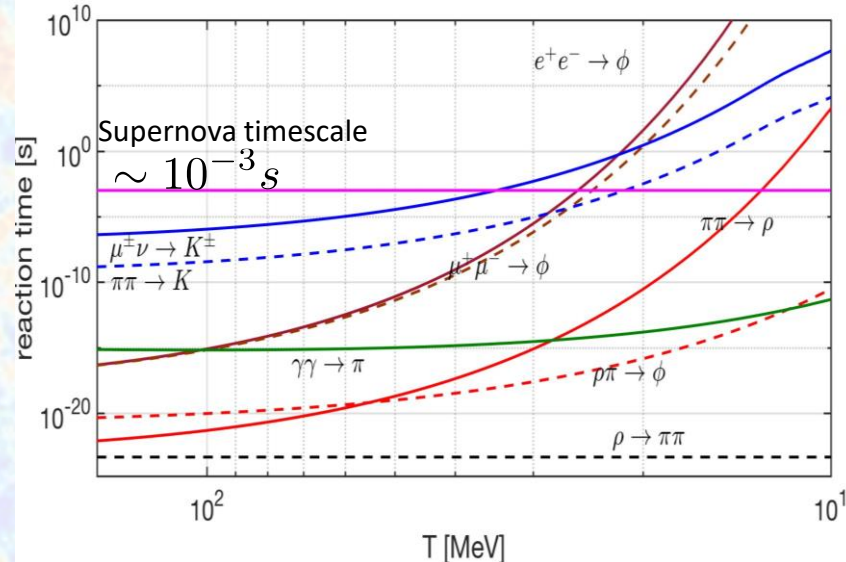



- **For $T < 20 \text{ MeV}$ we have $s = \bar{s}$:**
The reactions for the hyperon Λ production is dominated by $\bar{K} + N \leftrightarrow \Lambda + \pi$. Both strangeness and anti-strangeness disappear from the Universe via the reactions $\Lambda \rightarrow N + \pi$ and $K \rightarrow \pi + \pi$,
- **For $T = 12.9 \text{ MeV}$, we have $s \gg \bar{s}$:**
The dominant reaction is $\Lambda \leftrightarrow N + \pi$, which shows that at a lower temperature we still have (very little) strangeness remnant in the Λ

Where else is strangeness content dynamic?

Our results presented so far depend on the baryon-per-entropy ratio and the chemical potential during the Universe's evolution. **But these techniques are also relevant to astrophysical systems where the strangeness content in dense baryonic matter is dynamic:**

- Supernova explosions
- Strangeness formation quark star cores






Contents lists available at [ScienceDirect](https://www.sciencedirect.com)

Physics Letters B

www.elsevier.com/locate/physletb



Is the remnant of GW190425 a strange quark star?

J. Sedaghat^a, S.M. Zebarjad^{a,b}, G.H. Bordbar^{a,c}, B. Eslam Panah^{d,e,f,*}, R. Moradi^{f,g}

^a Department of Physics, Shiraz University, Shiraz 71454, Iran
^b Department of Physics, University of California at San Diego, La Jolla, CA 92093, USA
^c Department of Physics and Astronomy, University of Waterloo, 200 University Avenue West, Waterloo, Ontario N2L3G1, Canada
^d Sciences Faculty, Department of Physics, University of Mazandaran, P. O. Box 47415-416, Babolsar, Iran
^e ICRANet-Mazandaran, University of Mazandaran, P. O. Box 47415-416, Babolsar, Iran
^f ICRANet, Piazza della Repubblica 10, I-65122 Pescara, Italy
^g ICRA, Dipartimento di Fisica, Universit'a di Roma "La Sapienza", Piazzale Aldo Moro 5, I-00185 Roma, Italy

ARTICLE INFO

Article history:
 Received 9 June 2022
 Received in revised form 12 August 2022
 Accepted 15 August 2022
 Available online 18 August 2022
 Editor: J.-P. Blaizot

ABSTRACT

This study investigates the effects of different QCD models on the structure of strange quark stars (SQS). In these models, the running coupling constant has a finite value in the infrared region of energy. By imposing some constraints on the strange quark matter (SQM) and exploiting the analytic and background perturbation theories, the equations of states for the SQM are obtained. Then, the properties of SQSs in general relativity are evaluated. By using component masses of GW190425 [1] as well as some conversion relations between the barvonic mass and the gravitational mass, the remnant mass of

Special topic: Heavy quarks

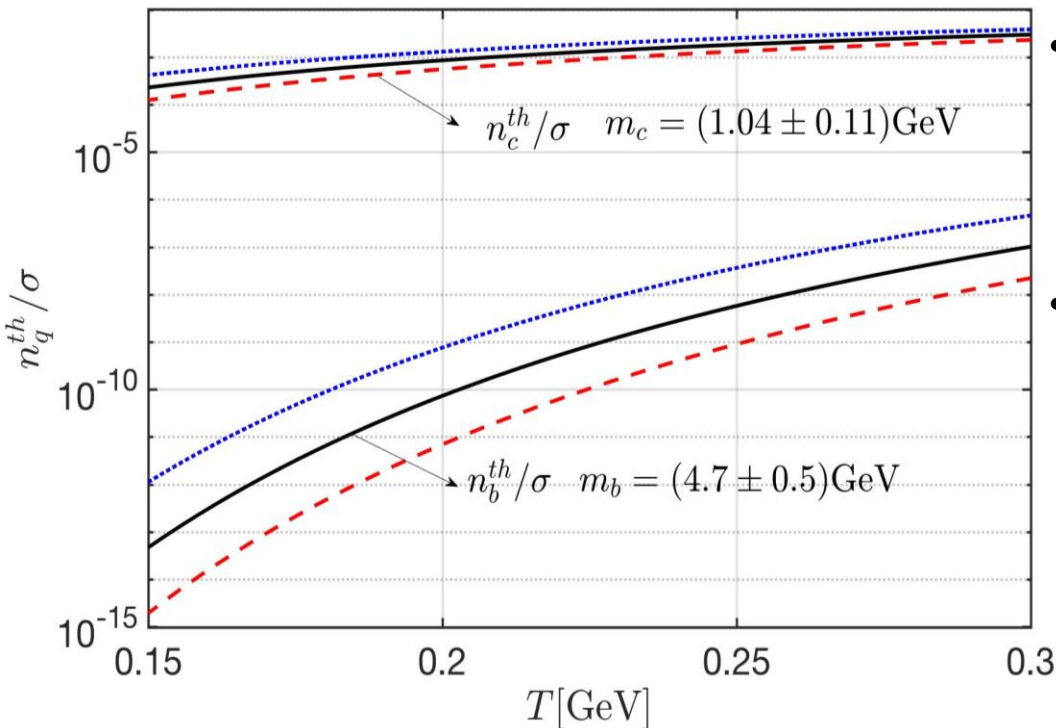
Bottom heavier than baryons – **Origin of baryogenesis?**

(Heavy) Quark Universe: Charm and Bottom Freeze-out

Experimentally accessible thermal temperature range

Thermal equilibrium abundance for charm and bottom

(Comparison to the Universe entropy density)



- The charm abundance is $10^4 \sim 10^9$ time greater than the bottom quarks in the temperature range $0.15 < T < 0.3$ GeV.

- This implies that the small bottom quark abundance is embedded in a large background comprising all lighter quarks (u, d, s, c) and antiquarks, as well as gluons.

Heavy quark dynamics with Tsallis statistics in thermal QGP

We have shown that thermalization of charmed quarks in a quark-gluon plasma by collisional processes on light quarks and gluons leads to a spectral shape well parameterized by the two parameter **Tsallis distribution**, and we have determined the pertinent spectral parameters for the published microscopic drag/diffusion coefficients.

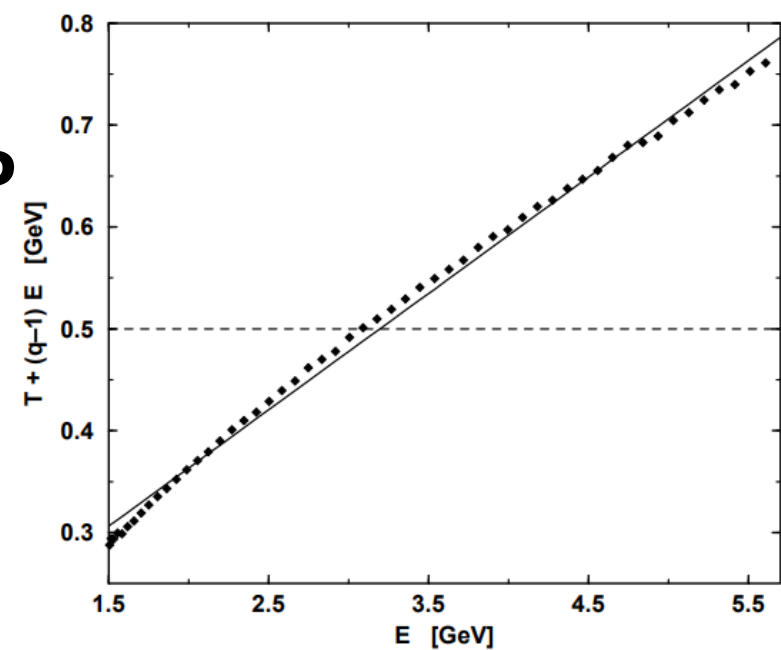


FIG. 1. Calculated data (diamonds) and linear fit for the ratio in Eq. (25) for a charmed quark $m_c = 1.5$ GeV thermalizing in gluon background at $T_b = 500$ MeV. Dashed line: result expected for a Boltzmann-Jüttner distribution, $T = T_b$.

VOLUME 84, NUMBER 1 PHYSICAL REVIEW LETTERS

3 JANUARY 2000

Equilibrium Distribution of Heavy Quarks in Fokker-Planck Dynamics

D. Brian Walton^{1,*} and Johann Rafelski^{2,†}

¹*Program in Applied Mathematics, University of Arizona, Tucson, Arizona 85721*

²*Physics Department, University of Arizona, Tucson, Arizona 85721*

(Received 8 July 1999)

We obtain an explicit generalization, within Fokker-Planck dynamics, of Einstein's relation between drag, diffusion, and the equilibrium distribution for a spatially homogeneous system, considering both the transverse and longitudinal diffusion for dimension $n > 1$. We provide a complete characterization of the equilibrium distribution in terms of the drag and diffusion transport coefficients. We apply this analysis to charm quark dynamics in a thermal quark-gluon plasma for the case of collisional equilibration.

PACS numbers: 12.38.Mh, 05.10.Gg, 25.75.-q



Brian Walton

Bottom quark production/decay

In the primordial QGP, the bottom quarks can be produced via the strong interaction gluon/quark pair fusion processes and disappear via the weak interaction decay .

Production

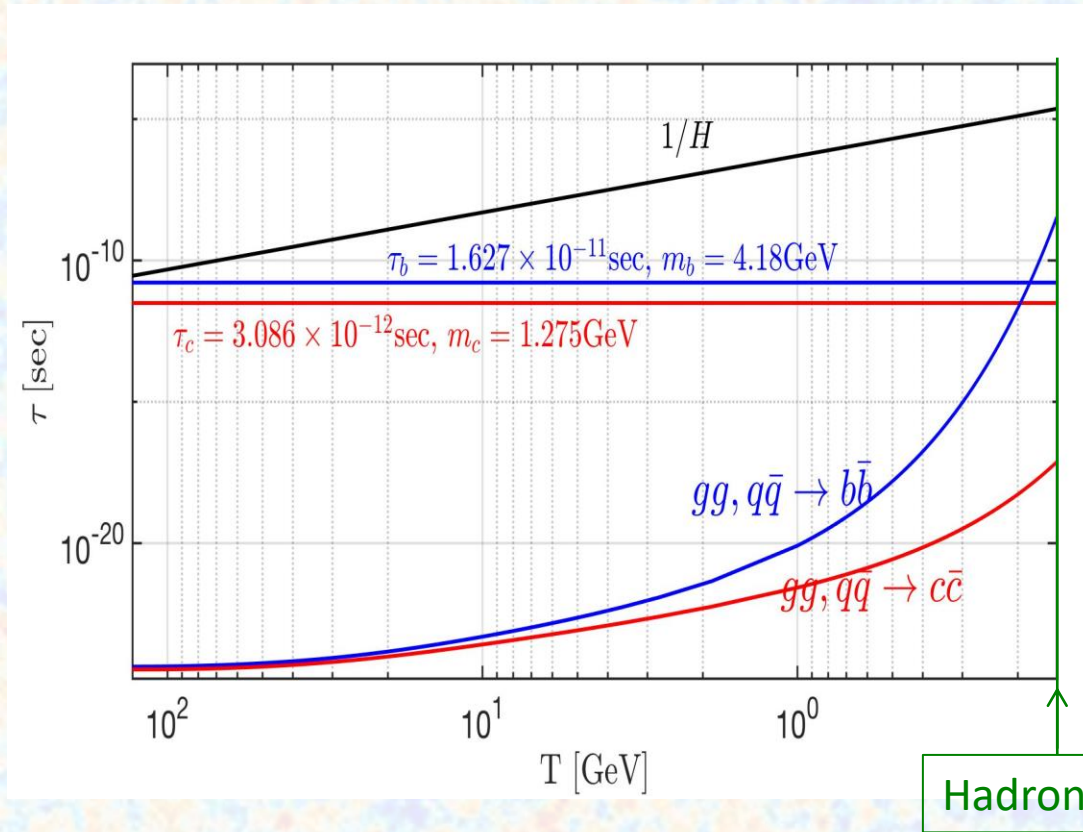
$$q + q \longrightarrow b + \bar{b}, c + \bar{c}$$

$$g + g \longrightarrow b + \bar{b}, c + \bar{c}$$

Decay

$$b \longrightarrow c + l + \nu_l, \quad b \longrightarrow c + q + \bar{q}$$

$$c \longrightarrow s + l + \nu_l, \quad c \longrightarrow s + q + \bar{q}$$



- The relaxation time for b-quark production intersects with b-quark decay at temperature $T=0.18$ GeV.

➔ **Dynamic bottom abundance in QGP**

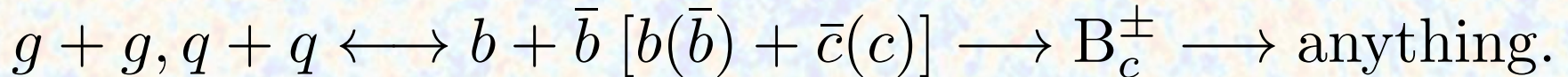
- The relaxation time for c-quark production is faster than the c-quark decay in QGP.

➔ **Charm disappear in the hadronic phase**

Hadronization $T=150$ MeV

Bottom Flavor Abundance Non-equilibrium

The heavy bottom quarks are embedded in a large background comprising all lighter u, d, s, c quarks and antiquarks, and can form the B_c meson via the reaction



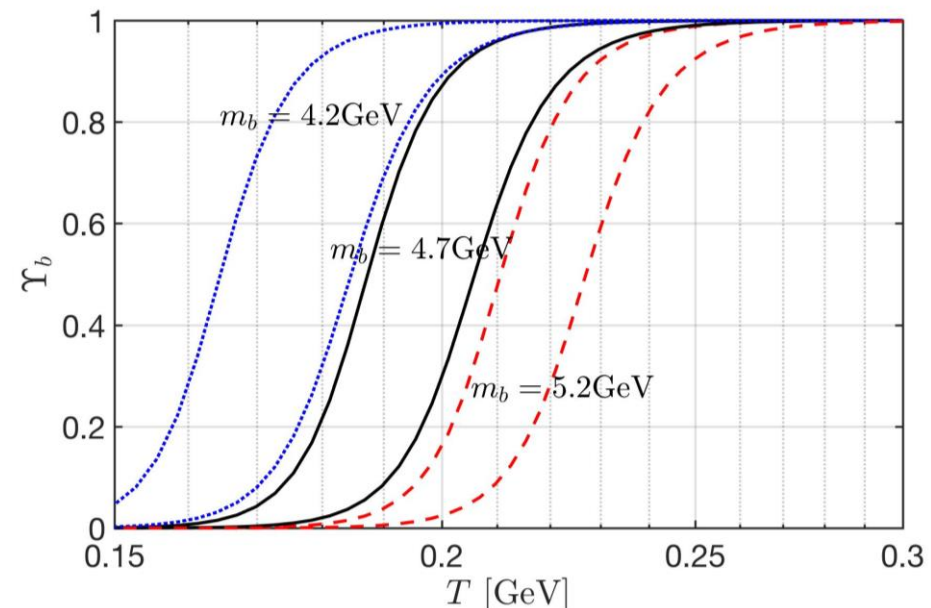
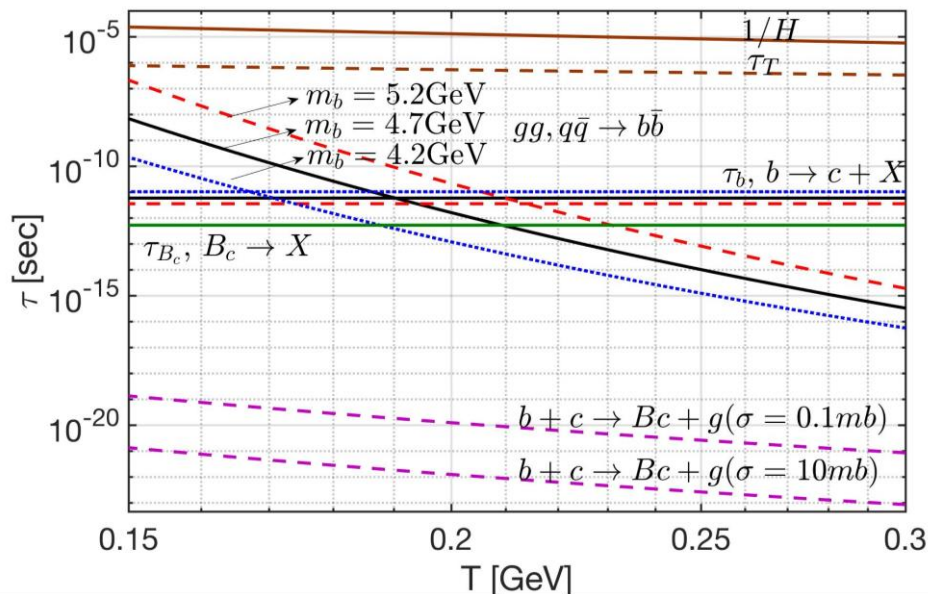
The fugacity equation for b-quark:

$$\frac{d\Upsilon_b}{dt} = (1 - \Upsilon_b^2) \frac{1}{\tau_b^{\text{Source}}} - \Upsilon_b \left(\frac{1}{\tau_b^{\text{Decay}}} + 3H - \frac{1}{\tau_T} \right)$$

Adiabatic approximation

$$\Upsilon_b = \frac{\tau_b^{\text{Source}}}{2\tau_b^{\text{Decay}}} \left[\sqrt{1 + \left(2\tau_b^{\text{Decay}} / \tau_b^{\text{Source}} \right)^2} - 1 \right]$$

Two dominant terms allowing the adiabatic solution



Bottom in QGP: Comparison with Entropy

After formation, the heavy bottom quarks are embedded in a large background comprising all lighter u, d, s, c quarks and antiquarks, and can form the Bc meson.

The number density of Bc meson:

$$n_{B_c} = \Upsilon_b n_b^{th} P_{B_c}$$

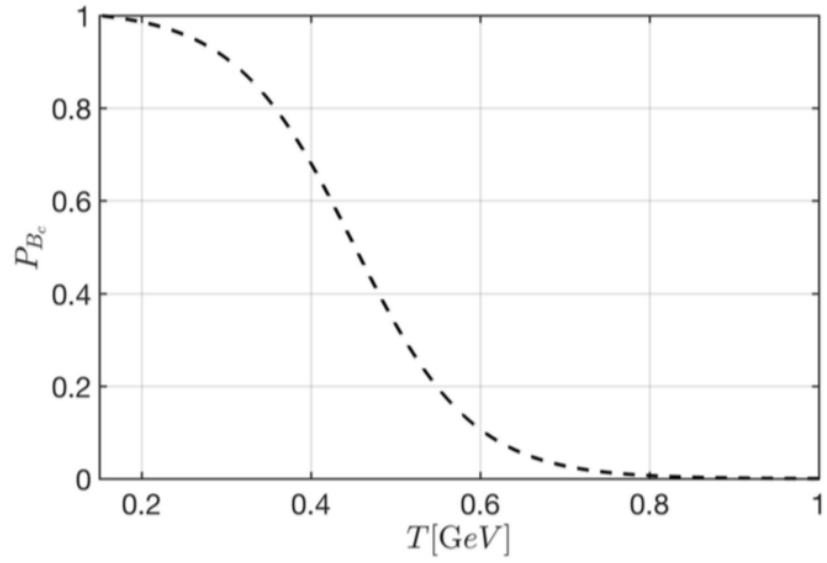
$$n_b^{th} = \frac{g_b}{2\pi^2} T^3 \left(\frac{m_b}{T}\right)^2 K_2(m_b/T)$$

$$\Upsilon_b = \frac{\tau_b^{Source}}{2\tau_b^{Decay}} \left[\sqrt{1 + \left(2\tau_b^{Decay} / \tau_b^{Source}\right)^2} - 1 \right]$$

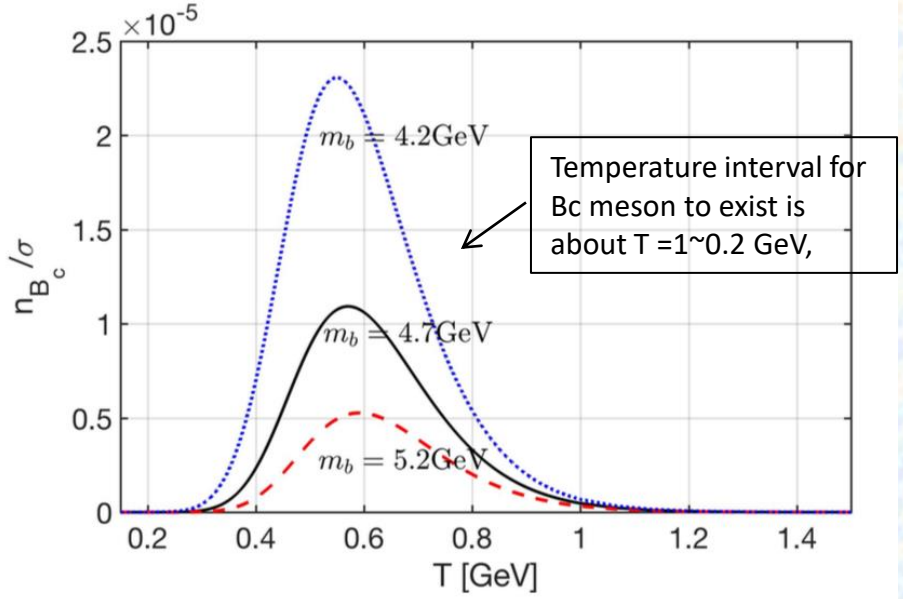
The survival probability of one Bc meson as a function of temperature

$$P_{B_c} = \mathcal{N} \left[1 - \tanh\left(\frac{T - 0.45 \text{ GeV}}{0.14 \text{ GeV}}\right) \right] \quad \mathcal{N} = 0.506882$$

M. Schroedter, R. L. Thews and J. Rafelski, "Bc meson production in nuclear collisions at RHIC," Phys. Rev. C 62, 024905 (2000)



The Bc number density normalized by entropy density



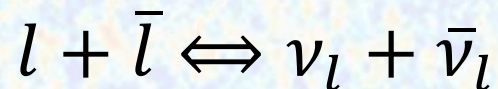
Module 7: Neutrino freeze-out in the Early Universe

In the literature one finds estimates of freeze-out temperatures based on a comparison of Hubble expansion with neutrino scattering length and considering only number changing (i.e. chemical) processes.

We employ a similar definition of freeze-out temperature in the context of the Boltzmann equation and refine the results by noting that there are three different freeze-out processes.

1. Neutrino chemical freeze-out:

At this point, annihilations/ productions cease, and relic population of particles remain.



2. Neutrino kinetic freeze-out:

At that time, elastic scattering processes cease, and the relic particles do not interact with other particles in the primordial plasma anymore.



3. Collisions between neutrinos:

Those collisions are capable of re-equilibrating energy within and between flavor families. **These processes end at a yet lower temperature and the neutrinos will be truly free-streaming from that point on.**

Neutrino decoupling as a function of natural constants

We studied the impact of SM parameter values on the neutrino freeze-out temperature in the Early Universe. In particular, we show the impact of the strength parameters η and $\sin 2\theta_W$ on N_ν .



Available online at www.sciencedirect.com

ScienceDirect



Nuclear Physics B 890 (2015) 481–517

www.elsevier.com/locate/nuclphysb

Relic neutrino freeze-out: Dependence on natural constants

Jeremiah Birrell^{a,b,*}, Cheng Tao Yang^{b,c}, Johann Rafelski^b

^a Program in Applied Mathematics, The University of Arizona, Tucson, AZ 85721, USA

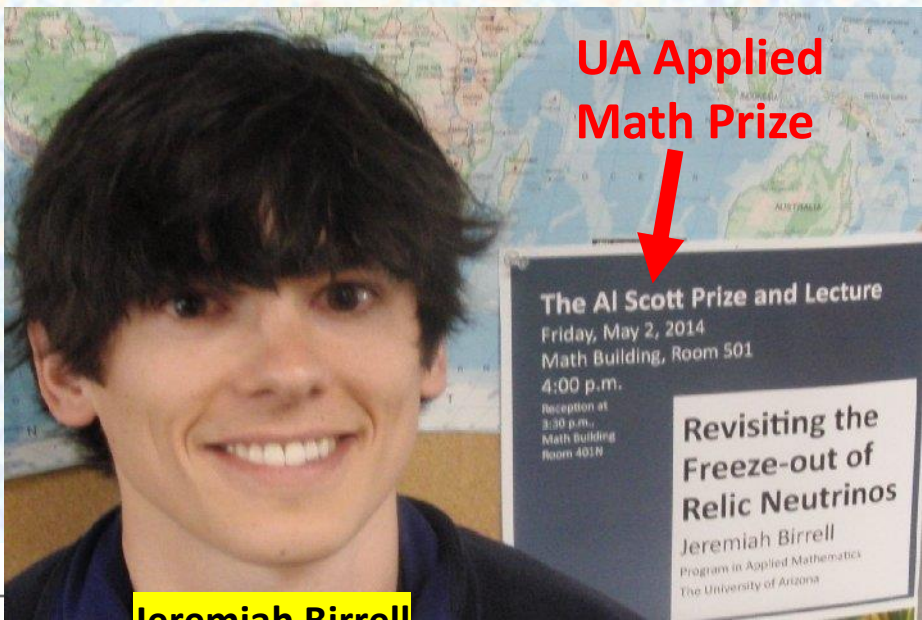
^b Department of Physics, The University of Arizona, Tucson, AZ 85721, USA

^c Department of Physics and Graduate Institute of Astrophysics, National Taiwan University, Taipei, 10617, Taiwan

Received 9 June 2014; received in revised form 2 November 2014; accepted 22 November 2014

Available online 27 November 2014

Editor: Tommy Ohlsson



Jeremiah Birrell

Abstract

Analysis of cosmic microwave background radiation fluctuations favors an effective number of neutrinos, $N_\nu > 3$. This motivates a reinvestigation of the neutrino freeze-out process. Here we characterize the dependence of N_ν on the Standard Model (SM) parameters that govern neutrino freeze-out. We show that N_ν depends on a combination η of several natural constants characterizing the relative strength of weak interaction processes in the early Universe and on the Weinberg angle $\sin^2 \theta_W$. We determine numerically the dependence $N_\nu(\eta, \sin^2 \theta_W)$ and discuss these results. The extensive numerical computations are made possible by two novel numerical procedures: a spectral method Boltzmann equation solver adapted to allow for strong reheating and emergent chemical non-equilibrium, and a method to evaluate Boltzmann equation collision integrals that generates a smooth integrand.

© 2014 The Authors. Published by Elsevier B.V. This is an open access article under the CC BY license (<http://creativecommons.org/licenses/by/3.0/>). Funded by SCOAP³.

Freeze-out dependance on natural constants

Neutrinos could participate in reheating of the Universe if natural constants were different in the Early Universe.

$$\eta \equiv M_p m_e^3 G_F^2,$$

$$M_p^2 \equiv \frac{1}{8\pi G_N},$$

Solving the relativistic Boltzmann equation numerically, we show the impact of the strength parameter η and $\sin 2\theta_W$ on N_ν and neutrino freeze-out temperature

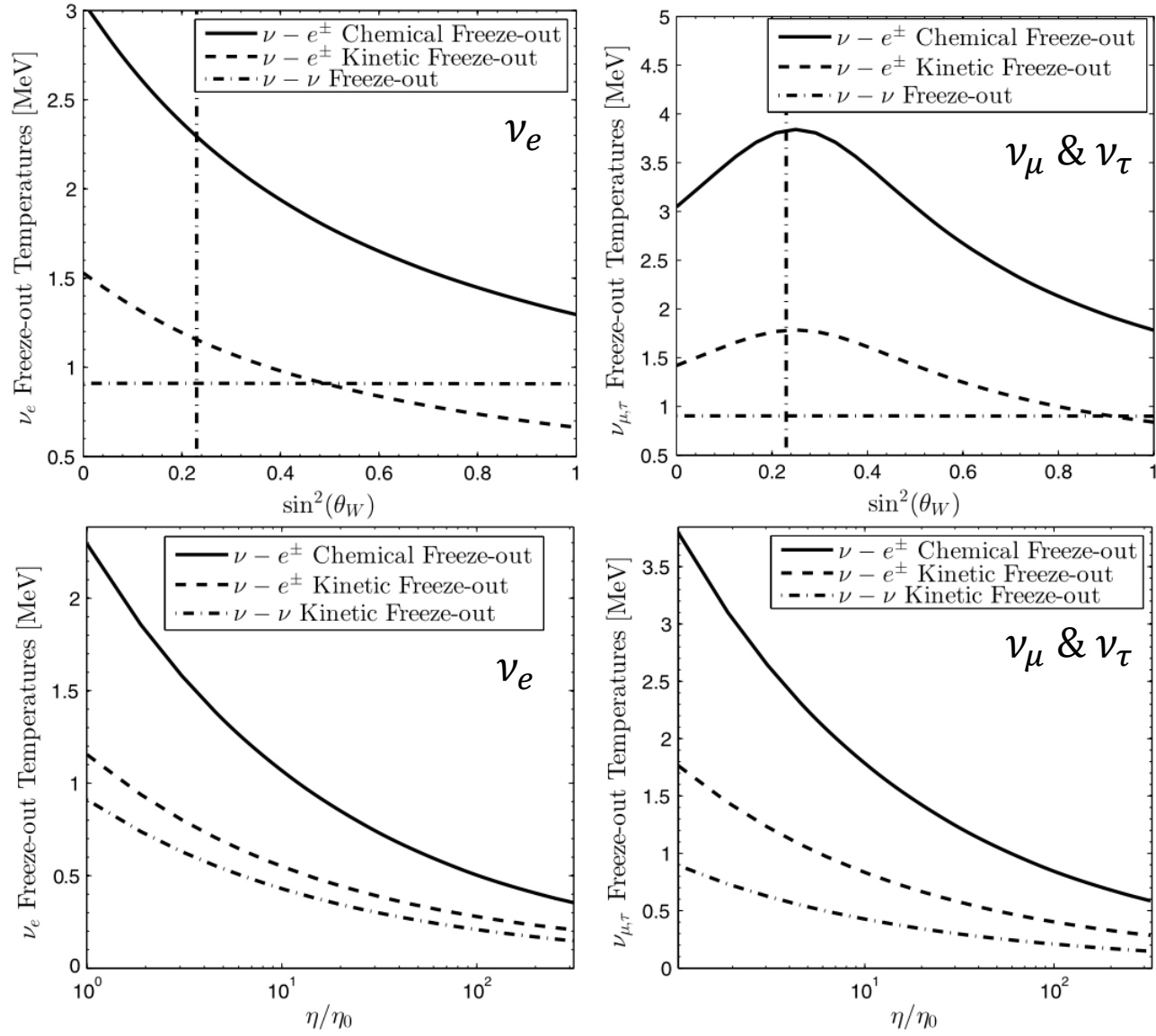


Fig. 3. Freeze-out temperatures for electron neutrinos (left) and μ, τ neutrinos (right) for the three types of processes, see text. Top panels as functions of $\sin^2 \theta_W$ for $\eta = \eta_0$, vertical line is $\sin^2 \theta_W = 0.23$; bottom panels as a function of relative change in interaction strength η/η_0 obtained for $\sin^2 \theta_W = 0.23$.

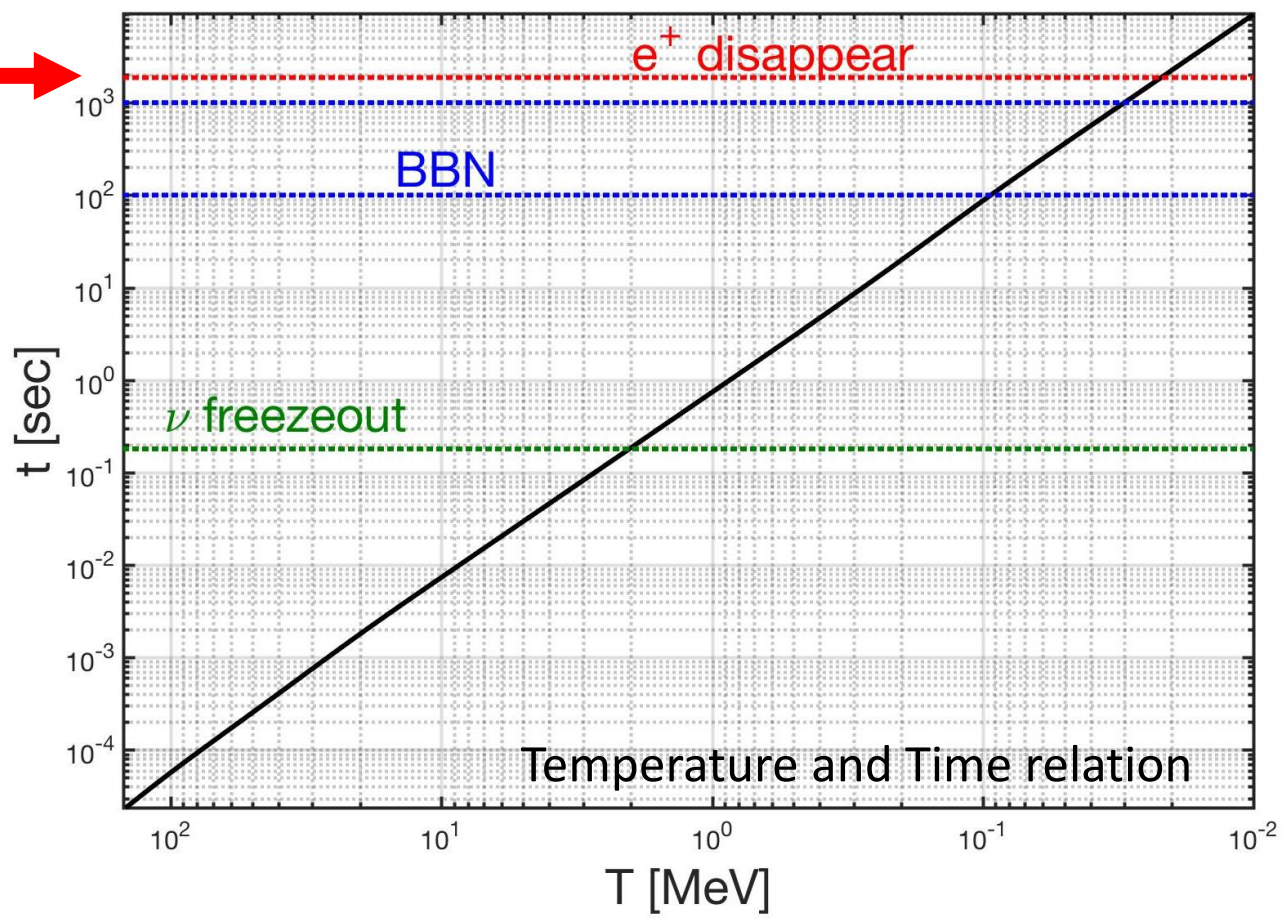
Module 8: Big Bang Nucleosynthesis epoch

Needed connection between time and temperature

There is very little non-equilibria during the Universe's expansion, thus the comoving entropy is practically constant.

$$\frac{d}{dt} (g_*^s T^3 a^3) = 0 \quad \rightarrow \quad 3H + 3\frac{\dot{T}}{T} + \dot{T} \frac{d}{dt} (\ln g_*^s) = 0$$

Despite common assumption, $e^+ e^-$ plasma disappears AFTER BBN.



Standard Model of Big Bang Nucleosynthesis

The Big Bang Nucleosynthesis produce the primordial abundances of the light elements in early universe around the typical temperature $T_{BBN} = 86 - 50 \text{ keV}$

C.Pitrou, A.Coc, J.P.Uzan and E.Vangioni, "Precision big bang nucleosynthesis with improved Helium-4 predictions," Phys. Rept. 754, 1-66 (2018)

Measurements:

$$Y_p = 0.245 \pm 0.003$$

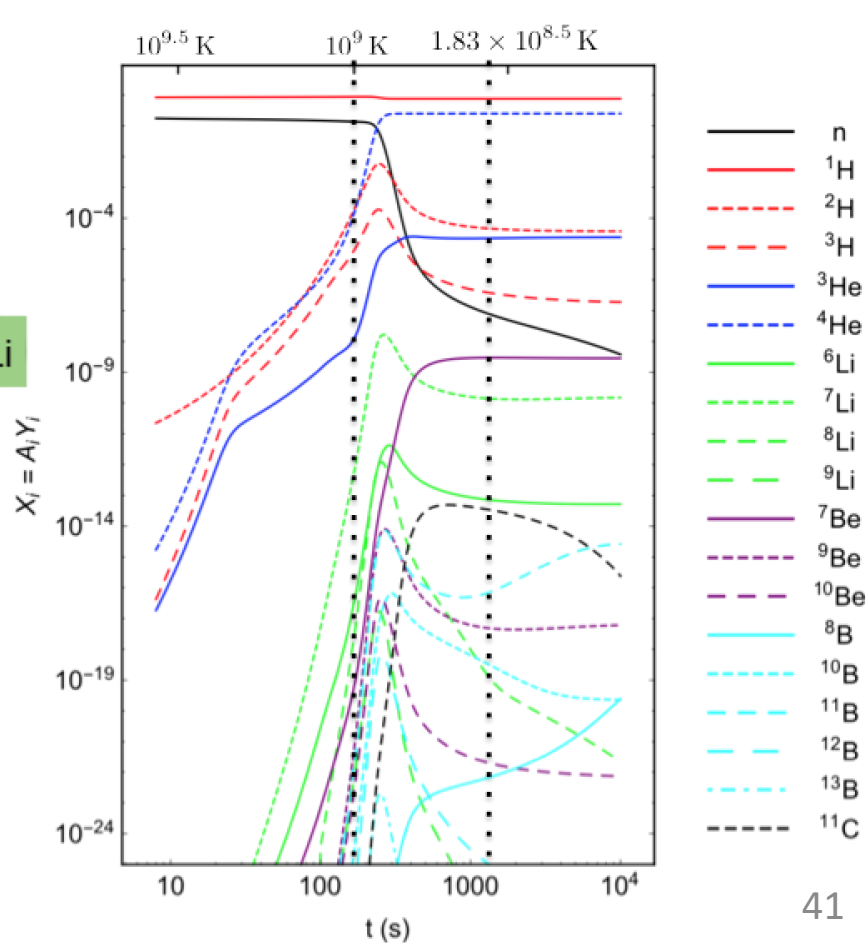
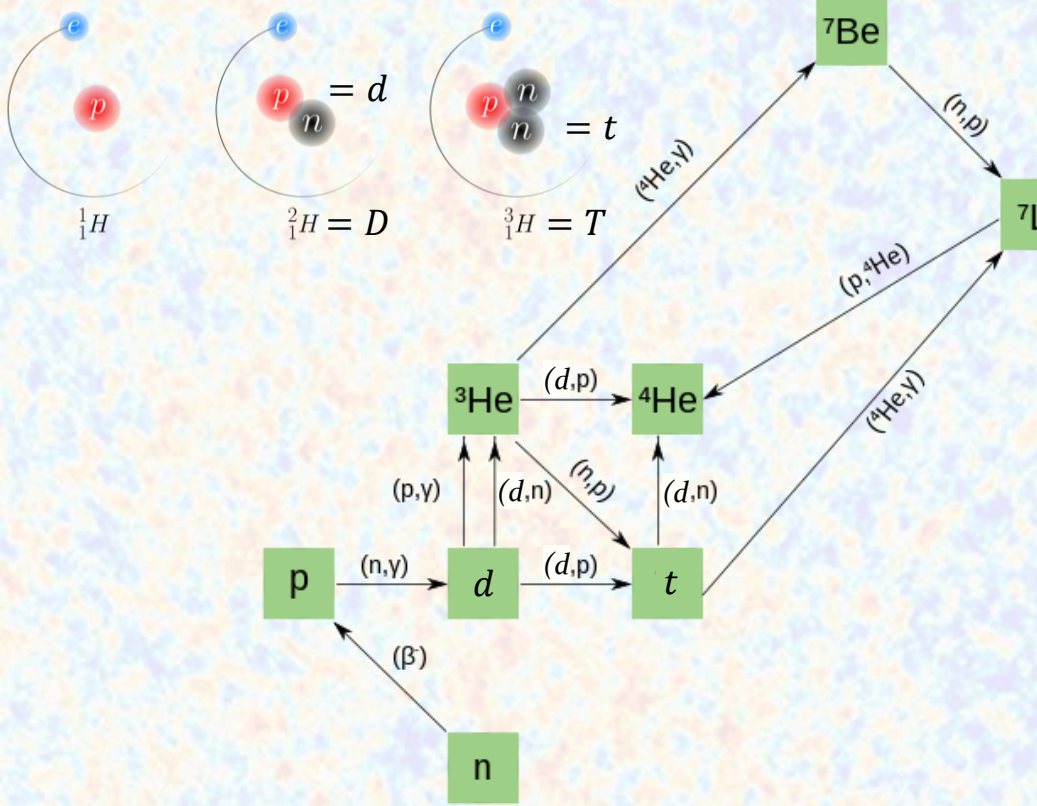
$${}^2\text{H}/\text{H} = (2.569 \pm 0.027) \times 10^{-5}$$

$${}^3\text{He}/\text{H} = (1.1 \pm 0.2) \times 10^{-5}$$

$${}^7\text{Li}/\text{H} = (1.6 \pm 0.3) \times 10^{-10}$$

$$T = 86 \text{ keV} \approx 1 \times 10^9 \text{ K}$$

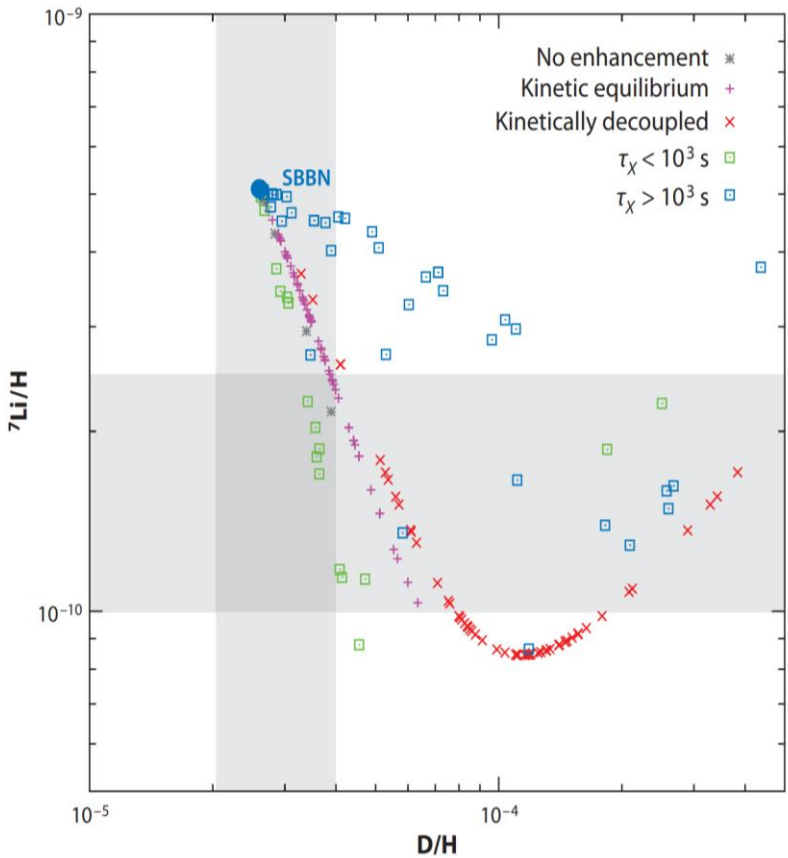
$$T = 50 \text{ keV} \approx 6 \times 10^8 \text{ K}$$



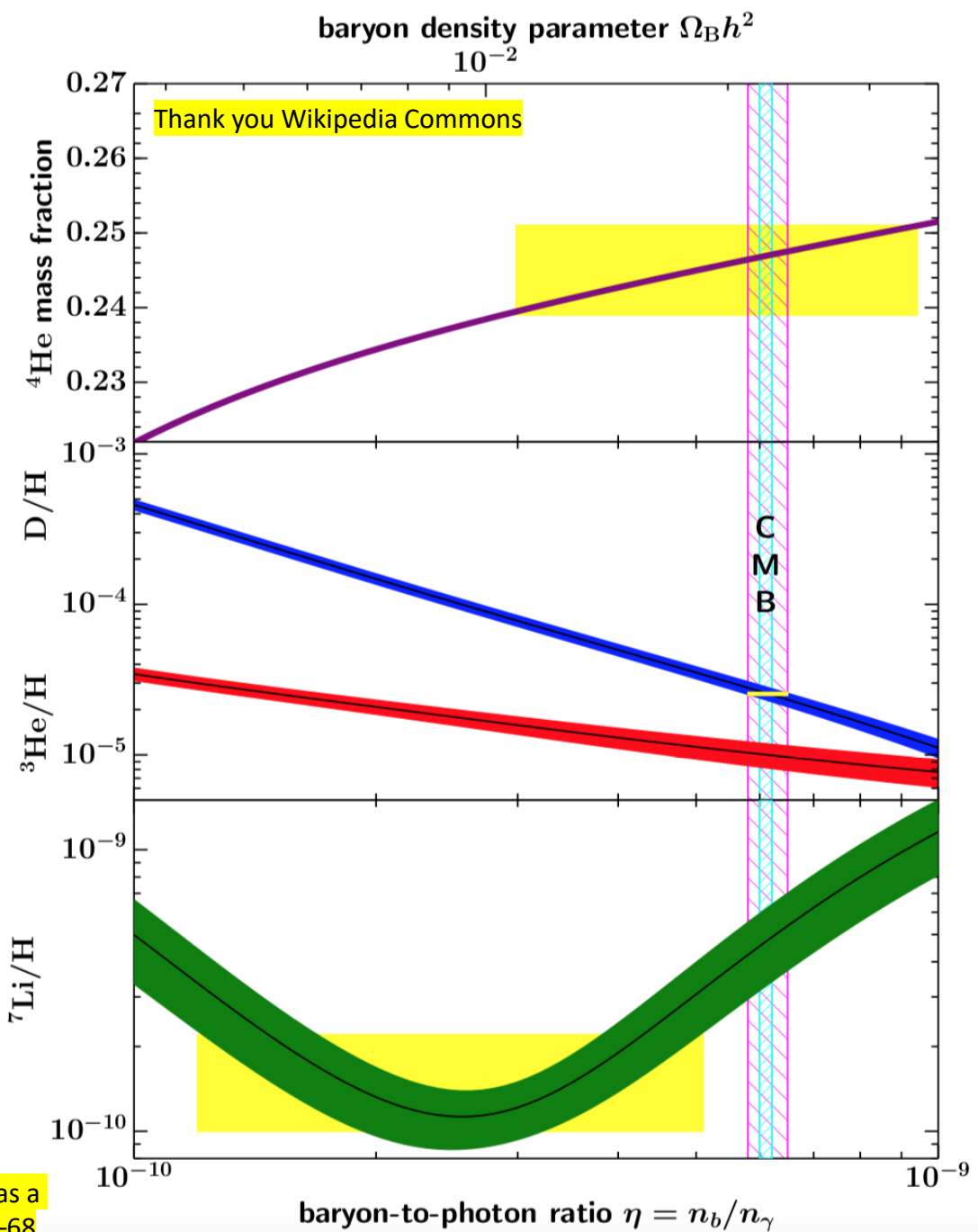
Open problem in BBN

There is a lack of consistency between baryon, lithium, deuterium and helium abundance.

Efforts to reconcile using nuclear reaction rates calculated in vacuum are not successful.



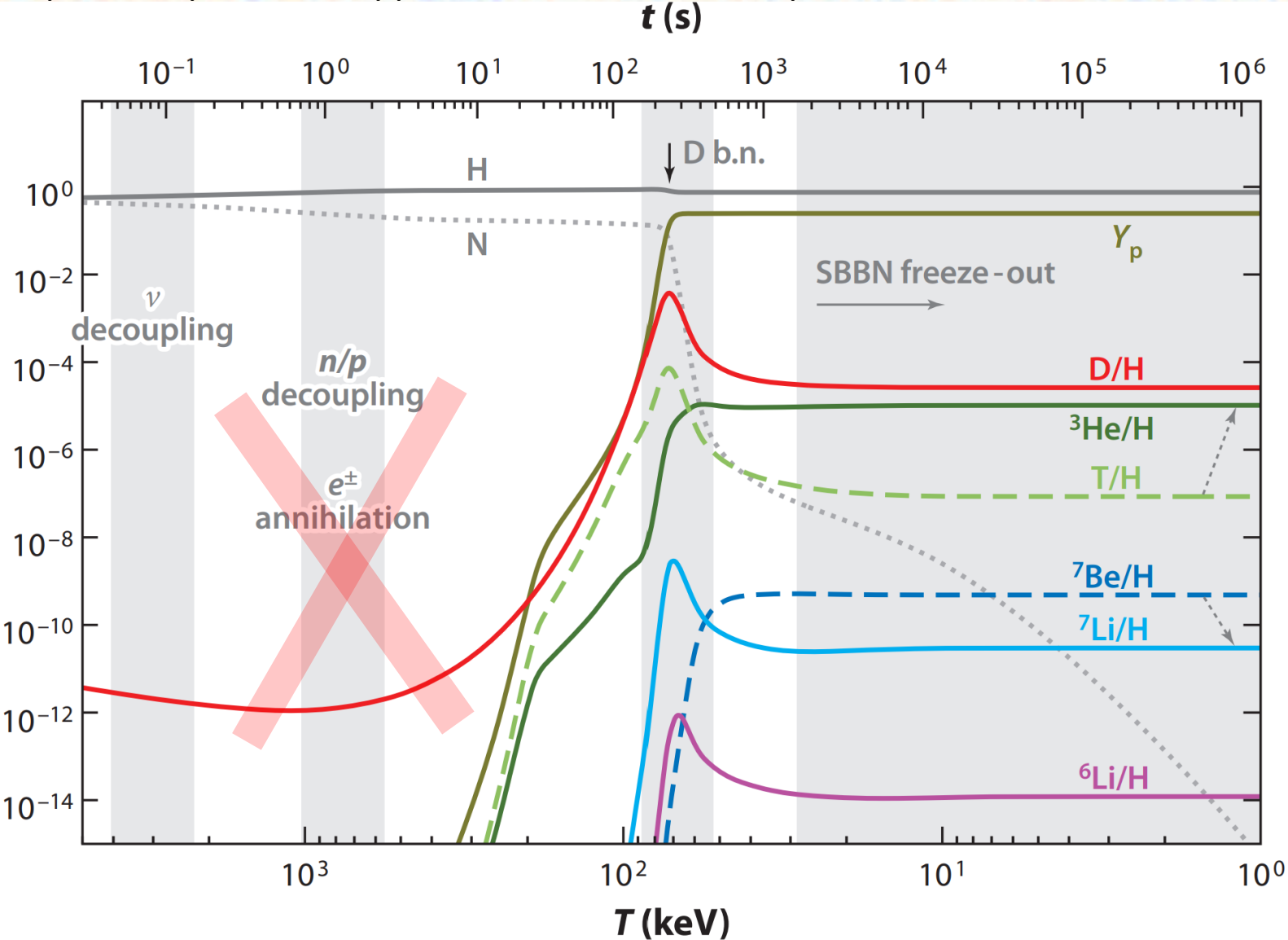
Pospelov, Maxim, and Josef Pradler. "Big bang nucleosynthesis as a probe of new physics." Annu. Rev. Nucl. Part. Sci. 2010. 60:539–68



baryon density parameter $\Omega_B h^2$
 10^{-2}

Open problem in BBN

The origin of the problem is possibly due to the mistaken belief that the electron-positron plasma disappeared before the BBN epoch.



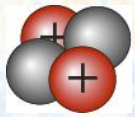
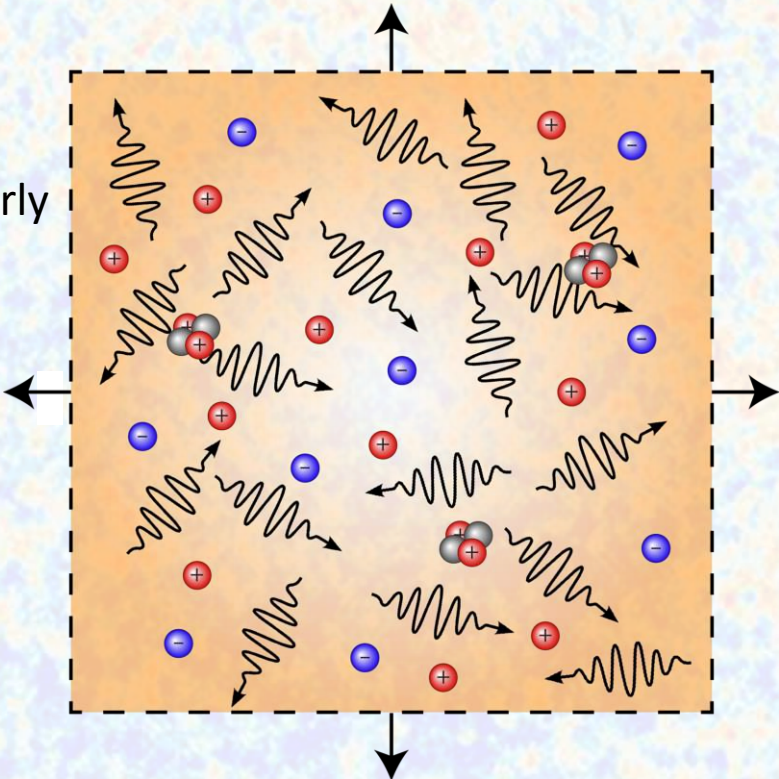
Does $e^+ e^-$ plasma impact BBN in the universe?

Infinite electron-positron photon plasma with electromagnetic perturbations caused by nuclei

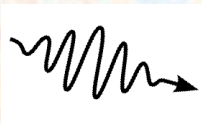
Applying previous quark-gluon-plasma (QGP) oriented work to electron-positron-photon QED plasma in the Early Universe:

Electromagnetic Perturbations $\leftrightarrow e^+ e^- \gamma$ Plasma

In the Early Universe, the standard assumption of a homogenous and infinitely extended plasma applies.



Nuclei



Photons



Positrons & Electrons

When do pairs $e^+ e^-$ disappear? Three principles used to determine the electron chemical potential

Our objective is to explore the dense electron/positron plasma in early universe under the hypothesis **charge neutrality** and **entropy and baryon conservation**

$$(n_B - n_{\bar{B}}) / n_\gamma = (0.609 \pm 0.06) \times 10^{-9} (\text{CMB})$$

$$\frac{n_B - n_{\bar{B}}}{s} = \left(\frac{n_B - n_{\bar{B}}}{s} \right)_{t_0} = \left(\frac{n_B}{s_{\gamma e} (1 + s_\nu / s_{\gamma e})} \right)_{t_0} = (0.865 \pm 0.008) \times 10^{-10}$$

1. Charge neutrality of the Universe:

$$n_e - n_{\bar{e}} = n_p - n_{\bar{p}} \approx n_p,$$

where n_ℓ denotes the number density of particle type ℓ .

2. Total comoving entropy is conserved. At $T \leq T_f$ the dominant contributors to entropy are photons, e^\pm , and neutrinos. In addition, after neutrino freezeout, neutrino comoving entropy is independently conserved. This implies that the combined comoving entropy in γ, e^\pm is also conserved for $T_\gamma \leq T_f$. On the other hand, comoving baryon number is also conserved, hence the ratio n_B/s is conserved, and we have

$$\frac{n_B}{s} = \frac{n_B}{\sum_i s_i} = \text{constant.}$$

$$n_e - n_{\bar{e}} = \frac{n_p}{n_B} \left(\frac{n_B}{s_{\gamma, e, \bar{e}}} \right)$$

$$n_e - n_{\bar{e}} = \frac{g_e}{2\pi^2} \left[\int_0^\infty \frac{p^2 dp}{\exp((E - \mu_e) / T_\gamma) + 1} - \int_0^\infty \frac{p^2 dp}{\exp((E + \mu_e) / T_\gamma) + 1} \right]$$

3. Neutrinos decouple (freeze out) at a temperature $T_f \simeq 2\text{MeV}$, after which they free stream through the Universe with an effective temperature

$$T_\nu(t) = T_f a(t_f) / a(t),$$

where $a(t)$ is the FLRW Universe scale factor.

Dense electron/positron plasma in the BBN epoch

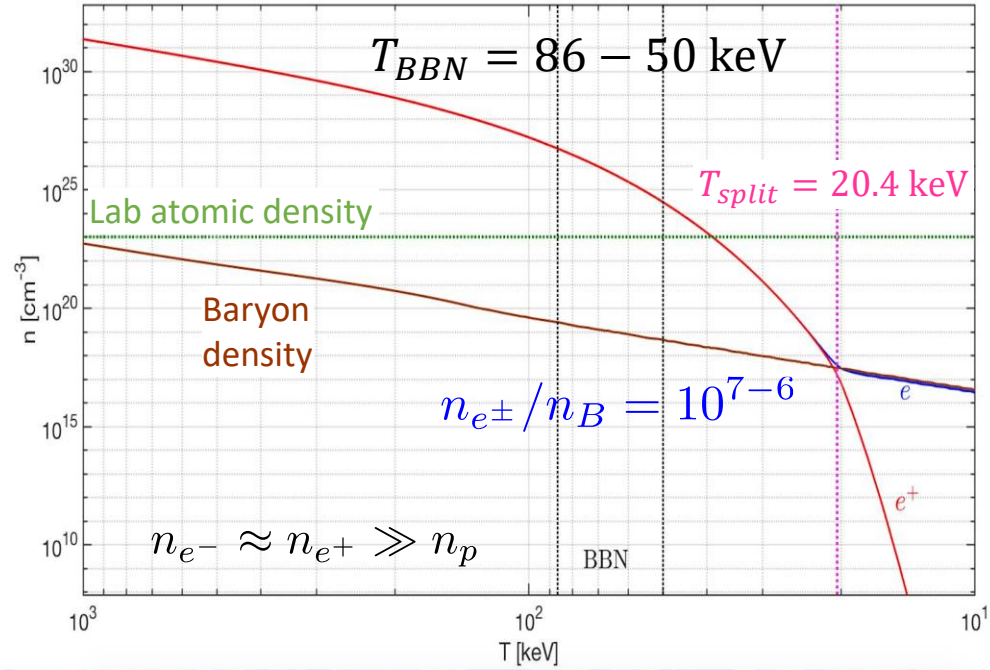
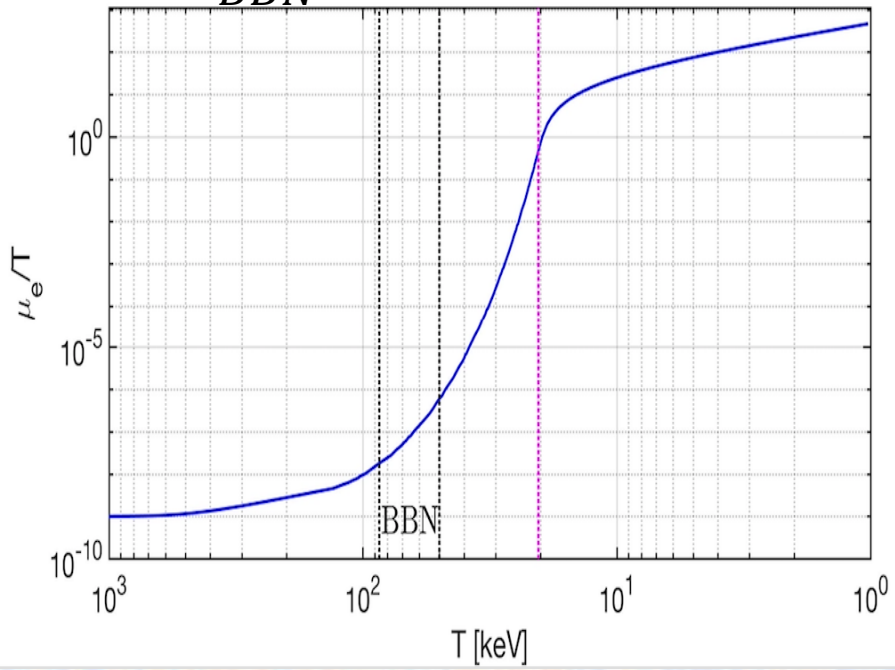
We know baryon density and charge neutrality fixes the electron chemical potential.

$$n_e - n_{\bar{e}} = \frac{n_p}{n_B} \left(\frac{n_B}{s_{\gamma, e, \bar{e}}} \right) s_{\gamma, e, \bar{e}}$$

$$\left(\frac{n_B}{s_{\gamma, e, \bar{e}}} \right) = \left(\frac{n_B}{s_{\gamma}} \right)_{t_0} = \left(\frac{n_B}{n_{\gamma}} \right)_{t_0} \left(\frac{n_{\gamma}}{s_{\gamma}} \right)$$

$$(n_B - n_{\bar{B}}) / n_{\gamma} = (0.609 \pm 0.06) \times 10^{-9} (\text{CMB})$$

$T_{BBN} = 86 - 50 \text{ keV}$



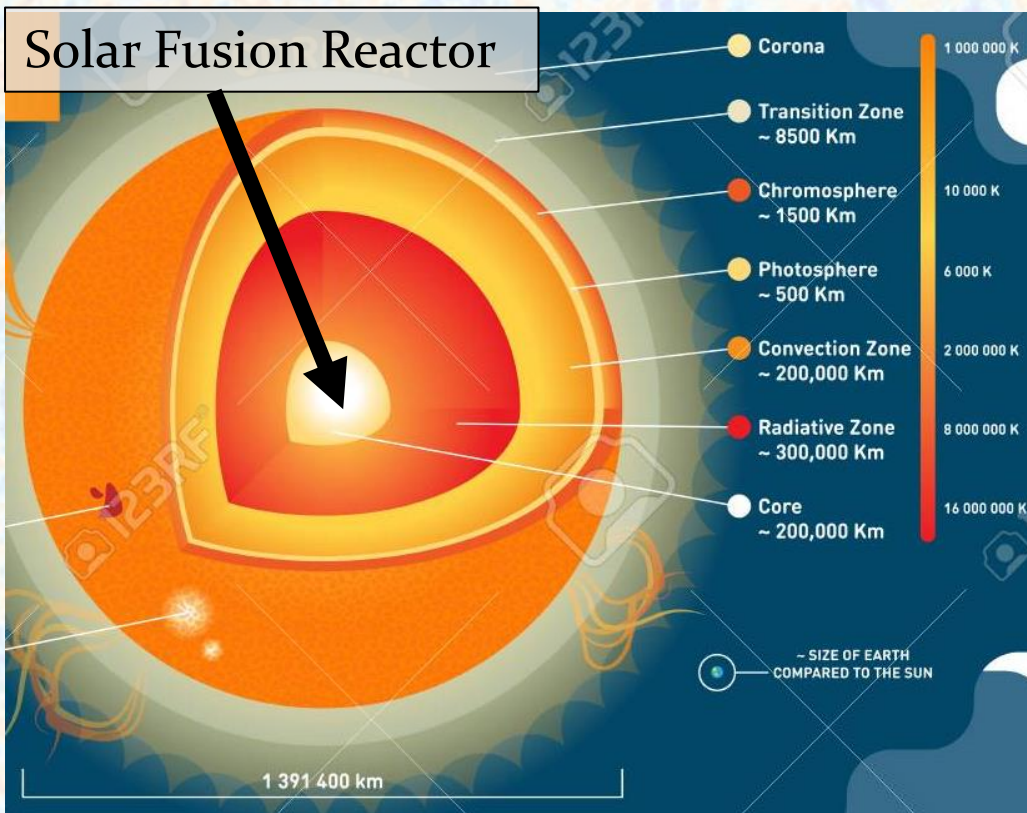
We find that in the Big Bang Nucleosynthesis epoch (BBN) we have a lot of e^+e^- pairs in the cosmic plasma with $n_{e^\pm}/n_B = 10^7$, and after temperature $T_{split} = 20.36 \text{ keV}$ the positron density decrease because of annihilation. **In this case the BBN happened in the electron-positron rich plasma** in presence of large number of electron and positron pairs during the BBN temperature range. **However, all BBN processes have been evaluated in empty space.**

Module 9: Fusion energy for mankind

Natural plasma fusion

The fusion reactor powering the solar system

The sun is primarily made up of primordial hydrogen and helium.

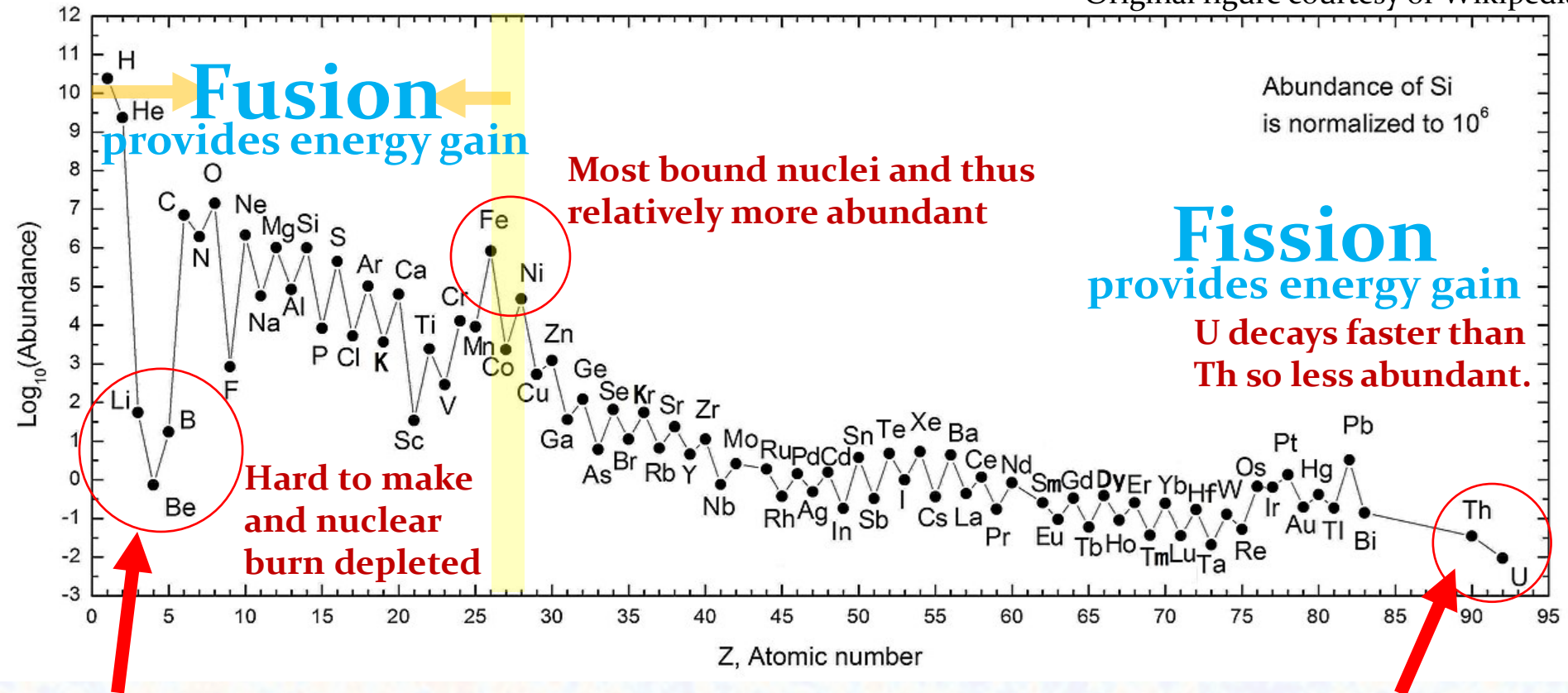


- The Sun produces energy by converting hydrogen into helium-4. Two processes are well known:
 - Proton-Proton (PP) chain
 - Carbon-Nitrogen-Oxygen (CNO) cycle
- Gravity provides the confining force which balances the explosive radiative pressure.
- It produces 3.8×10^{26} W and has been continuously running for 4.6 billion years.
- The Earth is habitable by the grace of our “local” **stable** Solar core fusion nuclear reactor.

The outcome of BBN and stellar nucleosynthesis

These are the ashes!

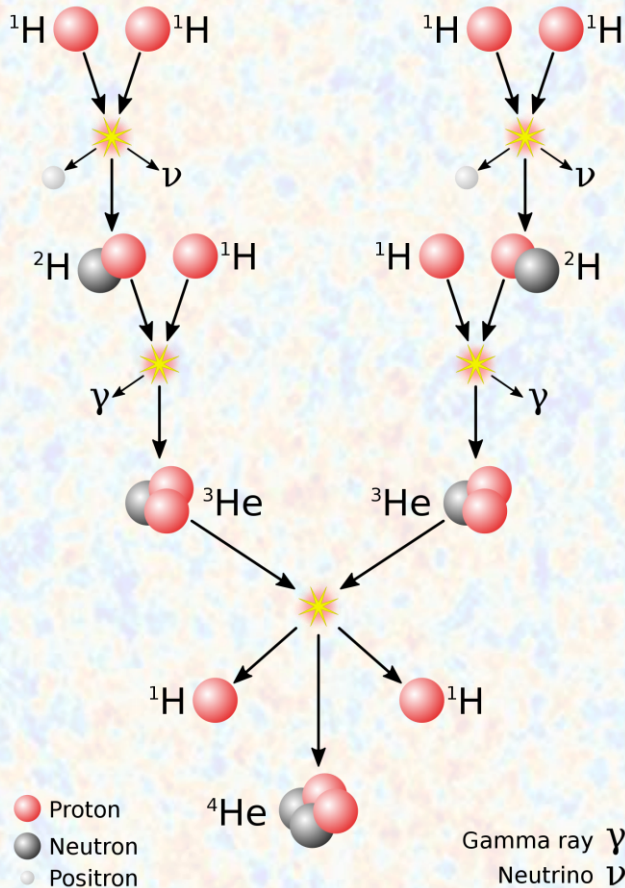
Original figure courtesy of Wikipedia



The light elements of lithium, boron and beryllium are suitable for aneutronic fusion.

Fuel for standard fission reactors

Primary power source of our Sun: The proton-proton chain



- This process is responsible for most of the energy production within the Sun as well as most low-mass stars.
- Every alpha produced releases about 14 MeV of energy from the binding energy per nucleon.
- The PP chain uses both the weak and strong interactions:
 - The weak interaction in the first step converts protons into deuterons.
 - The strong interaction then accomplishes the second and third steps to make intermediate helium-3 and finally the product helium-4.

Graphic courtesy of Wikipedia

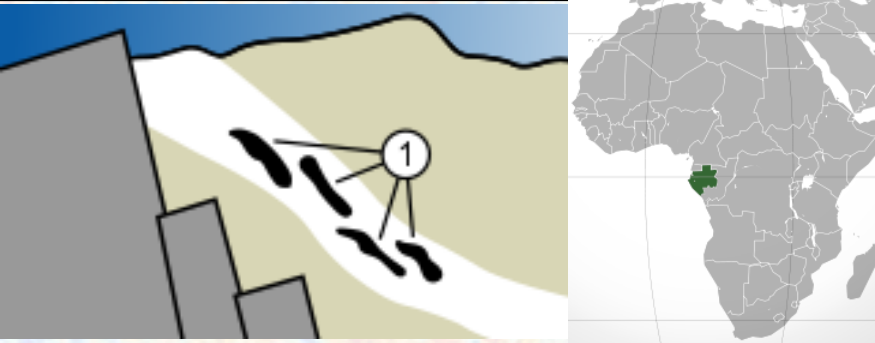
Fission versus fusion

Fission processes break apart large nuclei

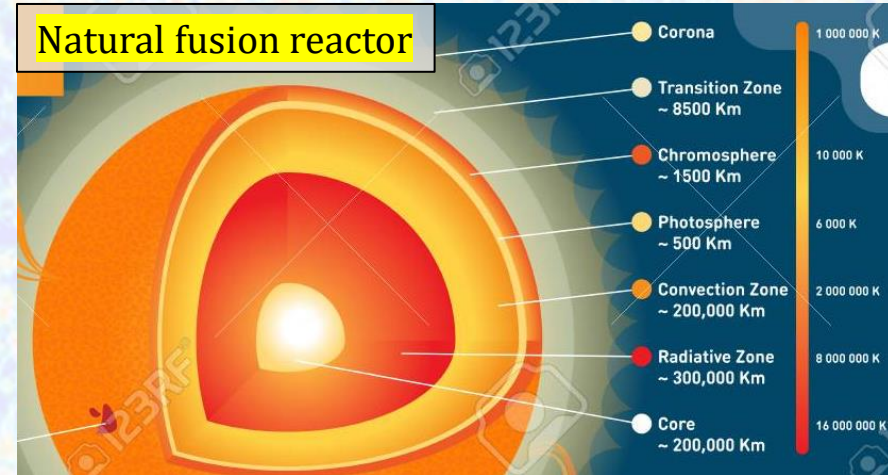
Fusion processes “fuse” or combine smaller nuclei into larger ones

Natural fission reactor

Present 2 billion years ago at Oklo, Gabon in Africa

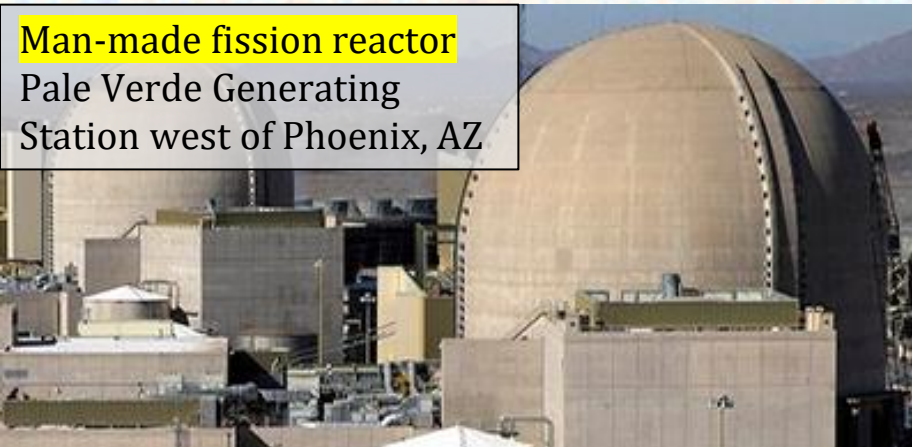


Natural fusion reactor



Man-made fission reactor

Pale Verde Generating Station west of Phoenix, AZ



Future man-made fusion



Movie: Passengers (2016)

Brute force & clever paths to manmade fusion

There are many different fusion reactors natural and (planned) manmade

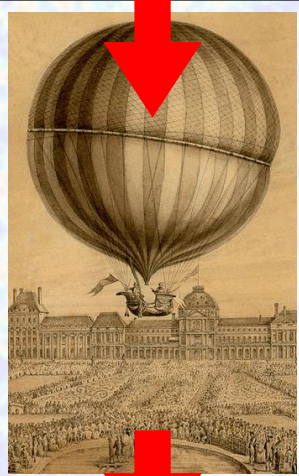
Can we facilitate nuclear fusion via a different path as compared to early Universe Big Bang nucleosynthesis (BBN) or stellar core reactors?

What can we change compared to natural plasma fusion?

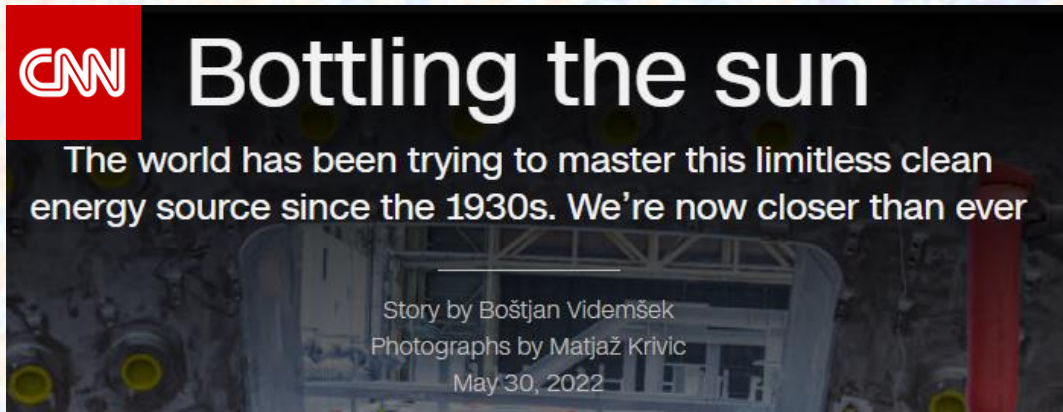


We can change the type of nuclear fusion fuel used and method of confinement e.g. replacing gravity force with magnetic fields. Result: Development of deuterium-tritium fusion reactor for past 70 years. **This is like the evolution of the chariot (1,000s of years).**

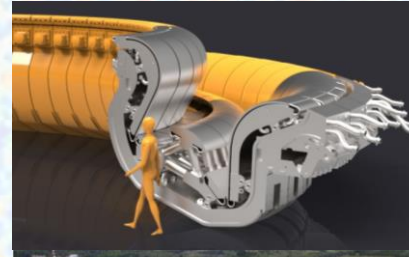
We can change the mechanism and process entirely by using lasers, plasmonics and light elements and their isotopes. **Transport without wheels (200 years).**



ITER = International Thermonuclear Experimental Reactor
ITER is a \$70 billion experiment: Start 2050?



ITER Divertor



scientific reports Potential design problems for ITER fusion device

www.nature.com/scientificreports

A. Hassanein & V. Sizyuk



The ITER reactor design was simulated in full and exact 3D geometry including all known relevant physical processes involved during these transient events. The current ITER divertor design may not work properly and may require significant modifications or new innovative design to prevent serious damage and to ensure successful operation.

Center for Materials Under Extreme Environment (CMUXE), Purdue University, West Lafayette, IN 47907, USA.
✉ email: hassanein@purdue.edu

ISSUES & EVENTS

PHYSICS TODAY | MAY 2022

Further delays at ITER are certain, but their duration isn't clear

A halt to construction, pandemic-caused delays in deliveries, labor strife, and concerns about potential beryllium exposure are among recent challenges to the fusion project.

Inertial confinement fusion

REVIEW ARTICLES | INSIGHT

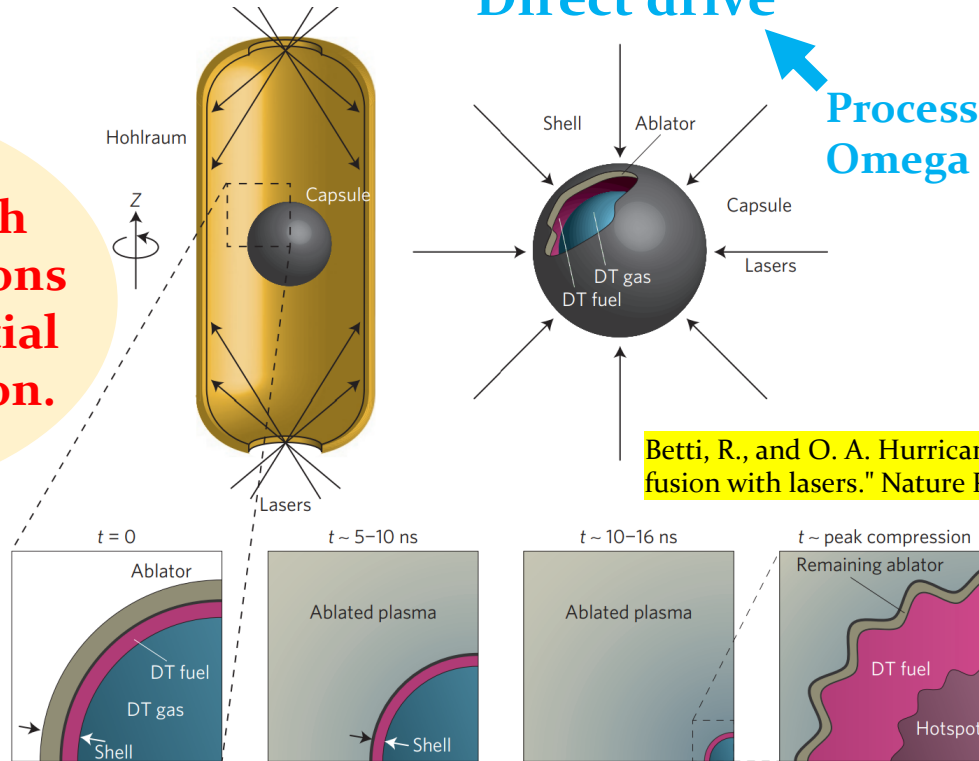
NATURE PHYSICS DOI: 10.1038/NPHYS3736

Indirect drive

Direct drive

Process used by NIF, Omega and Megajoule

Reminder:
All problems with tritium and neutrons also apply to inertial confinement fusion.



Originally envisioned with heavy-ions, but ultimately developed using laser pulses.

Figure 1 | Schematics of indirect- and direct-drive ICF. Typical targets used in laser-driven ICF are indirectly driven (upper left) or directly driven (upper right). In either case, a spherical capsule is prepared at $t = 0$ with a layer of DT fuel on its inside surface. As the capsule surface absorbs energy and ablates, pressure accelerates the shell of remaining ablator and DT fuel inwards—an implosion. By the time the shell is at approximately one-fifth of its initial radius it is travelling at a speed of many hundreds of kilometres per second. By the time the implosion reaches minimum radius, a hotspot of DT has formed, surrounded by colder and denser DT fuel.

Problems with inertial fusion

Personal point of view: Direct drive inertial confinement laser fusion unsuitable for any meaningful power generation. It is useful for a femto-version of an H-bomb. This is also where the funding of NIF came from.



Inside the target chamber at the US National Ignition Facility.

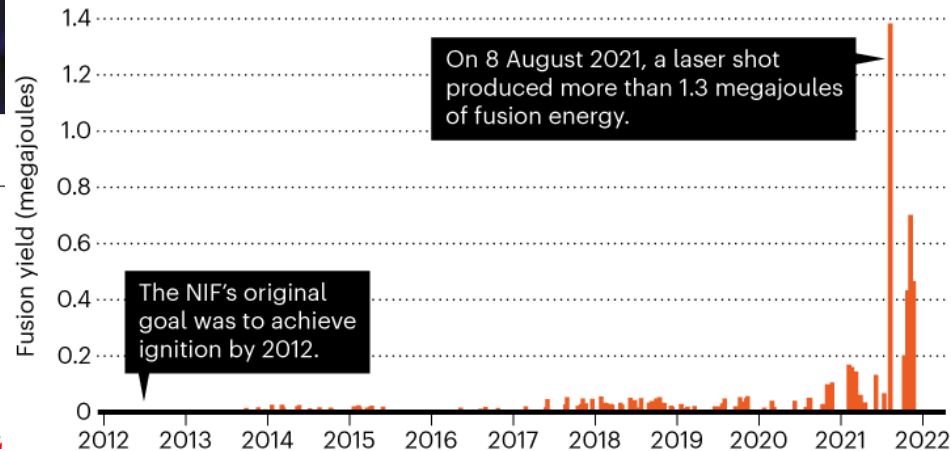
LASER-FUSION FACILITY HEADS BACK TO THE DRAWING BOARD

Published July 22nd, 2022

US scientists evaluate their options after failing to replicate record-setting experiment from 2021.

THE ROAD TO IGNITION

The National Ignition Facility (NIF) struggled for years before achieving a high-yield fusion reaction (considered ignition, by some measures) in 2021. Repeat experiments, however, produced less than half the energy of that result.



©nature

Tollefson, Jeff. "Exclusive: Laser-fusion facility heads back to the drawing board." *Nature* 608.7921 (2022): 20-21.

dt-fusion **safety** and **radioactive** waste

Appelbe, B., and J. Chittenden. "Relativistically correct DD and DT neutron spectra." High Energy Density Physics 11 (2014): 30-35.

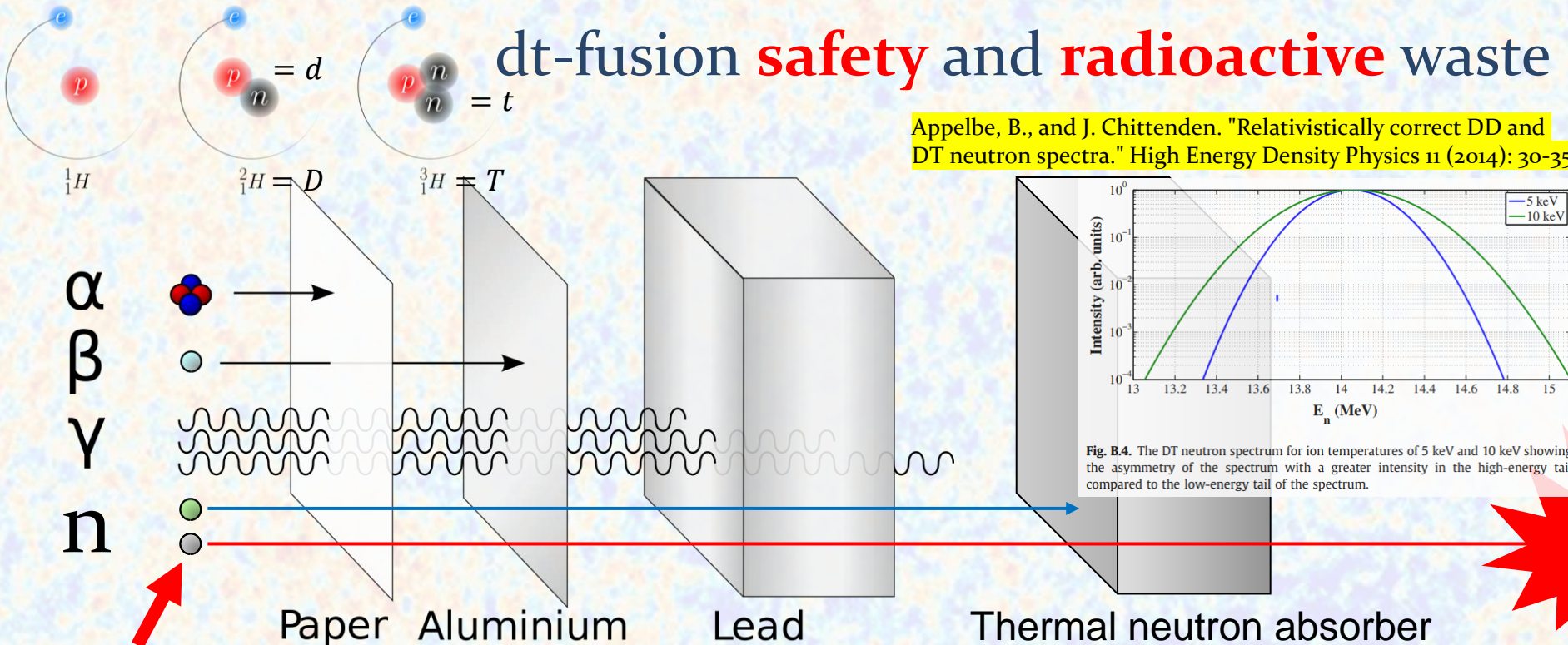


Fig. B.4. The DT neutron spectrum for ion temperatures of 5 keV and 10 keV showing the asymmetry of the spectrum with a greater intensity in the high-energy tail compared to the low-energy tail of the spectrum.

14 MeV neutrons
(dt process)
 $v_n = 0.173c$

$$m_n c^2 = 940 \text{ MeV}$$



dt-fusion leads to super-fast neutrons and associated problems: My objective today is the development of aneutronic fusion in a dynamic regime i.e. non-thermal equilibrium, forbidden by brems-losses.

MeV energy units: M = million and eV is the kinetic energy a unit charged particle acquires in a 1 Volt step

Tabletop approaches to fusion

Approach A: Muon-catalyzed fusion

J.D. Jackson reminisces in 2010: “Luis Alvarez and colleagues discovered muon-catalyzed fusion of hydrogen isotopes by chance in late 1956. On sabbatical leave at Princeton University during that year, I read the first public announcement of the discovery at the end of December in that well-known scientific journal, The New York Times. A nuclear theorist by prior training, I was intrigued enough in the phenomenon to begin some calculations.”

Jackson, J.D. A Personal Adventure in Muon-Catalyzed Fusion. Phys. Perspect. 12, 74–88 (2010). <https://doi.org/10.1007/s00016-009-0006-9>

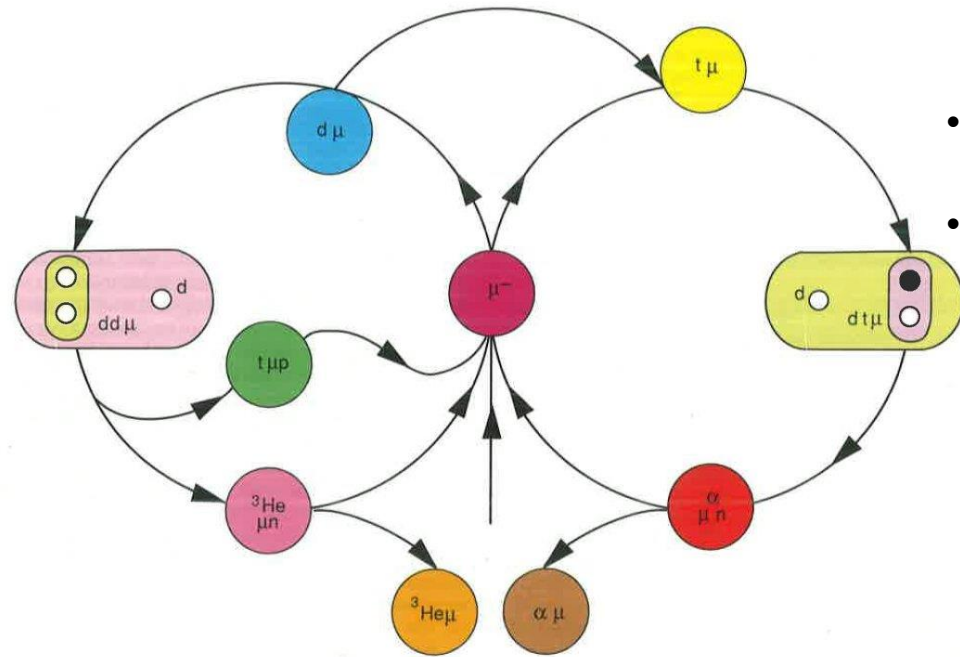


Modern nuclear fusion processes occur under inequilibrium conditions with the objective to spark a nano-fusion explosion which is short lived.

Muon-catalyzed fusion (μCF) cycle

The muon is the catalyzer for dt-fusion allowing a single muon to facilitate many fusion events.

Representation of the cycle of $dt\mu$ MuCF fusion processes.



- The muon is a heavy electron with 207 times more mass therefore muonic atoms are shrunk by a factor of 207.
- Muonic molecules of hydrogen are then also shrunk which allows rapid spontaneous fusion at any temperature and pressure.
- For $dt\mu^+$ molecules, the fusion rate is a million times faster than the natural decay of the muon.
- The greatest challenge to μCF is the loss of the muon due to binding with the produced alpha particles. This limits the number of observed fusions to about 200 per muon.

The physics breakeven point for $dt\mu$ cycle was achieved around 1988.

Approach B: Laser driven aneutronic proton-boron fusion

news@nature.com
The best in science journalism

Published online: 26 August 2005; | doi:10.1038/news050822-10

Lasers trigger cleaner fusion

Neutron-free reaction makes less radioactive waste.

Mark Peplow

Belyaev, V.S.; et al. (2005). "Observation of neutronless fusion reactions in picosecond laser plasmas". *Physical Review E*. 72 (2): 026406. doi:10.1103/physreve.72.026406

Two-laser process

Aneutronic fusion reactions require a spark of protons in the 0.01-1 MeV energy range

Patent Production of energy via laser-initiated
 aneutronic nuclear fusion reactions

Abstract

The invention relates to the production of energy with laser beams, involving: a) exciting a fuel target (4) into a plasma state using a first set of laser beams (1); b) bombarding the fuel target in the plasma state with particles generated using a second set of laser beams (2), the fuel and the particles being chosen so that the interaction between the fuel target in the plasma state and the particles produce non-thermal equilibrium aneutronic nuclear reactions; and c) recovering energy from the ions generated by the aneutronic nuclear reactions.

WO2013144482A1

WIPO (PCT)

2013-10-03 • Publication of WO2013144482A1

Other languages: French

Application PCT/FR2013/050558

2012-03-27 • Priority to FR1252750A

Inventor: Christine LABAUNE, Johann Rafelski, Sylvie DEPIERREUX, Clément GOYON, Vincent YAHIA

Two-laser pB process

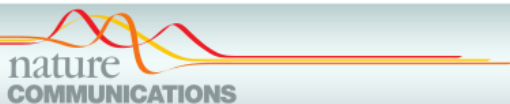
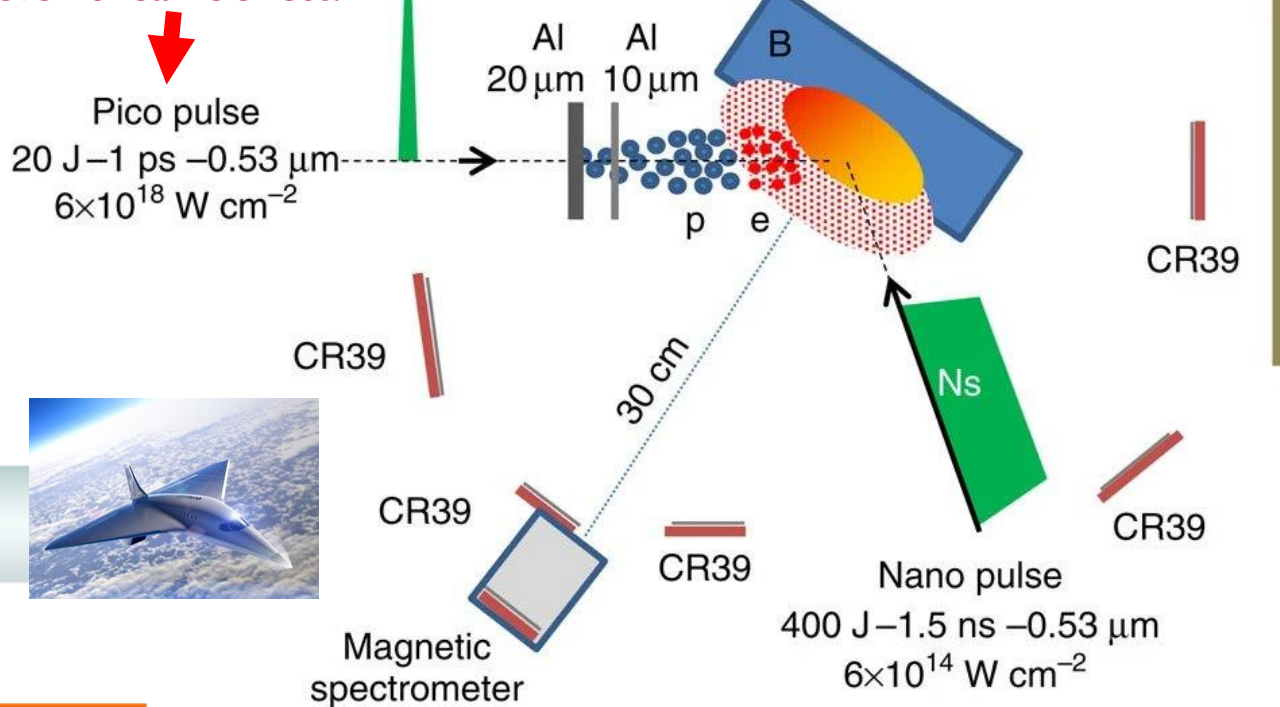
The long-pulsed nano-laser produces plasma and sweeps electrons away.

The short-pulsed pico-laser produces a beam of reactant protons. Fusion reactions occur prior to protons reaching thermal equilibrium.

Fusion reactions initiated by laser-accelerated particle beams in a laser-produced plasma

Scheme of the experimental set-up showing the laser beam configuration, the target arrangement and the diagnostics

Alternative short pulse lasers are milli-Joule femto-second level for same effect.



ARTICLE

Received 24 Jan 2013 | Accepted 27 Aug 2013 | Published 8 Oct 2013

DOI: 10.1038/ncomms3506

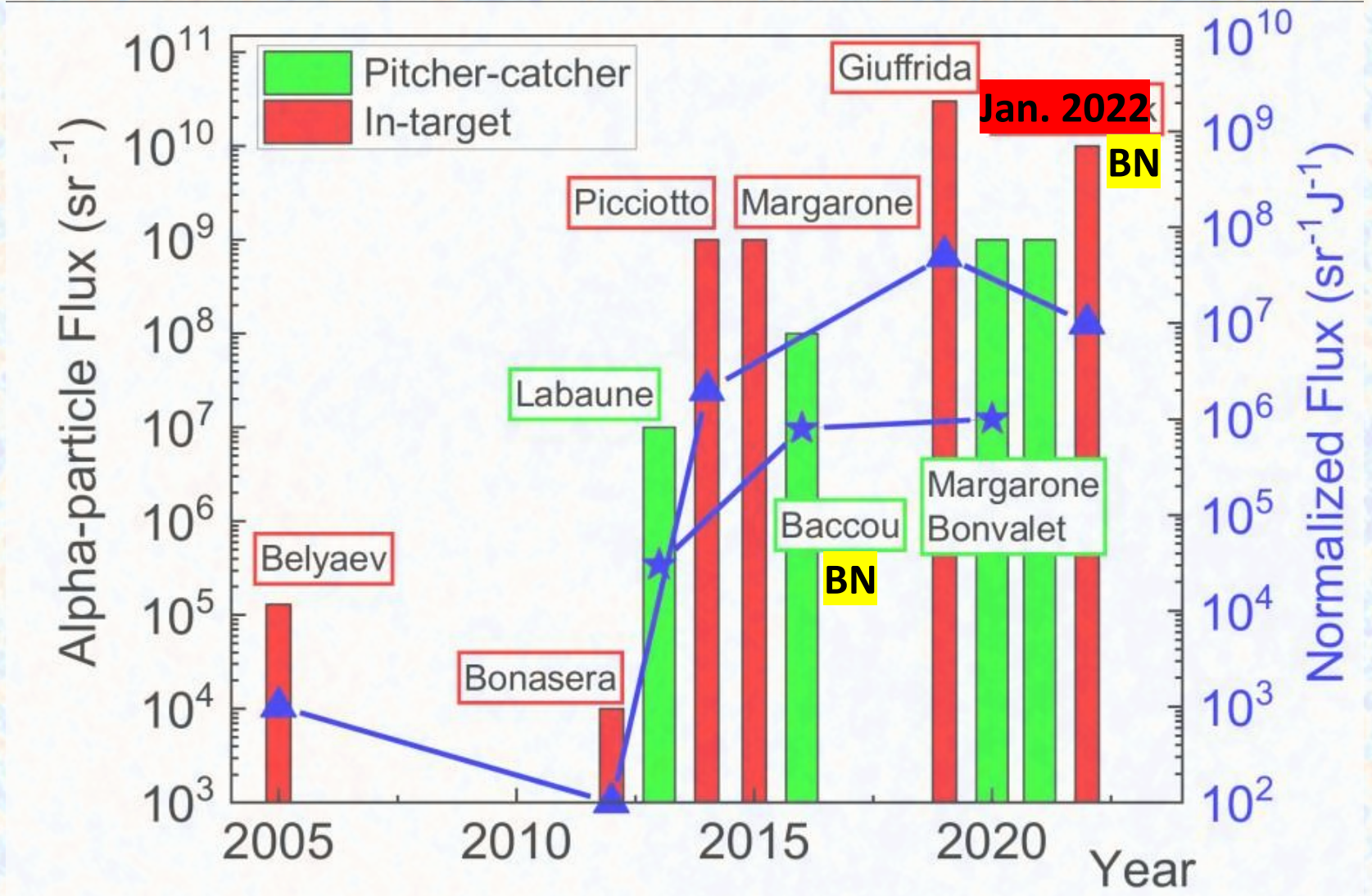
Fusion reactions initiated by laser-accelerated particle beams in a laser-produced plasma

C. Labaune¹, C. Baccou¹, S. Depierreux², C. Goyon², G. Loisel¹, V. Yahia¹ & J. Rafelski³

$$\text{Laser Contrast Ratio: } R = \frac{\text{Pulse Intensity}}{\text{Prepulse/pedestal Intensity}}$$

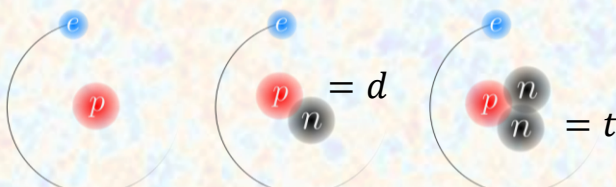
The laser contrast ratio is a crucial parameter in achieving laser-driven nuclear fusion.

The experimental progress in pB fusion measured in terms of α production

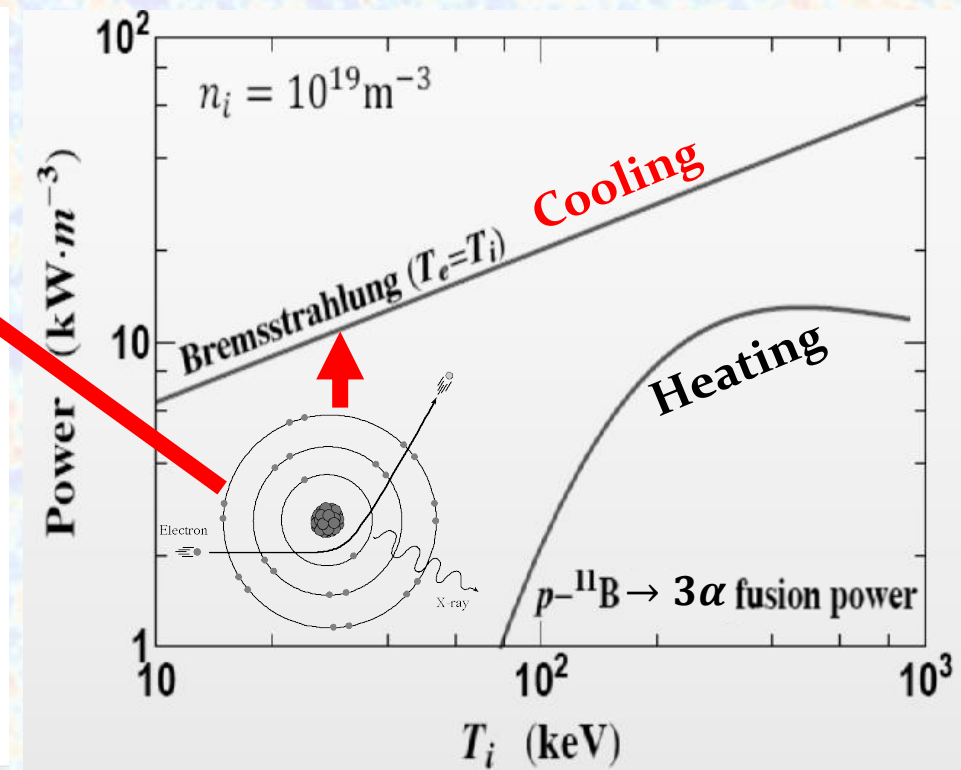
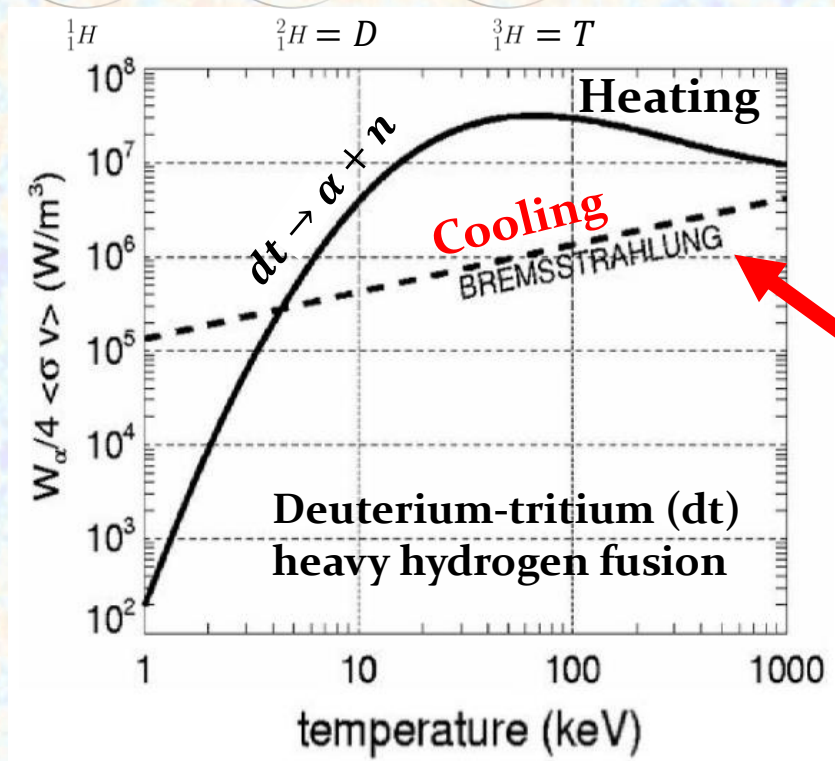


proton-Boron requires non-equilibrium processes rather than a thermal reactor

Comparing neutronic and aneutronic fusion



Some advanced fuels (such as boron) do not allow steady state thermal fusion because of fusion output versus radiation loss.



Approach C: Plasmonic fusion

Antennas for light

Lukas Novotny^{1*} and Niek van Hulst^{2,3}

nature
photonics

REVIEW ARTICLE

PUBLISHED ONLINE: 1 FEBRUARY 2011 | DOI: 10.1038/NPHOTON.2010.237

Optical antennas are devices that convert freely propagating optical radiation into localized energy, and vice versa. They enable the control and manipulation of optical fields at the nanometre scale, and hold promise for enhancing the performance and efficiency of photodetection, light emission and sensing. Although many of the properties and parameters of optical antennas are similar to their radiowave and microwave counterparts, they have important differences resulting from their small size and the resonant properties of metal nanostructures. This Review summarizes the physical properties of optical antennas, provides a summary of some of the most important recent developments in the field, discusses the potential applications and identifies the future challenges and opportunities.

IOP Publishing | Royal Swedish Academy of Sciences

Invited Comment

Physica Scripta

Phys. Scr. 91 (2016) 053010 (13pp)

Published 22 April 2016

doi:10.1088/0031-8949/91/5/053010

Surface plasmons: a strong alliance of electrons and light

Norbert Kroó^{1,3}, Sándor Varró^{1,2},
Péter Rácz¹ and Péter Dombi^{1,2}

¹Wigner Research Centre for Physics of the Hungarian Academy of Sciences, Institute for Solid State Physics and Optics, H-1525 Budapest, Pf. 49, Hungary ²ELI-ALPS, H-6720 Szeged, Dugonics tér 13, Hungary

Surface plasmon polaritons (SPPs) have several unique properties, including their strong-field enhancing effect in near field. This means, among other things, that nonlinear phenomena may be studied at much lower laser intensities. The present paper describes in detail the theory of basic properties of SPPs, and our model of a laser-induced oscillating double-layer potential. The SPPs may decay into photons and hot electrons. The latter may be emitted by a multi-plasmon process. Experiments on both photon and electron emission from a gold film are briefly

PRX ENERGY

Kinetic Model Evaluation of the Resilience of Plasmonic Nanoantennas for Laser-Induced Fusion

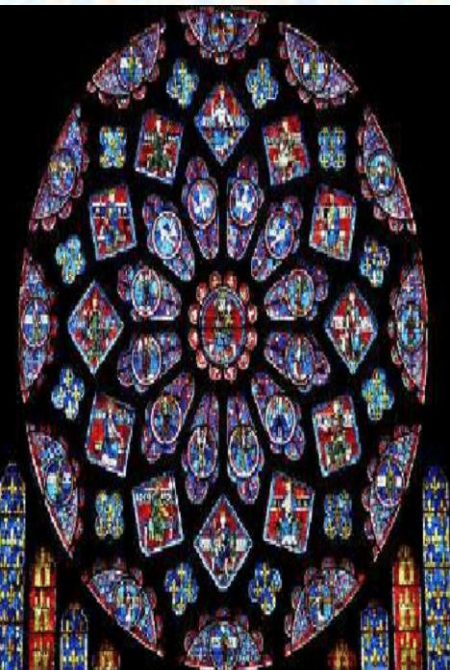
István Papp, Larissa Bravina, Mária Csete, Archana Kumari, Igor N. Mishustin, Dénes Molnár, Anton Motornenko, Péter Rácz, Leonid M. Satarov, Horst Stöcker, Daniel D. Strottman, András Szenes, Dávid Vass, Tamás S. Biró, László P. Csernai, and Norbert Kroó (NAPLIFE Collaboration)

PRX Energy 1, 023001 – Published 7 July 2022

Recently, a new version of laser-induced fusion was proposed where implanted nanoantennas regulated and amplified the light absorption in the fusion target [L.P. Csernai *et al.*, Phys. Wave Phenom. 28, 187–99 (2020)]. In this paper we estimate the nanoantenna lifetime in a dynamical kinetic model and describe how electrons are leaving the nanoantenna's surface, and for how long the plasmonic effect is maintained. Our model successfully shows a nanorod antenna lifetime that will allow future fusion studies with top-energy short laser ignition pulses.

Antennas for light invented in ancient Imperial Rome

A nano-sized piece of metal can be viewed as a box trapping free electron plasma. The domain of physics describing how light interacts with metallic nano-structures embedded in an insulator is called **plasmonics**. Extreme daily light absorption properties of metallic nano particles have been empirically recognized and used in **medieval stained glass** (see e.g. The Grande Rose of the Chartres Cathedral); and in precious objects made of glass during the **Roman era (e.g. Lycurgus drinking cup)**.

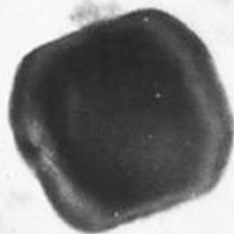


The Lycurgus Cup A Roman Nanotechnology

Ian Freestone¹, Nigel Meeks²,
Margaret Sax² and Catherine Higgitt²

Transmission electron microscopy (TEM) image of a silver-gold alloy particle within the glass of the Lycurgus Cup

50 nm



The Lycurgus Cup 1958,1202.1 in reflected (a) and transmitted (b) light. Scene showing Lycurgus being enmeshed by Ambrosia.

The NAPlife plasmonic fusion project

Tamás Biró

László Pál Csernai

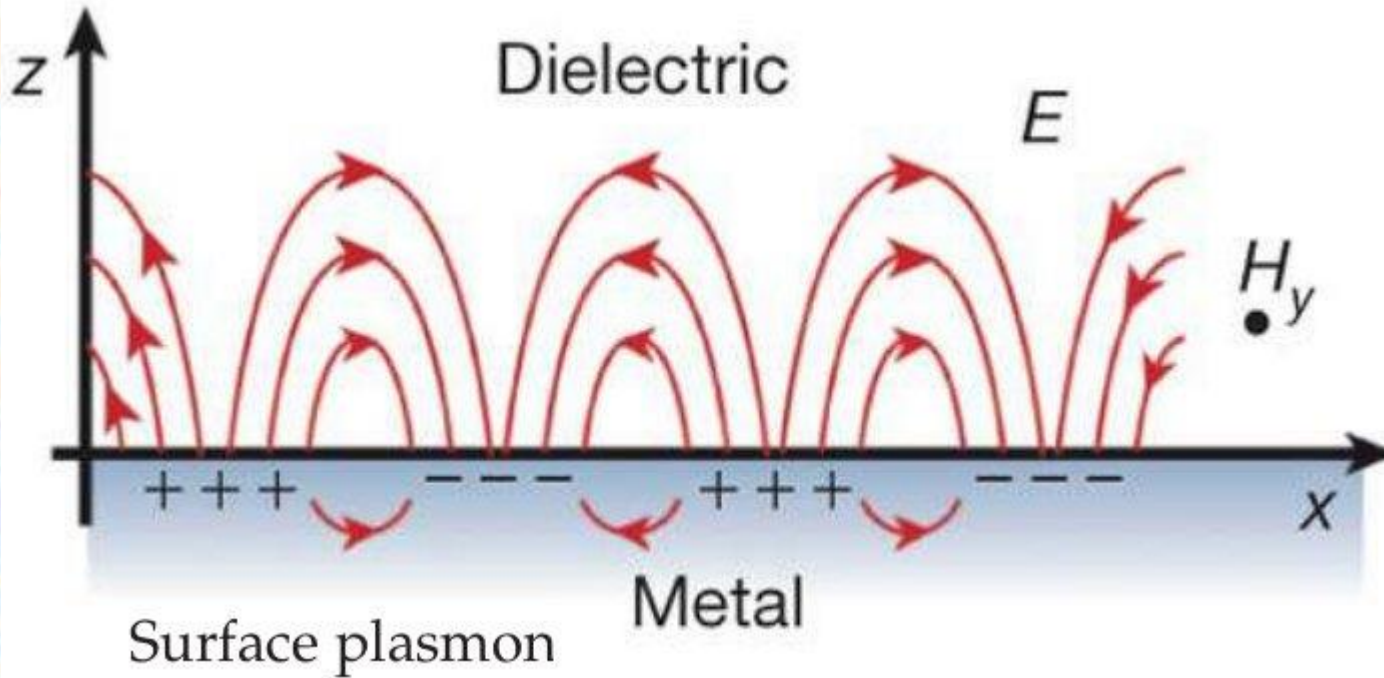
Norbert Kroó



NAPlife Collaboration:

Márk Aladi, Tamás S Biró, Attila Bonyár, Alexandra Borók, László P Csernai, Mária Csete, Attila Czirják, Péter Dombi, Olivér Fekete, Péter Földi, Gábor Galbács, Román Holomb, Csaba Horváth, Judit Kámán, Miklós Kedves, Norbert Kroó, Archana Kumari, Ágnes N Szokol, István Papp, Péter Petrik, Béla Ráczkevi, Péter Rácz, István Rigó, Melinda Szalóki, András Szenes, Ádám Takács, Csaba Tóth, Emese Tóth, Dávid Vass, Miklós Veres, Shereen Zangna

Antenna response: Surface electro-magnetic fields 1000-fold (in numerical model) amplified



Nanoparticles act as resonant antennas working at a fraction of the incident light's wavelength.

Resonance wavelength is determined by the electron density and geometry of the antenna.

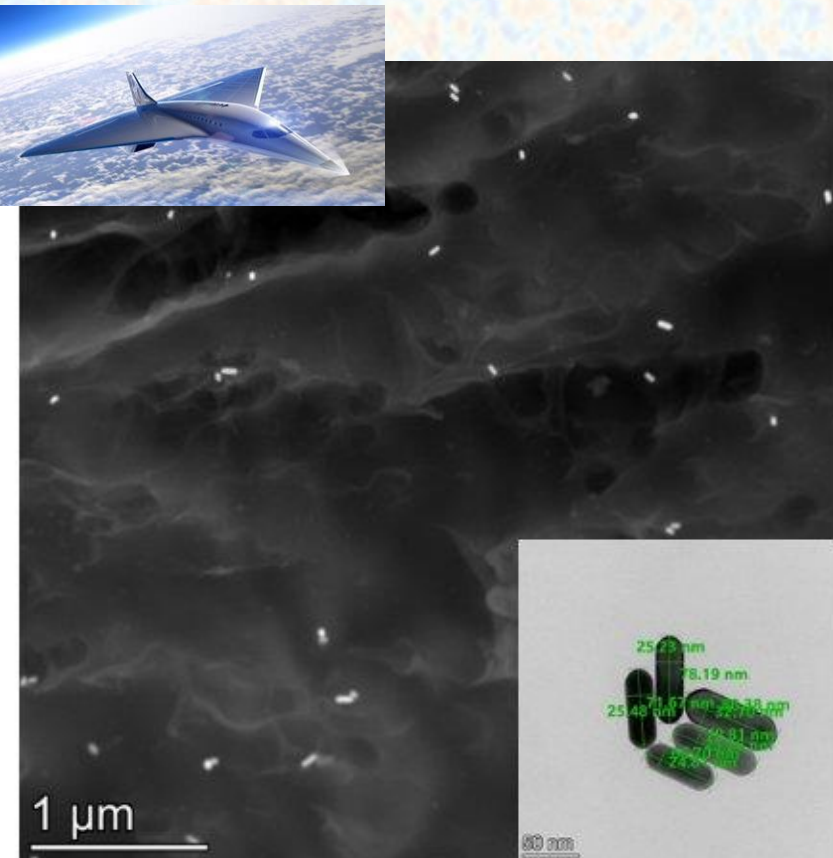
Plasmon coherent dynamics lifespan requires sub-picosecond laser pulses.

Commercially available femto-sec mJ lasers can excite surface plasmons in dielectrics which can accelerate protons to MeV energies.

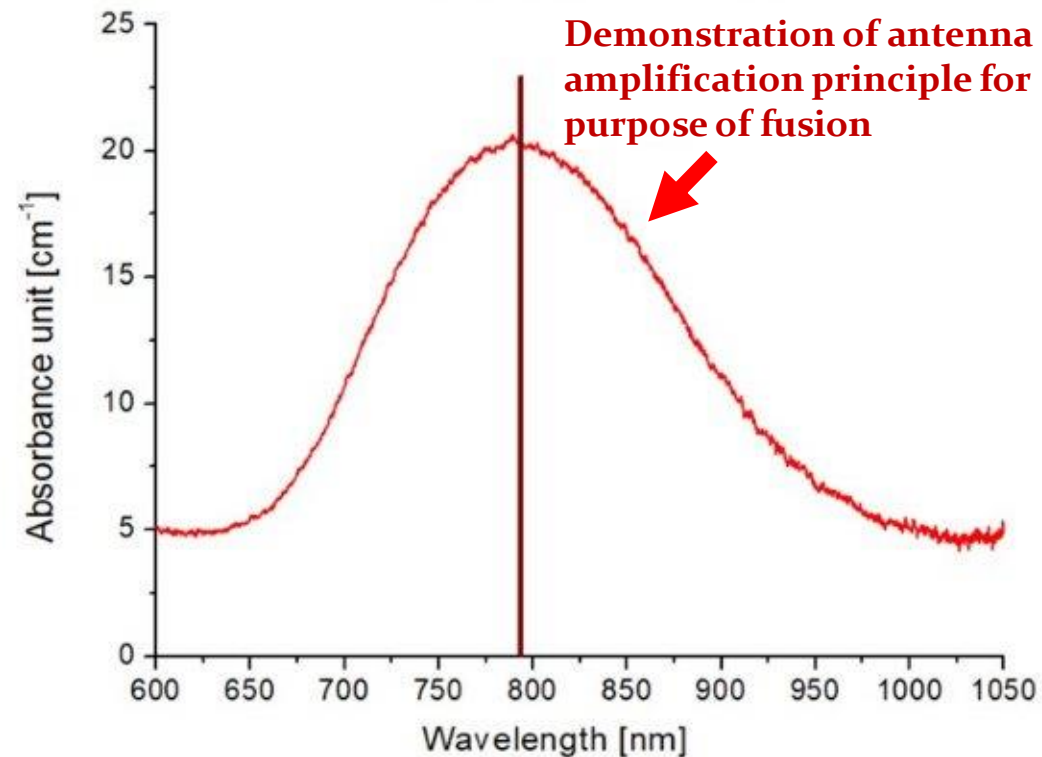
The NAPlife plasmonic fusion project

UDMA polymer with resonant gold nano-rods

Gold nano-rods embedded in polymer matrix:
Transmission electron microscope image;
insert shows actual nano-rods



Actual absorption curve for nano composites
measured by optical spectroscopy. The
absorption peak is tuned to resonate with laser
wavelength at 795 nm



Module 10: Nuclei in non-relativistic $e^+ e^-$ plasma

The response of a relativistic plasma to electromagnetic fields in the framework of the Boltzmann equation incorporating a collision term in the relaxation rate approximation.

$$(p \cdot \partial) f(x, p) + q F^{\mu\nu} p_\nu \frac{\partial f(x, p)}{\partial p^\mu} = (p \cdot u) C(x, p)$$

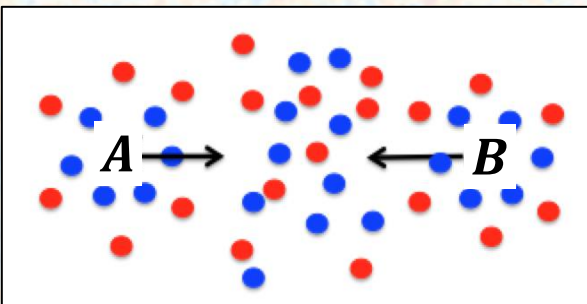
$$C(x, p) = \kappa \left(f_{\text{eq}}(p) \frac{n(x)}{n_{\text{eq}}} - f(x, p) \right)$$

Since,

$$\frac{1}{H} \gg \gg \frac{1}{\kappa}$$

to a very good approximation all plasma phenomena can be considered in a static universe.

Polarization response



Nuclei in EM plasma example:

The alpha particle is surrounded by the electron cloud and the electron cloud moves with the ion in plasma together.

- Linear response approximation**

Linear response does not separate electron and positron

$\rightarrow \mu_e(x, t)$

No self-interaction between screening charges and a small polarization perturbation.

The electron/positron medium is perturbed by alpha particle electromagnetically when it travels in the plasma.

$$f(x, p) = f_{\text{eq}}(p) + \delta f(x, p)$$

To study the damped dynamic screening in electron/positron plasma, more detail study of linear response theory required.

Still working in progress!



Chris Grayson

Beyond Vlasov Boltzmann equations

The fundamental starting point for our study is the Vlasov Boltzmann equation

$$p_k^\mu \partial_\mu f_k(x, p_k) + q_k F^{\mu\nu} p_{k\nu} \frac{\partial f_k(x, p_k)}{\partial p_k^\mu} = \sum_{l=1}^N C_{kl}(x, p_k)$$

Boltzmann "Flow" term: Represents diffusion of particles

Vlasov force term: Electromagnetic force on particles

ADDED Collision term: Microscopic collision between all other constituents

$k = e^-, e^+, \gamma$ Each species k is described by their own Boltzmann equation.

The collision term is given by

Transition Rate for Process

$$C_{kl}(x, p_k) = \frac{1}{2} \sum_{i=1}^N \sum_{j=1}^N \int \frac{d^3 p_l}{(2\pi)^3 p_l^0} \frac{d^3 p_i}{(2\pi)^3 p_i^0} \frac{d^3 p_j}{(2\pi)^3 p_j^0} \times [f_i f_j - f_k f_l] W_{kl|ijl}$$

Particles entering $dx^3 dp^3$

Particles leaving $dx^3 dp^3$

Photon depends on the debye mass through collisions with the plasma

Photons don't have charge!

For most part of the Universe's evolution $\kappa_{e\gamma} \ll \kappa_{e\bar{e}}$ so the photons do not respond to e^+e^- plasma density fluctuations.

$$f_\gamma(x, p) \approx f_\gamma^{\text{eq}}(p)$$

Photon transport equation in plasma:

$$p^\mu \partial_\mu f_\gamma(x, p) = \sum_{l=1}^N C_{\gamma l}(x, p_\gamma)$$

Linearized collision term – BGK Simplification

General transport equation in BGK approximation for the plasma:

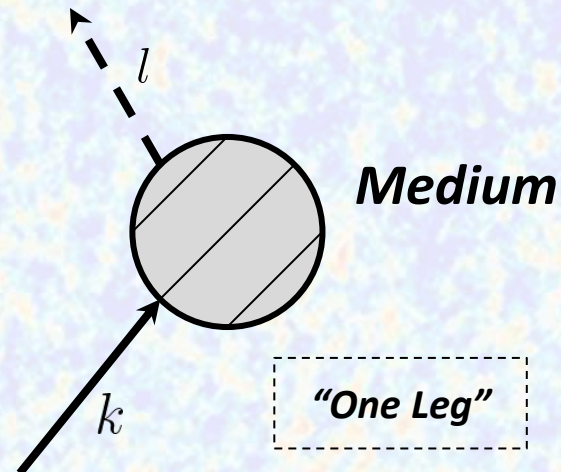
$$p_k^\mu \partial_\mu f_k(x, p_k) + q_k F^{\mu\nu} p_{k\nu} \frac{\partial f_k(x, p_k)}{\partial p_k^\mu} = \sum_{l=1}^N (p_k \cdot u) \kappa_{kl} \left(f_k^{\text{eq}}(p) \frac{n_k(x)}{n_k^{\text{eq}}} - f_k(x, p_k) \right)$$

The usual relaxation time collision term turns all collisions into a medium effect.

This neglects all process that allow particles to change from one species to another.

- Pair production
- Bremsstrahlung
- Compton scattering
- Electromagnetic force does not impact photons, but they can Compton scatter from both electrons and positrons

$$\delta f_k = f_k^{(0)} \delta \phi_k$$



Current-conserving relativistic BGK damped linear response



Chris Grayson



Martin Formanek



Berndt Müller


- Develops methods to calculate linear response in infinite homogeneous plasmas for which damping is important.
- Publication shown applied only to magnetic fields.
- Present extension now includes electrical fields in electron-positron plasmas.

PHYSICAL REVIEW D **106**, 014011 (2022)

Dynamic magnetic response of the quark-gluon plasma to electromagnetic fields

Christopher Grayson^{Ⓜ,*}, Martin Formanek^{Ⓜ,†,||} and Johann Rafelski^{Ⓜ,‡}
Department of Physics, The University of Arizona, Tucson, Arizona 85721, USA

Berndt Müller^{Ⓜ,§}
Department of Physics, Duke University, Durham, North Carolina 27708-0305, USA

 (Received 2 May 2022; accepted 26 June 2022; published 18 July 2022)

We investigate the electromagnetic response of a viscous quark-gluon plasma in the framework of the relativistic Boltzmann equation with current conserving collision term. Our formalism incorporates dissipative effects at all orders in linear response to the electromagnetic field while accounting for the full space and time dependence of the perturbing fields. As an example, we consider the collision of two nuclei in a stationary, homogeneous quark-gluon plasma. We show that for large collision energies the induced magnetic fields are governed by the response of quark-gluon plasma along the light cone. In this limit, we derive an analytic expression for the magnetic field along the beam axis between the receding nuclei and show that its strength varies only weakly with collision energy for $\sqrt{s_{\text{NN}}} \geq 30$ GeV.

DOI: 10.1103/PhysRevD.106.014011



Andrew Steinmetz

Strong magnetic fields govern early state quark-gluon-plasma in the universe

The intergalactic magnetic field B_{relic} is not strongly constrained at the mega-parsec scale:

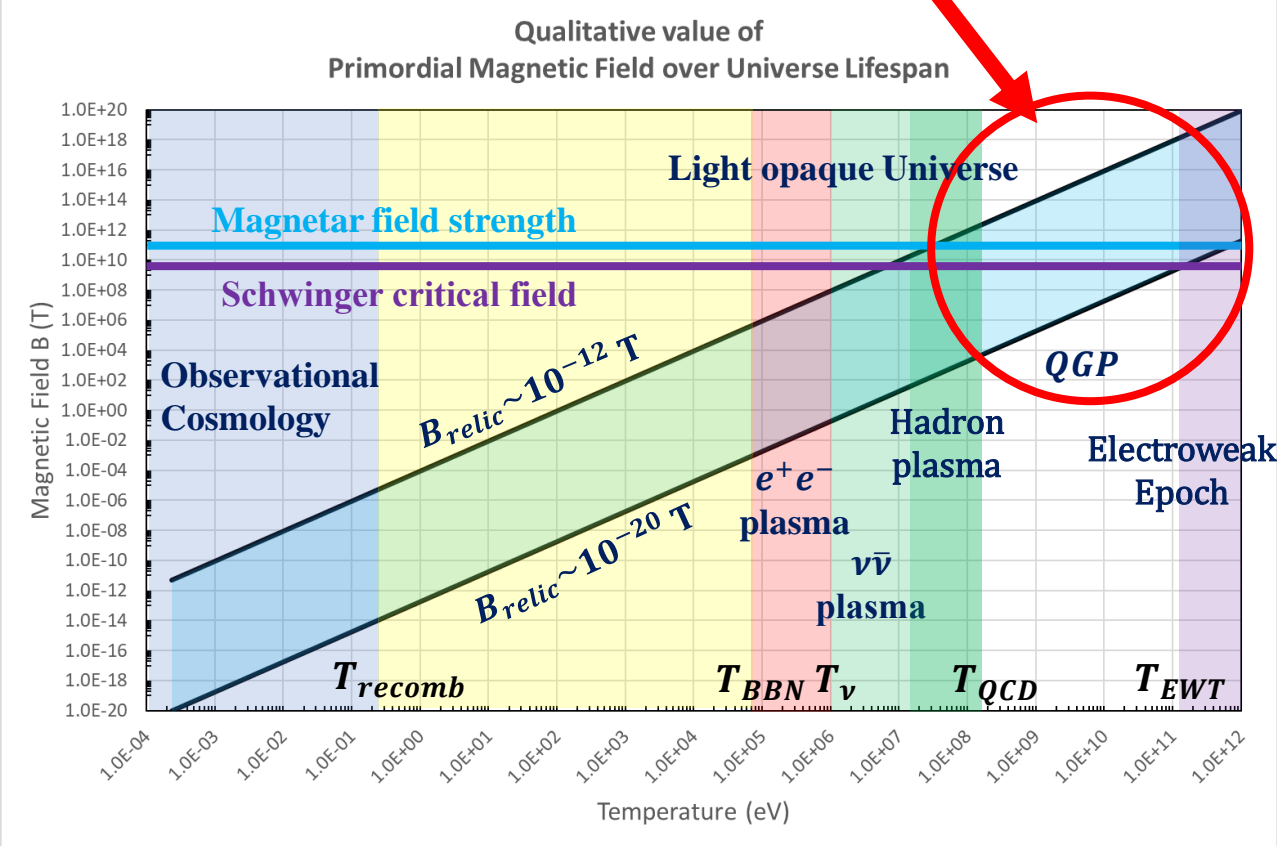
$$10^{-20} \text{ T} < B_{relic} < 5 \times 10^{-12} \text{ T}$$

Relic fields are diluted in the universe's expansion due to the conservation of magnetic flux:

$M(t) \rightarrow 0$

$$B(t) = M(t) + \frac{B_{relic}}{a(t)^2}$$

Could strong EM fields in the Early Universe be related to mysteries such as baryon asymmetry?



T. Vachaspati, "Progress on Cosmological Magnetic Fields" Rep. Prog. Phys.84(2021) 074901
 S. Mchedlidze, et al. "Evolution of primordial magnetic fields during large-scale structure formation." arXiv preprint arXiv:2109.13520 (2021).
 K. Subramanian, "The origin, evolution and signatures of primordial magnetic fields." Reports on Progress in Physics 79.7 (2016): 076901.

Dynamic damped screening potential: Debye Mass

The screened potential of nuclei can be obtained by solving Maxwell equations algebraically in Fourier space, in the presence of electron/positron medium.

C. Grayson, M. Formanek, J. Rafelski and B. Müller, arXiv:2204.14186 [hep-ph]

M. Formanek, C. Grayson, J. Rafelski and B. Müller, Annals Phys 434, 168605 (2021)

Longitudinal permittivity

$$\tilde{\phi}(\omega, \mathbf{k}) = \frac{\tilde{\rho}_{\text{ext}}(\omega, \mathbf{k})}{\epsilon_{\parallel}(\omega, \mathbf{k})(k^2 - \omega^2)}$$

Fourier transformed charge distribution of the traveling nuclei

$$\epsilon_{\parallel}(\omega, \mathbf{k}) = \epsilon_0 \left(\frac{\Pi_{\parallel}(\omega, \mathbf{k})}{\omega^2} + 1 \right)$$

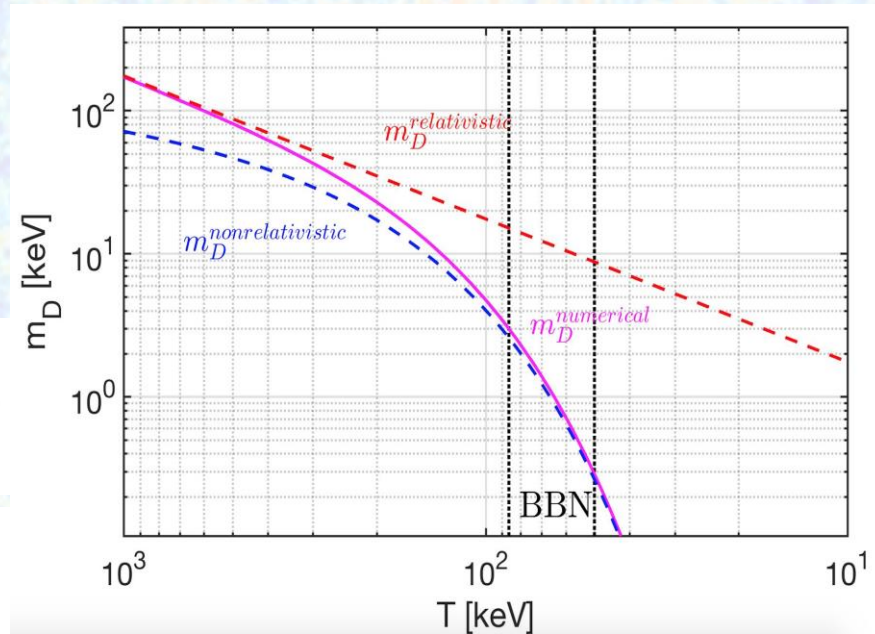
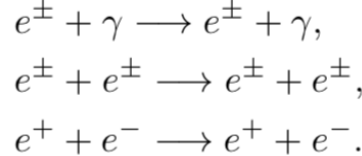
Using Linear response theory, the longitudinal polarization tensor for nonrelativistic electron-positron plasma

$$\Pi_{\parallel} = -m_D^2 \frac{\omega^2}{(\omega + i\kappa)^2} \frac{1}{1 - \frac{i\kappa}{\omega + i\kappa} \left(1 + \frac{Tk^2}{m(\omega + i\kappa)^2} \right)}$$

Non-relativistic Debye mass:

$$m_D^2 = -\frac{2e^2}{\pi^2} \int_0^{\infty} d|\mathbf{p}| |\mathbf{p}|^2 \frac{\partial f_{eq}}{\partial p_0}$$

$$= \frac{2e^2}{\pi^2} T^2 \int_{m_e/T}^{\infty} dx x \sqrt{x^2 - (m_e/T)^2} \frac{e^{-x}}{(1 + e^{-x})^2}$$



Chris Grayson



Cheng-Tao Yang

Boltzmann approximation taken by limit $e^{-x} \ll 1$

Damped dynamic screening with scattering friction κ

In electron-positron plasma the major reactions between photons and electron/positron pairs are inverse Compton scattering, Møller scattering, and Bhabha scattering. The general reaction rate per volume in two-body reaction in the Boltzmann approximation: Jean Letessier, Johann Rafelski, "Hadrons and Quark-Gluon Plasma"



Cheng-Tao Yang

$$R_{12 \rightarrow 34} = \frac{g_1 g_2}{32\pi^4} \frac{T}{1 + I_{12}} \int_{sth}^{\infty} ds \sigma(s) \frac{\lambda_2(s)}{\sqrt{s}} K_1(\sqrt{s}/T)$$

$$\lambda_2(s) = [2 - (m_1 + m_2)^2] [2 - (m_1 - m_2)^2]$$

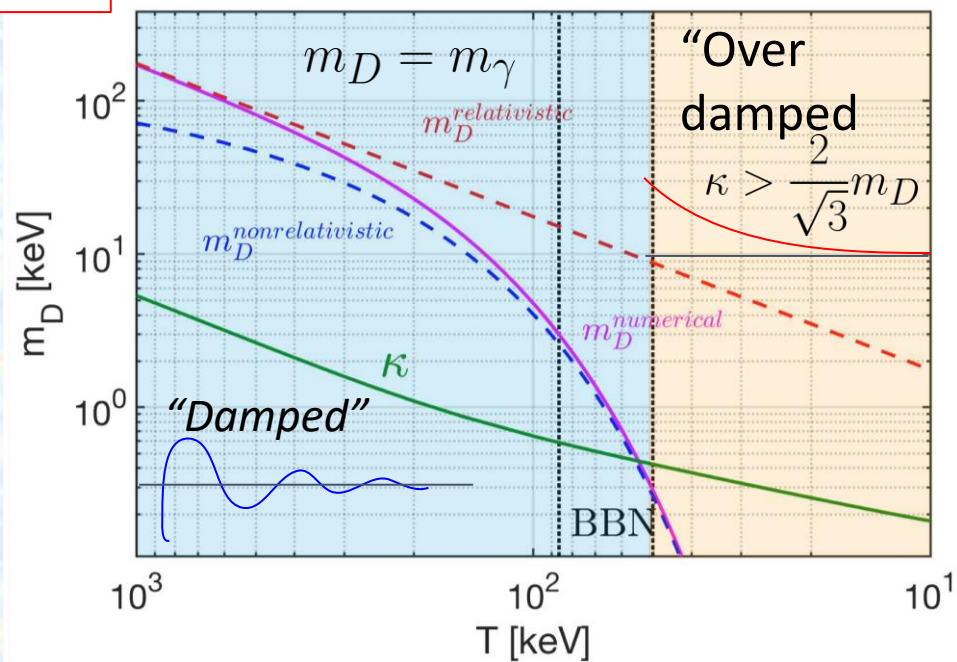
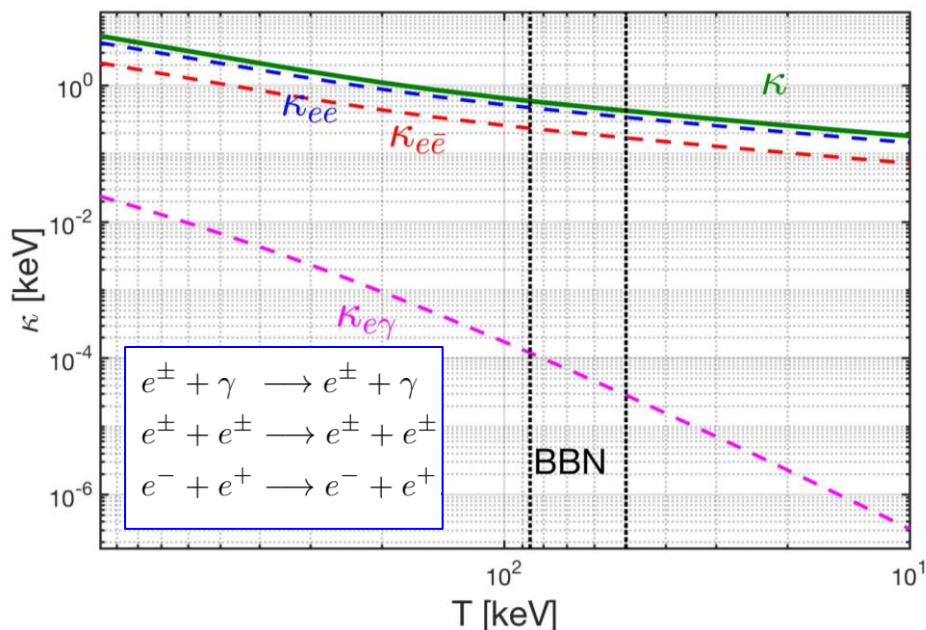
Debye mass in Boltzmann approximation

$$m_D^2 = \frac{16\alpha}{\pi} T^2 \left(\frac{m}{T}\right)^2 K_2\left(\frac{m}{T}\right) \cosh\left(\frac{\mu}{T}\right)$$

The damping rate for the electron-positron plasma is:

$$\kappa = \frac{(R_{e-\gamma} + R_{e+\gamma}) + (R_{e-e^-} + R_{e+e^+}) + R_{e-e^+}}{2\sqrt{n_{e^-} n_{e^+}}}$$

$$\sqrt{n_{e^-} n_{e^+}} = \frac{g_e}{2\pi^3} T^3 \left(\frac{m_e}{T}\right)^2 K_2(m_e/T)$$



Damped dynamic screening with scattering friction κ

Analytic solution in momentum phase space for the screened potential: **Dynamic and damped**

- The self consistent potential in an infinite stationary plasma can be found to be

$$\tilde{\phi}(\omega, \mathbf{k}) = \frac{\tilde{\rho}_{\text{ext}}(\omega, \mathbf{k})}{\varepsilon_0(\mathbf{k}^2 - \omega^2) (\Pi_{\parallel}/(\omega^2 \varepsilon_0) + 1)} \quad A \approx 0 \quad \text{“non-relativistic”}$$

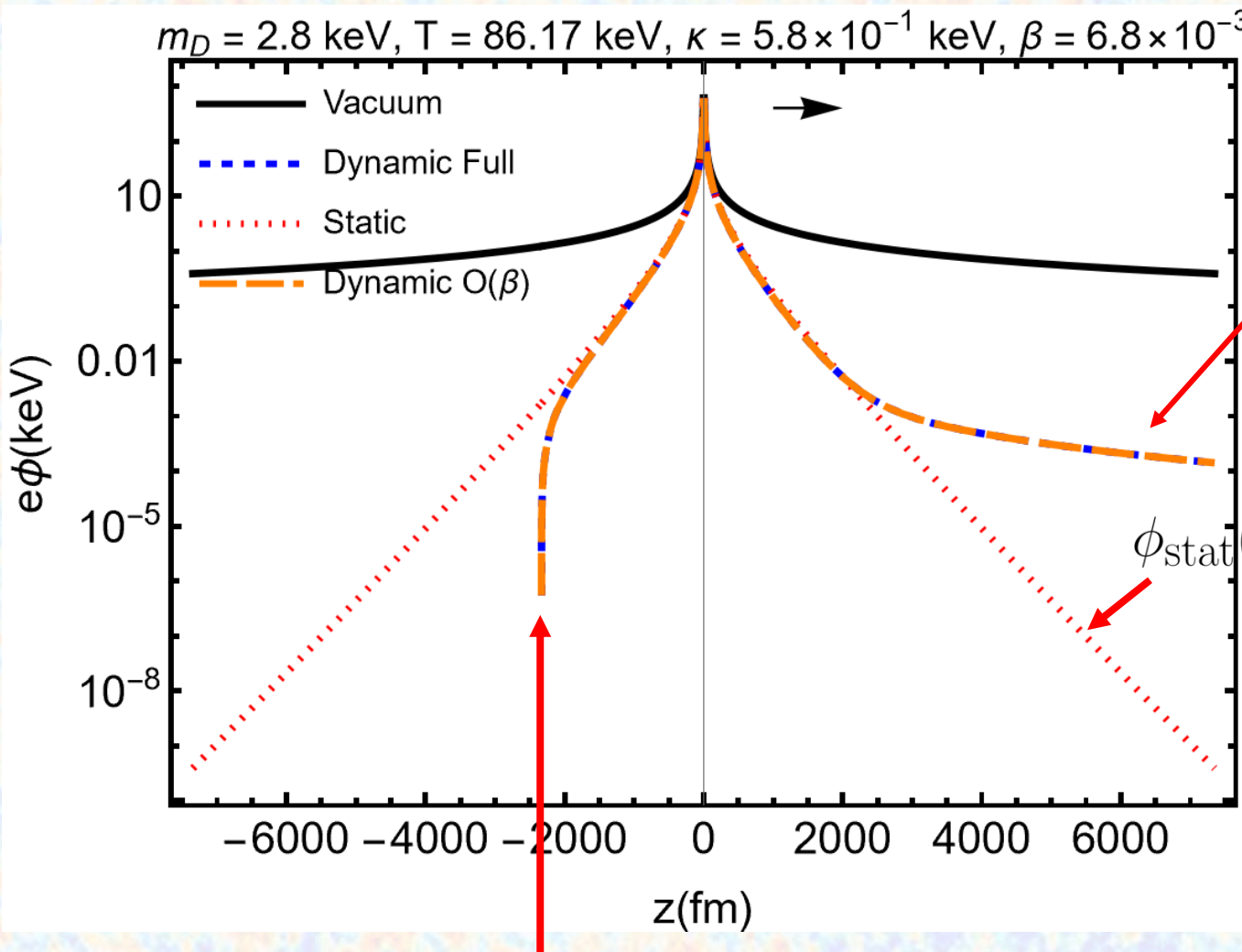
- $\Pi_{\parallel}(\omega, k)$ is the non-relativistic longitudinal polarization function found by solving,

$$(p \cdot \partial) f(x, p) + q F^{\mu\nu} p_{\nu} \frac{\partial f(x, p)}{\partial p^{\mu}} = (p \cdot u) \kappa \left(f_{\text{eq}}(p) \frac{n(x)}{n_{\text{eq}}} - f(x, p) \right)$$

$$\text{With } f_{\text{eq}} \approx \exp\left(-\frac{p \cdot u}{T}\right) \quad \text{and} \quad (p \cdot u) = p^0 = m \left(1 + \frac{|\mathbf{p}|^2}{2m^2} + \dots\right)$$

$$\Pi_{\parallel} = -m_D^2 \frac{T}{m(\omega + i\kappa)^2} \frac{\omega^2}{1 - \frac{i\kappa}{\omega + i\kappa} \left(1 + \frac{T|\mathbf{k}|^2}{m(\omega + i\kappa)^2}\right)}$$

Damped Dynamic Screening Comparison of Alpha Particles



Approaching a $1/r$ vacuum potential with a lower effective charge as already noted by L. Stenflo, M. Y. Yu, and P. K. Shukla *Shielding of a slow test charge in a collisional plasma The Physics of Fluids* 16, 450 (1973)

$$\phi_{\text{stat}}(r) = \frac{Ze}{4\pi\epsilon_0 r} e^{-m_D r}$$



Chris Grayson

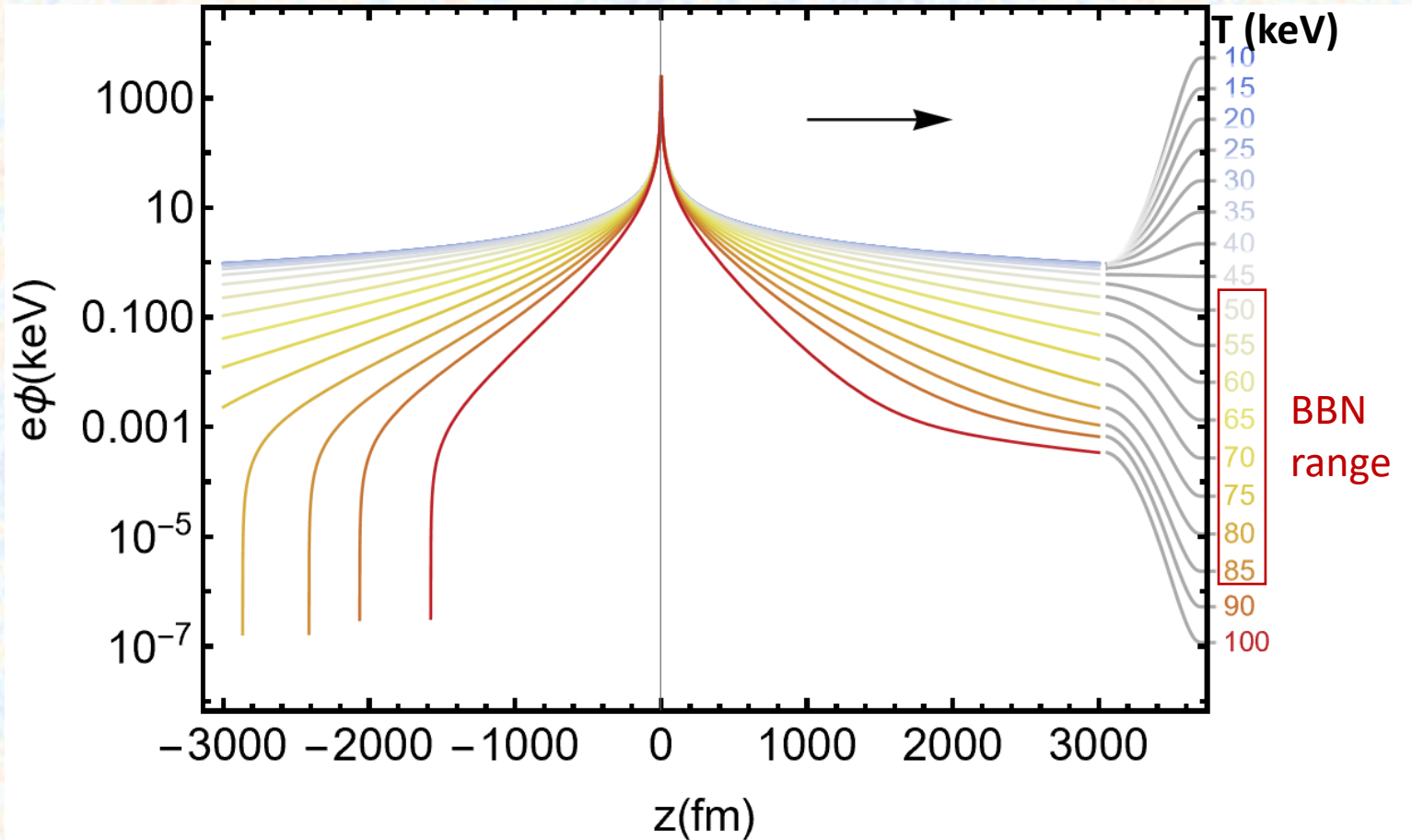
Wake charge build up (potential goes to zero)

$$v_{\text{th}} \approx \sqrt{\frac{2T}{m_N}} = 6.8 \times 10^{-3} c \text{ at } T = 86.2 \text{ keV}$$

Damped Dynamic Screening:

Coulomb Potential of a moving alpha

BBN reactions can be dynamically screened



Chris Grayson

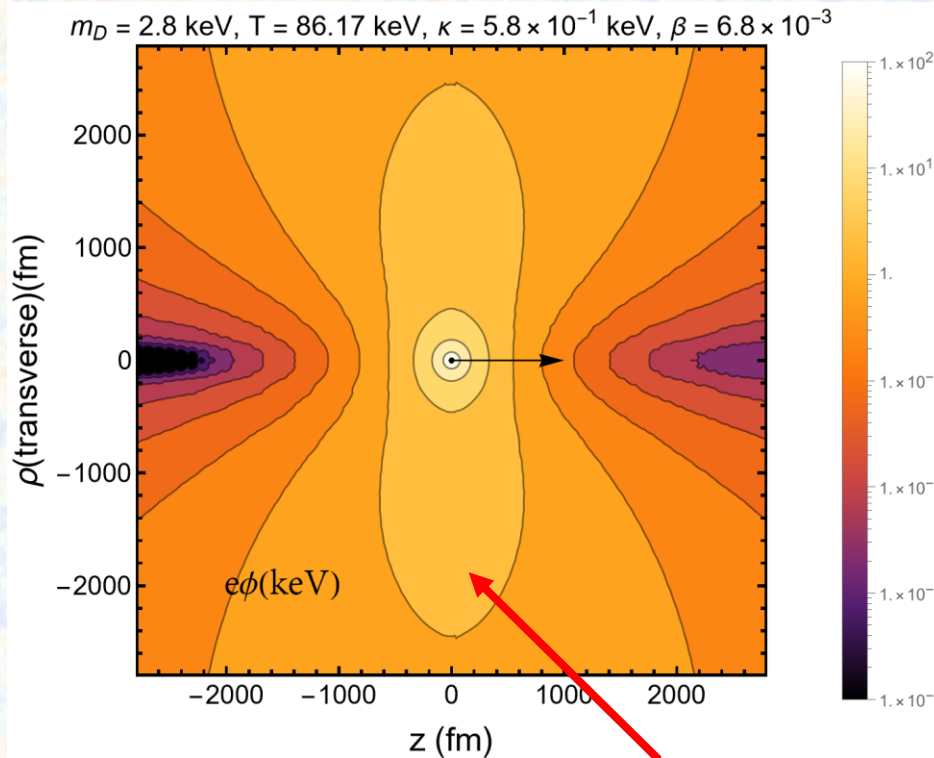
$$v_{\text{th}} \approx \sqrt{\frac{2T}{m_N}}$$

All light element components (p, d, t, He-3) approach faster from back due to their lighter masses compared to the alpha.

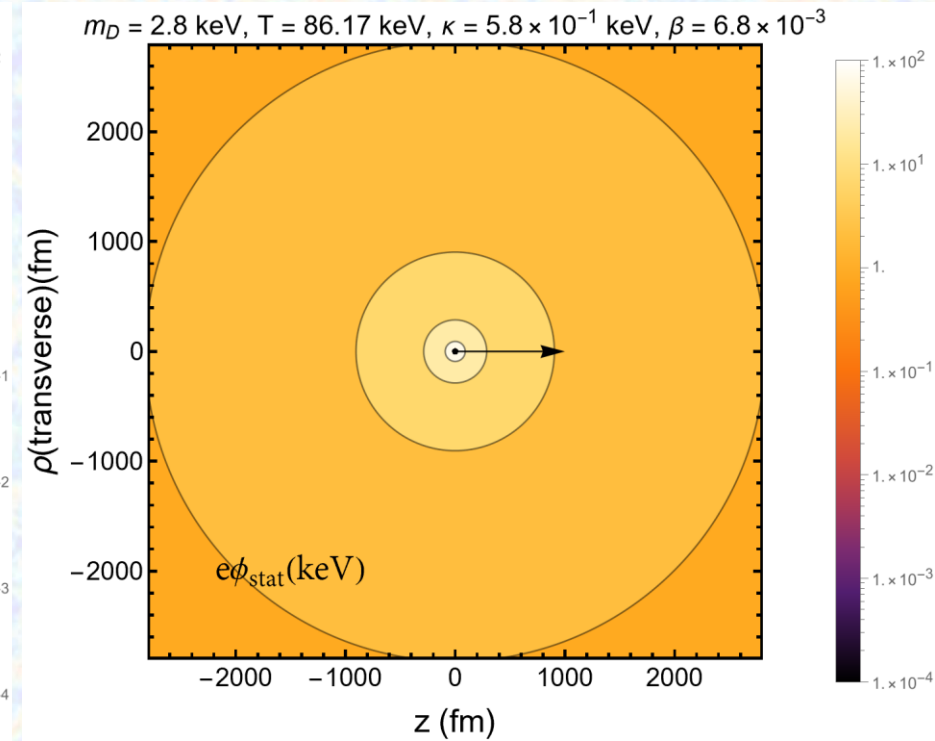


Chris Grayson

Damped Dynamic Screening



Static Screening



Less screening in the transverse direction

December 2022 Fusion conclusion

- The universe's evolution contains distinct eras of different particles and plasmas
- Special role of electron-positron plasma in BBN fusion recognized
- Fusion for mankind requires new ideas beyond what has been promised for 70 years without much success
- We describe screening effects that are relevant for BBN reactions. **Future research needed: Are screening effects of key importance in understanding dynamical tabletop fusion?**

